



AAV9-mediated SMN gene therapy rescues cardiac desmin but not lamin A/C and elastin dysregulation in Smn2B/- spinal muscular atrophy mice

Journal:	<i>Human Molecular Genetics</i>
Manuscript ID	HMG-2023-CE-00351.R1
Manuscript Type:	Original Article
Date Submitted by the Author:	n/a
Complete List of Authors:	<p>Brown, Sharon; Keele University, School of Pharmacy and Bioengineering; Robert Jones and Agnes Hunt Orthopaedic Hospital NHS Foundation Trust, Wolfson Centre for Inherited Neuromuscular Disease</p> <p>Šoltić, Darija; Keele University, School of Pharmacy and Bioengineering; Robert Jones and Agnes Hunt Orthopaedic Hospital NHS Foundation Trust, Wolfson Centre for Inherited Neuromuscular Disease</p> <p>Synowsky, Silvia; University of St Andrews, BSRC Mass Spectrometry and Proteomics Facility</p> <p>Shirran, Sally; University of St Andrews, BSRC Mass Spectrometry and Proteomics Facility</p> <p>Chilcott, Ellie; Royal Holloway University of London, AGCTlab.org, Centre of Gene and Cell Therapy, Centre for Biomedical Sciences, Department of Biological Sciences, School of Life Sciences and the Environment</p> <p>Shorrock, Hannah; The University of Edinburgh, Edinburgh Medical School: Biomedical Sciences; Euan MacDonald Centre for Motor Neurone Disease Research</p> <p>Gillingwater, Thomas; The University of Edinburgh, Euan MacDonald Centre for Motor Neurone Disease Research</p> <p>Yáñez-Muñoz, Rafael ; Royal Holloway University of London, School of Biological Sciences</p> <p>Schneider, Bernard; Ecole Polytechnique Federale de Lausanne, Brain Mind Institute</p> <p>Bowerman, Melissa; Keele University, School of Medicine</p> <p>Fuller, Heidi; Keele University, Wolfson Centre for Inherited Neuromuscular Disease; Robert Jones and Agnes Hunt Orthopaedic Hospital NHS Foundation Trust, Wolfson Centre for Inherited Neuromuscular Disease</p>
Key Words:	spinal muscular atrophy, lamin A/C, desmin, elastin, AAV9

1
2
3
4
5
6
7
8
9
10
11
12
13
14
15
16
17
18
19
20
21
22
23
24
25
26
27
28
29
30
31
32
33
34
35
36
37
38
39
40
41
42
43
44
45
46
47
48
49
50
51
52
53
54
55
56
57
58
59
60

AAV9-mediated *SMN* gene therapy rescues cardiac desmin but not lamin A/C and elastin dysregulation in *Smn*^{2B/-} spinal muscular atrophy mice

Sharon J. Brown^{a1,b2}, Darija Šoltić^{a1,b2}, Silvia A. Synowsky^{e3}, Sally L. Shirran^{e3}, Ellie Chilcott^{d4}, Hannah K. Shorrocks^{e5}, Thomas H. Gillingwater^{e5}, Rafael J. Yáñez-Muñoz^{d4}, Bernard Schneider^{f6,g7}, Melissa Bowerman^{b2,h8} and Heidi R. Fuller^{a1,b2*}

^{a1}School of Pharmacy and Bioengineering, Keele University, ST5 5BG, UK; ^{b2}Wolfson Centre for Inherited Neuromuscular Disease, TORCH Building, RJA Orthopaedic Hospital, Oswestry SY10 7AG, UK; ^{e3}BSRC Mass Spectrometry and Proteomics Facility, University of St Andrews, St Andrews KY16 9ST, UK; ^{d4}AGCTlab.org, Centre of Gene and Cell Therapy, Centre for Biomedical Sciences, Department of Biological Sciences, School of Life Sciences and the Environment, Royal Holloway University of London, Egham Hill, Egham, Surrey TW20 0EX, UK; ^{e5}Edinburgh Medical School: Biomedical Sciences, University of Edinburgh, UK; Euan MacDonald Centre for Motor Neurone Disease Research, University of Edinburgh, Edinburgh EH8 9XD, UK; ^{f6}Bertarelli Platform for Gene Therapy, Ecole Polytechnique Fédérale de Lausanne (EPFL), Geneva, Switzerland; ^{g7}Brain Mind Institute, Ecole Polytechnique Fédérale de Lausanne (EPFL), 1015 Lausanne, Switzerland; ^{h8}School of Medicine, Keele University, ST5 5BG, UK.;

*Corresponding author E-mail: h.r.fuller@keele.ac.uk

Postal Address: [Wolfson Centre for Inherited Neuromuscular Disease, TORCH Building, RJA Orthopaedic Hospital, Oswestry SY10 7AG, UK](#)

Telephone: +44(0)1782734546

Abstract

Structural, functional and molecular cardiac defects have been reported in spinal muscular atrophy (SMA) patients and mouse models. Previous quantitative proteomics analyses demonstrated widespread molecular defects in the severe Taiwanese SMA mouse model. Whether such changes are conserved across different mouse models, including less severe forms of the disease, has yet to be established. Here, using the same high-resolution proteomics approach in the less-severemilder *Smn*^{2B/-} SMA mouse model, 277 proteins were found to be differentially produced-abundant at a symptomatic timepoint (post-natal day (P) 18), 50 of which were similarly dysregulated in severe Taiwanese SMA mice. Bioinformatics analysis linked many of the differentially produced-abundant proteins to cardiovascular development and function, with intermediate filaments highlighted as an enriched cellular compartment in both datasets. Lamin A/C was increased in cardiac tissue whilst another intermediate filament protein, desmin, was reduced. The extracellular matrix (ECM) protein, elastin, was also robustly decreased in the heart of *Smn*^{2B/-} mice. AAV9-*SMNI*-mediated gene therapy rectified low levels of survival motor neuron (SMN) protein and restored desmin levels in heart tissues of *Smn*^{2B/-} mice. In contrast AAV9-*SMNI* therapy failed to correct lamin A/C or elastin levels. Intermediate filament proteins and the ECM have key roles in cardiac function and their dysregulation may explain cardiac impairment in SMA, especially since mutations in genes encoding these proteins cause other diseases with cardiac aberration. Cardiac pathology may need to be considered in the long-term care of SMA patients, as it is unclear whether currently available treatments can fully rescue peripheral pathology in SMA.

Introduction

Spinal muscular atrophy (SMA) arises from insufficient levels of survival motor neuron (SMN) protein due to a homozygous mutation/deletion in the *SMN1* gene (1). Although humans possess the *SMN2* gene (2), this generates only a limited amount of functional SMN (~10%) with the majority (~90%) being an unstable, truncated form of the protein (3). SMA patients present with a range of clinical phenotypes with varying severity, which generally, but not always, have an inverse relationship with *SMN2* copy number (4). Recent advances in SMA treatments aim to increase the levels of full-length SMN by either upregulating the *SMN2* gene or by delivering the *SMN1* gene directly to the cells via a viral vector (5). Neither treatment option is fully effective and evidence is emerging of new patient phenotypes with long-term treatment outcomes remaining unknown (5).

Although SMA is typically considered a motor neuron disease, the ubiquitous nature of SMN production has prompted research into the effects of reduced levels of SMN in peripheral tissues and organs, in both patients and animal models of SMA. Evidence demonstrating that SMA is a multisystem disease has been accruing (6,7) and impairment of cardiac function in mouse models of SMA and in SMA patients described (8–15). Examples of cardiac dysfunction include observations of bradycardia, dilated cardiomyopathy, and decreased contractility in *SMN Δ 7* mice (12), and [electrocardiogram](#) ECG abnormalities and thickened myocardium in patients with milder forms of SMA (9,16); whilst a retrospective study of patients with SMA Type I identified ~24% of patients with severe symptomatic bradycardia (10). Congenital heart defects, such as septal defects, in severe Type I patients (11) and in the severe Taiwanese SMA mouse model (14) have also been noted. A study in which the incidence of health insurance claims in Type I to III patients pre-SMA diagnosis were compared to control patients found valve disorders, cardiomyopathies, septal defects and premature beats to be increased (17).

1
2
3 Furthermore, a systematic review of more than 70 studies in which 264 SMA patients were
4 identified with cardiac pathology found a tendency for structural abnormalities to occur in the
5
6 more severe form of SMA (Type I) whilst in patients with less severe SMA, cardiac rhythm
7
8 disturbances were more common (18).
9
10

11
12
13 SMN protein is found in both the cytoplasm and nucleus of cells, and typically associated with
14
15 structures called Gemini of the coiled bodies (Gems) in the nucleus. There is also evidence that
16
17 SMN localises to structural components such as the sarcomere in striated muscle fibres (19)
18
19 and the Z-disc in mice cardiac myofibrils (20), but its function in cardiac muscle remains
20
21 unknown. Most studies have focussed on the more severe form of SMA, including our previous
22
23 quantitative proteomics study in which we demonstrated widespread molecular defects in heart
24
25 tissue from the severe Taiwanese SMA mouse model compared to healthy controls (15). In
26
27 particular, a robust increase in the intermediate filament protein, lamin A/C, was observed,
28
29 which we hypothesised may contribute to the impairment of cardiac function by causing
30
31 nuclear stiffness in the cardiomyocytes.
32
33
34
35
36
37
38
39

40 A recent study that focussed on the FoxO family of transcription factors in heart tissues from
41
42 the less-severe ~~milder~~ *Smn*^{2B/-} SMA mouse model, found no significant pathology related to
43
44 these factors or their downstream targets of proteosomal and autophagosomal degradation (21),
45
46 but the full extent of molecular consequences and their implications remain unknown for this
47
48 less-severe SMA mouse model. A recent transcriptome study of cardiomyocytes isolated from
49
50 a severe SMA mouse model and cardiomyocytes generated from induced pluripotent stem cells
51
52 (iPSCs) derived from an SMA Type II patient, however, found that SMN deficiency disrupts
53
54 muscle cell and fibre development, muscle function and Ca²⁺ handling (22). Cell studies are
55
56 extremely useful, but cell isolation and subsequent culture changes the physiological stresses
57
58
59
60

1
2
3 that they are exposed to in comparison to those experienced *in vivo*. Thus, we undertook a
4
5 quantitative proteomic comparison of heart tissues from the [less-severemilder](#) *Smn*^{2B/-} SMA
6
7 mouse model and age-matched wild-type (WT) mice and compared these findings with those
8
9 identified in our previous study of heart tissues from the severe Taiwanese SMA mouse model
10
11 (15).
12
13
14
15
16

17 We report evidence of widespread protein dysregulation in *Smn*^{2B/-} mouse hearts compared to
18
19 age-matched WT mice, some of which was common to the Taiwanese SMA mouse model. In
20
21 agreement with our previous findings from the Taiwanese model (15), the intermediate
22
23 filament protein, lamin A/C, was increased in expression in hearts from the [less-severemilder](#)
24
25 *Smn*^{2B/-} SMA mouse model, whereas desmin, another intermediate filament protein, was found
26
27 to be decreased in heart tissues in both mouse models. The extracellular matrix (ECM) protein,
28
29 elastin, was also significantly decreased in the heart tissues of the *Smn*^{2B/-} mouse. Whilst
30
31 AAV9-mediated *SMN1* delivery restored desmin levels in the *Smn*^{2B/-} SMA mouse model to
32
33 those seen in WT mice, this treatment did not rescue the increased levels of lamin A/C or the
34
35 decreased levels of elastin, even though levels of SMN were significantly enhanced when a
36
37 codon-optimised transgene was administered. Together these findings suggest that post-natal
38
39 AAV9-mediated *SMN1* delivery may not rectify all the dysregulated proteins [found in the](#)
40
41 [Smn^{2B/-} mouse model of associated with](#) SMA, and since these proteins have the potential to
42
43 detrimentally impact heart function, additional cardiac monitoring may prove useful in the
44
45 long-term care of SMA patients.
46
47
48
49
50
51
52
53

54 Results

55
56
57 **Quantitative proteomics analysis of heart tissue from a mouse model of [less-](#)**
58
59 **[severeintermediate](#) SMA [severity](#) reveals widespread molecular defects**
60

1
2
3 To determine the molecular consequences of SMN depletion in heart tissue from the
4 [intermediateless-severe](#) *Smn*^{2B/-} SMA mouse model, a relative quantitation proteomic
5 comparison against age-matched WT mouse hearts was undertaken using iTRAQ™ mass
6 spectrometry analysis at the symptomatic time-point of P18. This approach identified 3105
7 proteins in total (Supplementary Table 1) after removing proteins identified from 1 or more
8 peptides and those which matched to the decoy search (i.e., prefixed with “REVERSED...”).
9
10 Of these, 2479 were identified with a 5% local false-discovery rate. From these, 277 proteins
11 met the specified criteria (an unused ProtScore (conf) > 0.05, detected by ≥2 unique peptides,
12 and a statistically significant (p<0.05) fold change of ≥1.25 or ≤0.8) for differential expression
13 in the *Smn*^{2B/-} mouse heart compared to age-matched WT hearts, of which 156 proteins were
14 increased and 121 were decreased in expression in SMA mouse hearts (Supplementary Table
15 2).

16
17
18
19
20
21
22
23
24
25
26
27
28
29
30
31
32
33 To guide the direction of further studies, we were interested to understand whether any of the
34 differentially [expressed-abundant](#) proteins identified in heart tissue from the [milderless-severe](#)
35 *Smn*^{2B/-} SMA mouse model were conserved with those identified previously from the severe
36 Taiwanese SMA mouse model (15). The iTRAQ data pertaining to the Taiwanese model were
37 derived in the same experiment as the *Smn*^{2B/-} data reported here, but only the Taiwanese section
38 of the data was published previously (15). Compared to their respective age-matched WT mice
39 (i.e., P18 for the *Smn*^{2B/-} & P8 for the Taiwanese), and using the same criteria (p<0.05, [fold](#)
40 [change of >1.25 or <0.8, FC ≥ 0.25](#), >1 unique peptide), 50 proteins were found to be commonly
41 dysregulated in both mouse models of SMA (Supplementary Table 3). Of these, 30 were up-
42 regulated and 20 down-regulated with statistical significance in both models (Figure 1A) with
43 a similar fold-change in most dysregulated proteins (Figure 1B).

1
2
3 The list of differentially ~~expressed~~ abundant proteins from both mouse models was also
4 compared using the comparison analysis function of the curated bioinformatics platform,
5
6 Ingenuity Pathway Analysis (IPA®). This two-way comparison in which the enriched terms
7
8 were ranked by absolute *p*-value, demonstrated a similar enrichment of terms for “diseases &
9
10 disorders, physiological system development & function” after removal of cancer related terms.
11
12 In particular, “abnormal morphology” and “dilated cardiomyopathy” were highly enriched in
13
14 both mouse models (*Smn*^{2B/-} mouse model, *p*-value range 3.72 x 10⁻¹⁹ to 2.65 x 10⁻⁷; Taiwanese
15
16 mouse model, *p*-value range 9.52 x 10⁻²⁴ to 4.69 x 10⁻⁸) (Figure 1C). Similarly, for “molecular
17
18 & cellular functions”, terms relating to “translation, synthesis and metabolism of proteins” and
19
20 “cell & organismal death” were significantly enriched among the differentially ~~expressed~~
21
22 abundant proteins common to both mouse models (*Smn*^{2B/-} mouse model, *p*-value range 5.01 x
23
24 10⁻⁴⁰ to 2.65 x 10⁻⁷; Taiwanese mouse model, *p*-value range 9.52 x 10⁻²⁴ to 4.69 x 10⁻⁸) (Figure
25
26 1D). Various canonical pathways already linked to SMA such as “EIF2 signaling” (239) and
27
28 “mitochondrial dysfunction” (2409) were also enriched in the *Smn*^{2B/-} and Taiwanese mouse
29
30 models (Figure 1E). In addition, the “dilated cardiomyopathy signaling pathway” was
31
32 significantly enriched in both models (*Smn*^{2B/-} mouse model, *p*=6.52 x 10⁻¹¹, *z*-score = 1.043;
33
34 Taiwanese mouse model, *p*=2.72 x 10⁻¹⁸, *z*-score = -0.667).
35
36
37
38
39
40
41
42
43
44

45 Using the Database for Annotation, Visualization and Integrated Discovery (DAVID)
46
47 bioinformatics tool, the cellular components with which the significantly dysregulated proteins
48
49 in the *Smn*^{2B/-} mouse model were associated was ascertained (Figure 1F and Supplementary
50
51 Table 4A). Of particular interest were those cellular components pertinent to cardiomyocyte
52
53 function including the Z-disk (12 proteins; *p*=4.7x 10⁻⁶), the costamere (6 proteins; *p*=5.4 x 10⁻⁶),
54
55 focal adhesion (12 proteins; *p*=7.9 x 10⁻⁵) and adherens junction (10 proteins; *p*=3.2x10⁻⁴),
56
57 the sarcolemma (9 proteins; *p*=5.4 x 10⁻⁴), the intercalated disc (6 proteins; *p*=1.4 x 10⁻³), and
58
59
60

1
2
3 intermediate filaments (6 proteins; $p=2.5 \times 10^{-2}$). When the 50 proteins significantly
4 dysregulated in both the *Smn*^{2B/-} and Taiwanese SMA mouse models were considered in the
5 DAVID analysis, “intermediate filament” (3 proteins; $p=4.8 \times 10^{-2}$) remained an enriched
6 cellular component term (Supplementary Table 4B).
7
8
9
10
11
12
13
14

15 **The intermediate filament proteins, lamin A/C and desmin, are differentially ~~expressed~~**
16 **abundant in heart tissue from two mouse models of SMA**
17

18
19 The finding that intermediate filament proteins are differentially ~~expressed~~ abundant in both
20 SMA mouse models is of particular interest with regards to heart conditions. Mutations
21 affecting both lamin and desmin (type V and type III intermediate filament proteins,
22 respectively), commonly give rise to conditions associated with cardiomyopathy and heart
23 failure (4125). Of additional relevance is that mutations in *LMNA* -the lamin A/C gene- have
24 been attributed to adult-onset conditions with an SMA-like phenotype (426,2743). Lamin A
25 was identified by iTRAQ as being increased in both the Taiwanese (15) and *Smn*^{2B/-} SMA
26 mouse models (Supplementary Table 1) (albeit it just missed the criteria for differential
27 expression in the *Smn*^{2B/-} with $p=0.056$). Desmin, on the other hand, was decreased in
28 expression in both the Taiwanese (15) and *Smn*^{2B/-} SMA mouse models, but only met the
29 criteria for differential expression when peptides quantified with 99% confidence were used to
30 calculate the ratio, resulting in $p=0.049$).
31
32
33
34
35
36
37
38
39
40
41
42
43
44
45
46
47
48

49 To gain further insights into the involvement of these intermediate filament proteins in SMA,
50 we verified the differential expression of lamin A/C and desmin in heart tissue from the *Smn*^{2B/-}
51 and Taiwanese SMA mice. Quantitative western blotting confirmed a 1.94-fold and 2.06-fold
52 increase in lamin A and C expression, respectively, in heart tissue extracts from *Smn*^{2B/-} mice
53 compared to age-matched WT mice ($p=0.014$ and $p=0.030$, respectively) (Supplementary File
54
55
56
57
58
59
60

1
2
3 Figure 1A). Immunohistochemistry analysis also confirmed increased lamin A
4 immunoreactivity in heart tissues from the *Smn*^{2B/-} mouse model compared to those from WT
5 mice (1.74-fold increase, $p=0.007$; Supplementary File Figure 1B). This aligned with our
6 previous findings (15) where lamin A/C levels were increased in heart tissue from the severe
7 Taiwanese SMA mouse model. Immunohistochemistry analysis of *Smn*^{2B/-} mouse heart
8 sections revealed few lamin A/C positive cells in the ventricle lumen (Supplementary File
9 Figure 1C), in line with our previous observation from the Taiwanese SMA mouse model (15).
10 Although we cannot rule out a minor contribution, this result confirms that the increased lamin
11 A/C levels cannot be solely attributed to circulating blood cells. For reference, SMN levels in
12 heart tissue extracts from the *Smn*^{2B/-} mice were reduced to 0.08-fold ($p=0.007$) of that found
13 in WT mice (Supplementary File Figure 1A).
14
15
16
17
18
19
20
21
22
23
24
25
26
27
28
29
30

31 Decreased desmin expression was also confirmed in both mouse models of SMA by western
32 blotting, with levels being reduced in the *Smn*^{2B/-} mice compared to age-matched (P18) WT
33 mice to 0.73-fold ($p=0.033$) and in the Taiwanese mice compared to age-matched (P8) WT
34 mice to 0.76-fold ($p=0.007$) (Supplementary File Figure 2A). These findings were corroborated
35 by immunohistochemistry analysis (Supplementary File Figure 2B) with desmin
36 immunoreactivity in *Smn*^{2B/-} mice showing a decrease to 0.41-fold ($p=0.033$) compared to WT
37 (P18) mice and desmin staining in Taiwanese mice demonstrating a decrease to 0.26-fold
38 ($p=0.019$) compared to (P8) WT mice (Supplementary File Figure 2C).
39
40
41
42
43
44
45
46
47
48
49
50

51 **AAV9-mediated *SMN1* delivery to increase SMN expression in the hearts of *Smn*^{2B/-} SMA** 52 **mice** 53 54

55
56 To establish the impact of currently approved gene therapy treatments, which are designed to
57 increase SMN levels in SMA patients, on a peripheral tissue such as the heart, we examined
58
59
60

1
2
3 the extent to which AAV9-mediated *SMNI* treatment restored expression levels of lamin A/C
4 and desmin towards control mice. For these experiments, we chose to focus only on the less-
5
6
7
8 severe *Smn*^{2B/-} SMA model as these mice have a longer pre-symptomatic period compared to
9
10 the Taiwanese mouse model allowing for a better understanding of developmental defects
11 secondary to motor neuron loss. In addition, to validate our findings further, two distinct
12
13
14
15 vectors that have previously been used in *Smn*^{2B/-} mice were utilised (3128,329), in particular
16
17 the one vector results in enhanced expression of the *SMNI* gene (3128). SMN levels were
18 confirmed by quantitative western blotting to be significantly increased in extracts of heart
19
20
21 tissues from *Smn*^{2B/-} mice following AAV9-mediated *SMNI* replacement (Figure 2). As
22
23
24 expected (3128), delivery of the optimised cDNA transgene AAV9_*Co-hSMNI* resulted in
25
26 enhanced levels of SMN (169-fold; $p=0.0002$) compared to untreated *Smn*^{2B/-} mice with
27
28 increased levels of SMN beyond that expected in WT mice (~13.50-fold). Although the
29
30 scAAV9-*SMNI*-mediated delivery also resulted in an SMN increase (2.4-fold; $p=0.0003$)
31
32 compared to untreated *Smn*^{2B/-} mice, SMN levels remained below that found in WT mice
33
34 (~0.32-fold) (Figure 2A). There was no statistically significant difference in SMN expression
35
36 levels between untreated *Smn*^{2B/-} mice and vehicle controls (i.e., AAV9_*eGFP* (2.1-fold;
37
38 $p=0.14$); scAAV9-*GFP* (1.8-fold; $p=0.08$) (Figure 2A). Immunohistochemistry analysis of
39
40 heart tissues from *Smn*^{2B/-} mice revealed increased SMN immunoreactivity following SMN
41
42 replacement, particularly in those treated with AAV9_*Co-hSMNI* (Figure 2B).
43
44
45
46
47
48

49 **AAV9-mediated *SMNI* delivery restores desmin expression but does not correct** 50 **increased lamin A/C expression in the hearts of *Smn*^{2B/-} SMA mice**

51
52 Quantitative western blotting and immunohistochemistry analysis revealed that AAV9-
53
54 mediated *SMNI* treatment did not correct the increased production of lamin A/C in *Smn*^{2B/-}
55
56 mouse hearts. On western blots, lamin A expression levels following delivery of AAV9_*Co-*
57
58
59
60

1
2
3 *hSMN1* were 0.80-fold ($p=0.36$) compared to untreated *Smn*^{2B/-} mice and 1.56-fold ($p=0.04$)
4 compared to WT mice. Following scAAV9-*SMN1*-mediated delivery lamin A levels were 0.96-
5 fold ($p=0.44$) compared to untreated *Smn*^{2B/-} mice and 1.56-fold ($p=0.003$) compared to WT
6 mice (Figure 3A). Similarly, lamin C expression levels following delivery of AAV9_*Co-*
7 *hSMN1* were 0.77-fold ($p=0.26$) compared to untreated *Smn*^{2B/-} mice and 1.39-fold ($p=0.13$)
8 compared to WT mice and following scAAV9-*SMN1*-mediated delivery were 0.96-fold
9 ($p=0.50$) compared to untreated *Smn*^{2B/-} mice and 1.54-fold ($p=0.004$) compared to WT mice
10 (Figure 3A). There was no statistically significant difference in lamin A and C expression levels
11 between untreated *Smn*^{2B/-} mice and vehicle controls (i.e., AAV9_*eGFP* (1.06-fold ($p=0.46$)
12 for lamin A and 1.21-fold ($p=0.06$) for lamin C); scAAV9-*GFP* (0.96-fold ($p=0.59$) for lamin
13 A and 0.84-fold ($p=0.06$) for lamin C) (Figure 3B).

14
15
16
17
18
19
20
21
22
23
24
25
26
27
28
29
30
31 In heart sections from WT mice, lamin A/C immunoreactivity was largely confined to the
32 nuclear membrane, as expected, with a small proportion being localised to the sarcomere as
33 confirmed by double-label immunohistochemistry with alpha-actinin 2, a sarcomere marker
34 (Figure 3C & 3D). In heart sections from the *Smn*^{2B/-} mice, lamin A/C was significantly
35 increased in expression at the nuclear membrane alongside a strikingly increased distribution
36 of lamin A/C at the sarcomeres (Figure 3C). When quantified across each section, lamin A/C
37 immunoreactivity in heart tissues from *Smn*^{2B/-} mice showed a significant increase in lamin A/C
38 expression compared to age-matched (P18) WT mice (3.29 ± 1.13 -fold; $p=0.004$; Figure 3C),
39 and after treatment with AAV9_*Co-hSMN1* or scAAV9-*SMN1* lamin A/C levels in *Smn*^{2B/-}
40 mice remained increased compared to the untreated *Smn*^{2B/-} mice (3.66 ± 0.70 -fold ($p=0.54$)
41 and 4.25 ± 0.45 -fold ($p=0.13$), respectively (Figure 3C).

1
2
3 Western blot and immunohistochemistry analysis revealed that AAV9-mediated *SMNI*
4 treatment did, however, restore the decreased expression of desmin in *Smn*^{2B/-} mouse hearts
5 towards WT levels. From western blots, desmin expression levels following delivery of
6 AAV9_*Co-hSMNI* were 1.74-fold ($p=0.0095$) compared to untreated *Smn*^{2B/-} mice and 1.06-
7 fold ($p=0.44$) compared to WT mice and following scAAV9-*SMNI*-mediated delivery were
8 1.84-fold ($p=0.04$) compared to untreated *Smn*^{2B/-} mice and 1.31-fold ($p=0.13$) compared to
9 WT mice (Figure 4A). There was no statistically significant difference in desmin expression
10 levels between untreated *Smn*^{2B/-} mice and vehicle controls (i.e., AAV9_*eGFP*) (0.99-fold
11 ($p=0.88$)) and scAAV9-*GFP* (1.16-fold ($p=0.19$)) (Figure 4B). Desmin immunoreactivity in
12 heart sections from WT mice was typically present at the Z-disc (Figure 4C). Desmin
13 immunoreactivity in heart sections from the *Smn*^{2B/-} mice was clearly reduced ([Figure 4C, high](#)
14 [magnification images](#)), although some striations could still be seen, the staining appearing to
15 be variable in intensity and disorganised. Quantification of desmin immunoreactivity across
16 each heart section from the *Smn*^{2B/-} mice found desmin expression to be significantly decreased
17 compared to age-matched (P18) WT mice (0.61 ± 0.12 -fold ($p<0.001$)) (Figure 4C), but
18 treatment with AAV9_*Co-hSMNI* or scAAV9-*SMNI* confirmed that desmin levels in *Smn*^{2B/-}
19 mice were increased compared to the untreated *Smn*^{2B/-} mice (1.75 ± 0.19 -fold ($p<0.0001$) and
20 1.28 ± 0.22 -fold ($p=0.035$)), respectively (Figure 4C).

21 22 23 24 25 26 27 28 29 30 31 32 33 34 35 36 37 38 39 40 41 42 43 44 45 46 47 **Decreased elastin expression in *Smn*^{2B/-} mouse heart is also refractory to AAV9-mediated** 48 ***SMNI* delivery**

49
50
51 Lamin A/C is a significant regulator of cell stability and dynamics ([3044](#)), and its expression
52 correlates with the stiffness of tissue ([4531](#)). Increased rigidity of cardiomyocytes enhances
53 passive tension *in vitro* and *in vivo*, resulting in functional heart defects ([4632,4733](#)). To gain
54 insights into the wider impact of increased lamin A/C levels on the contractile apparatus of
55
56
57
58
59
60

1
2
3 cardiomyocytes and overall stiffness of heart tissues in the *Smn*^{2B/-} SMA mouse model, we
4 examined the levels of elastin, a protein essential for the elastic properties of many tissues.
5 Elastin was identified by iTRAQ analysis to be significantly reduced to 0.01-fold ($p=0.003$) in
6 heart tissue from the *Smn*^{2B/-} SMA mouse model compared to WT. This finding was confirmed
7 qualitatively by immunohistochemical analysis of van Gieson staining (i.e., a modified Miller's
8 stain which differentially stains elastin from collagen and muscle), and quantitatively by
9 higher-power immunofluorescence analysis (0.30 ± 0.14 -fold ($p<0.00001$) in *Smn*^{2B/-} vs WT)
10 (Figure 5). Elastin levels in *Smn*^{2B/-} mice following treatment with either AAV9_*Co-hSMN1* or
11 scAAV9-*SMN1* remained comparable to those observed in untreated *Smn*^{2B/-} mice (0.37 ± 0.16 -
12 fold ($p=0.41$), and 0.30 ± 0.13 -fold ($p=0.24$)) of WT levels respectively) (Figure 5).
13
14
15
16
17
18
19
20
21
22
23
24
25
26
27

28 Discussion

29
30 Over the last two decades, evidence has built to suggest that in severe forms of SMA, structural
31 and functional abnormalities in heart tissues exist (14,18,22), whilst in patients with less severe
32 types, a potentially milder impairment of cardiac function is suggested (9,16). The aim of this
33 study was to conduct a proteomic comparison of heart tissues from the [less-severemilder](#)
34 *Smn*^{2B/-} SMA mouse model and age-matched wild-type (WT) mice and compare these findings
35 with those identified in our previous study of heart tissues from the severe Taiwanese SMA
36 mouse model (15) to determine whether a conserved response to reduced SMN levels is
37 evident. We also investigated whether dysregulated proteins with a known role in heart
38 function are impacted and whether their levels could be rescued by increasing SMN levels in
39 the [less-severemilder](#) *Smn*^{2B/-} mouse model.
40
41
42
43
44
45
46
47
48
49
50
51
52
53
54
55

56 In each SMA mouse model, hundreds of proteins were found to be dysregulated compared to
57 age-matched WT mice. Bioinformatics analysis revealed a highly significant enrichment of
58
59
60

1
2
3 terms relating to “abnormal morphology” and “dilated cardiomyopathy” in reference to
4
5 “diseases & disorders, physiological system development & function” in both dysregulated
6
7 datasets. Previously, cardiac defects such as thinning of the interventricular septum and
8
9 cardiomyocyte disorganisation have been noted in the severe Taiwanese SMA mouse model
10
11 (14) as have atrial or ventricular septal defects (11) and thickened myocardium (9) in patients
12
13 with SMA type I. Out of 42 SMA type II and III patients, one patient had mitral valve prolapse,
14
15 7 had sinus tachycardia, and more than half had an elevated minimum 24-hour heart rate (16).
16
17 When “molecular and cellular functions” were considered, terms relating to the “translation,
18
19 synthesis and metabolism of proteins”, and “cell and organismal death” were highly significant.
20
21 Most of these terms are typically associated with SMA, in particular, SMN is known to be key
22
23 for protein homeostasis (348). Both *in vitro* and *in vivo* studies provide support for impaired
24
25 translation in SMA (4935,5036) and a comprehensive study involving rat primary neuron
26
27 culture, fibroblasts from SMA Type I patients and neurons from a severe mouse model of SMA
28
29 (*Smn*^{-/-}; *SMN2*^{tg/0}) demonstrated reduced *de novo* protein synthesis linked to mTOR signalling
30
31 (5137). In an earlier study, microfilament metabolism was found to be impacted by reduced
32
33 levels of SMN (5238), and with evidence building for a role of mitochondrial dysfunction in
34
35 SMA (240,539–5541), all these factors may contribute to altered protein metabolism. Most of
36
37 the significantly enriched “canonical pathways” common to both mouse models have also been
38
39 implicated in SMA, such as EIF2 signaling (239), mitochondrial dysfunction (240) and mTOR
40
41 signaling (5137), but of particular interest was the significant enrichment of “dilated
42
43 cardiomyopathy” and the “dilated cardiomyopathy signaling pathway” in both mouse models
44
45 of SMA.
46
47
48
49
50
51
52
53
54
55

56 While differentially expressed-abundant proteins from the *Smn*^{2B/-} dataset were associated with
57
58 several cellular components pertinent to cardiomyocyte function, the only cellular component
59
60

1
2
3 to be significantly enriched among proteins common to both mouse models was intermediate
4
5 filaments. Genetic mutations of the intermediate filaments lamin A/C and desmin are known
6
7 contributors of cardiomyopathies and heart failure (4125,5642). Both proteins form networks
8
9 within the cardiomyocyte and help maintain intra- and intercellular structure, with lamin A/C
10
11 at the nuclear envelope (5743) and desmin within the cytoplasm. In addition, lamin and desmin
12
13 have important functions in nucleo-cytoskeletal coupling and mechano-transduction, gene
14
15 regulation, metabolism, mitochondrial homeostasis and cardiomyocyte differentiation and
16
17 survival (5743–459), all of which are necessary for a fully functioning heart.
18
19
20
21
22

23
24 As previously confirmed in the Taiwanese mouse model of severe SMA (15), levels of lamin
25
26 A/C were significantly increased in heart tissues from the *Smn*^{2B/-} mouse model of [less-](#)
27
28 [severemilder](#) SMA. Increased levels of lamin A/C were localised to the nuclear envelope and
29
30 to the sarcomere of *Smn*^{2B/-} mouse hearts, and further support the concept that appropriate lamin
31
32 A/C production is SMN-dependent (15,4327,460). Previously, increased lamin A/C levels have
33
34 been described in muscle (6147) and Schwann cells from SMA mice (6248) and in motor
35
36 neurons obtained from Type I SMA patients (6349). In terms of impact on heart conditions and
37
38 development of dilated cardiomyopathy, impairment of the lamin A/C gene is a well-known
39
40 factor (6450) and results in conduction problems, arrhythmias, atrioventricular block and
41
42 sudden cardiac death (651–6955) with at least 260 *LMNA* mutations having been linked to
43
44 cardiac diseases (7056). In several studies, *LMNA* mutations have also resulted in an SMA-like
45
46 phenotype with cardiac involvement (426,4327).
47
48
49
50
51
52

53
54 An increase in lamin A/C may result in a “stiffer” nucleus which will alter the biomechanics
55
56 of the cardiomyocyte, and thus the heart tissue, and may be in response to increased stiffness
57
58 of the heart tissue (4531). Conditions where increased accumulation of lamin A at the nuclear
59
60

1
2
3 envelope is known to occur are Hutchinson-Gilford progeria syndrome and restrictive
4
5 dermopathy. Both conditions arise from improper post-translational processing of prelamin A,
6
7 the former from an *LMNA* mutation which results in a mutant farnesylated prelamin A
8
9 (progerin) whilst the latter is due to reduced levels of ZMPSTE24, the enzyme necessary for
10
11 processing prelamin A (574). Although not verified by immuno techniques in the current study,
12
13 ZMPSTE24 was significantly increased in the mass spectrometry data from both SMA mouse
14
15 models which may imply dysregulation of lamin A processing. In the current study, lamin A
16
17 was also prevalent at the sarcomere, especially in *Smn*^{2B/-} mice where it co-localised with alpha-
18
19 actinin 2. This may indicate an increase in unprocessed lamin A in SMA, as previously
20
21 prelamin A was identified at the sarcomere along with alpha-actinin 2 (6955). Since it has been
22
23 suggested that prelamin A may be toxic and could promote dilated cardiomyopathy (6955),
24
25 further investigations into understanding whether lamin A processing is defective in SMA may
26
27 prove useful. Additionally, the phosphorylation status of lamin A in SMA is worthy of
28
29 investigation as this may have implications for the regulation of lamin A levels since hypo-
30
31 phosphorylation renders lamin A more stable and less likely to be degraded (7258) and has
32
33 occurred in mesenchymal stem cells when subjected to increased tissue stiffness (7359).
34
35
36
37
38
39
40
41

42 Lamin A/C is the main provider of nuclear membrane mechanical strength and is key to
43
44 transmitting mechanical force from the ECM to the nucleus (7460,7561). Deficiency or
45
46 mutations in lamin A/C can cause mechano-transduction impairment (762) or impact whole-
47
48 cell biomechanical properties (7763). In a lamin A-deficient mouse model, the desmin network
49
50 was disrupted and detached from the nuclear surface (7864), suggesting defective force
51
52 transmission due to loss of lamin interactions with desmin and subsequent loss of cytoskeletal
53
54 tension. In another study of lamin A-deficient mice, desmin accumulation was increased in
55
56 both muscle and cardiac tissues (7965). It may prove useful to consider whether the reverse is
57
58
59
60

1
2
3 true in SMA cardiomyocytes whereby decreased levels of desmin result in increased lamin A
4
5 or *vice versa*.
6
7
8
9

10 Desmin is located throughout the cardiomyocyte and assists in transmitting force across the
11 ECM, sarcomere and cytoskeleton (8066), and has been implicated in SMA (8167). In
12 combination with microtubules and microfilaments, desmin helps to maintain the cytoskeleton
13 structure and organisation of sub-cellular organelles (682) and is thought to provide
14 cardiomyocyte nuclei with tension (8369). Structurally, desmin links individual myofibrils at
15 the Z-discs (8470,8571), connects Z-discs to the intercalated disc (8672), forms part of the
16 desmosomes, and is linked to the costamere enabling adhesion to the ECM (873). Overall,
17 desmin is key to the functioning of sarcomeres in efficient syncytia. Mutations often result in
18 loss of sarcomere integrity and myofibrillar structure (8874) and depletion causes muscle
19 architecture disruption (8975), which is not impacted during embryogenesis and myofibrillar
20 assembly but affects muscle regeneration resulting in weaker mice in a desmin knock-out
21 model (9076). In other studies, lack of desmin impacted contractile function (9177) and
22 increased fibrosis (9278) with muscle fibres lacking desmin being more susceptible to physical
23 damage (793) and desmin loss causing increased passive stiffness in muscle (9480).
24
25
26
27
28
29
30
31
32
33
34
35
36
37
38
39
40
41
42
43
44

45 Mechano-sensing within cardiomyocytes is a “two-way” system, with the nucleus being an
46 important mechanosensory organelle in the cell and intimately connected to the cytoskeleton,
47 and the latter in turn to the ECM. For optimal heart performance, both electrical and mechanical
48 stimuli are required with cardiomyocytes being subjected to cyclic contraction as the heart
49 beats (9581). Cardiomyocytes also experience passive mechanical stimuli such as that exerted
50 by the cardiac ECM. The cardiac ECM is a combination of elastin bundles, collagen and
51 interconnected basement membranes (9682), with intra- and extracellular components
52
53
54
55
56
57
58
59
60

1
2
3 contributing to overall myocardial stiffness (9581). Although collagen is the main extracellular
4 protein in myocardial tissue, elastin, which is found in the epicardium, endomysium and
5 structures such as arteries, atria and ventricles of the heart (9783), provides elasticity upon
6 mechanical demand (984). Elastin is a structural glycoprotein and an essential component of
7 myocardial stiffness (9985), so any alterations in its levels will impact heart function.
8 Typically, elastin is very stable with a considerably low turnover rate, with degradation or
9 damage indicating pathological remodelling of the tissue and cardiovascular disease (10086).
10 Reduced levels of elastin, as found in this study, will increase the heart tissue's passive
11 stiffness, potentially reducing cardiac function, since cardiomyocytes cultured on a stiff,
12 fibrotic-like matrix fail to beat properly (10187). Typically, following myocardial
13 infarction/ischaemia, elastin levels will decrease (10288), promoting ECM remodelling which
14 further increases the stiffness of the cardiac tissue and impairment of cardiac function (9985).
15 In Williams-Beuren syndrome, impairment of the elastin *ELN* gene results in 4 out of 5 patients
16 having cardiovascular abnormalities (10389), with mutations also resulting in congenital heart
17 disease (1904). Elastin fibres are crucial for the proper functioning of Purkinje's fibres (9105)
18 and blood vessels (10692), and impairment can cause arrhythmias (10793) or altered blood
19 flow respectively, again impacting heart function.
20
21
22
23
24
25
26
27
28
29
30
31
32
33
34
35
36
37
38
39
40
41
42
43
44

45 Two AAV9-mediated *SMN1* treatments were used in this study, both of which have previously
46 been used in *Smn*^{2B/-} mice (3128,329), but the novel codon-optimised cDNA transgene
47 demonstrated significantly enhanced expression of the human *SMN1* gene in *Smn*^{2B/-} mice
48 hearts. Both treatments restored desmin levels to that of WT mice, but lamin A/C levels
49 remained elevated and elastin levels decreased even though the codon-optimised cDNA
50 transgene generated SMN levels more than 10-fold greater than those found in WT mice. The
51 lack of effect of increased SMN levels on lamin A in this study may be due to several reasons:
52
53
54
55
56
57
58
59
60

1
2
3 (4i) lamin A is independent of SMN levels; (2ii) the impact of low SMN levels on lamin A is
4 greatest during embryonic development so post-natal treatment is too late; (3iii) cardiac
5 remodelling is influencing lamin A levels; and/or (4iv) dysregulation of proteins responsible
6 for post-translation processing or regulating the stability of lamin A are not independent of
7 SMN levels. In contrast, desmin levels were increased by both AAV9-mediated *SMN1*
8 treatments, indicating a direct relationship between these two proteins. Previously,
9 abnormalities in the Z-bands of a patient with SMA were identified (10894). Since low levels
10 of desmin appeared to be associated with sarcomere damage in a rat model of diabetes mellitus
11 (1095) and alpha-actinin staining showed disrupted sarcomere/costamere/z-disc striations in
12 desmin-null mice (11096), it is coherent that the improved levels of desmin in the AAV9-
13 treated *Smn*^{2B/-} mice result in improved sarcomere structure, although higher resolution
14 microscopy is required to confirm this. Interestingly, SMN has been found to be localised to
15 the I- and M-bands of sarcomeres in normal human skeletal fibres (11197) and the Z-disc in
16 mice (20) which suggests that sarcomeric SMN may directly or indirectly interact with the
17 cytoskeleton and thus be involved in sarcomere structure (11197), or its maintenance (20). In
18 addition, during heart development, desmin and lamin A are ~~expressed abundant~~ in the cardiac
19 conduction systems; desmin preferentially in the myocardium of the central conduction system
20 and lamin A more localised to the peripheral conduction system, then progressively to the
21 central conduction system (11298). It may be possible that AAV9-mediated treatment does not
22 rectify lamin A/C levels due to inherent problems with the central conduction system that are
23 established prior to treatment being administered. Additionally, abnormalities in conduction
24 usually occur before dilated cardiomyopathy development (11399) with elevated heart rate
25 being associated with cardiomyopathy in late adolescence and increased heart failure risk
26 (10014). In desmin mutant mice, distribution of lamin A/C was nucleoplasmic whilst in WT
27
28
29
30
31
32
33
34
35
36
37
38
39
40
41
42
43
44
45
46
47
48
49
50
51
52
53
54
55
56
57
58
59
60

1
2
3 mice, lamin A/C was mostly at the nuclear periphery (8672). Since AAV9-mediated treatment
4 restored desmin levels, lamin A/C's nuclear distribution may improve over time.
5
6
7
8
9

10 Other researchers have found the outcome of AAV9 treatment in SMA to be variable. A study
11 focussed on fibrosis, remodelling, vascular integrity and oxidative stress in two mouse models
12 of differing severity only found a partial rescue of cardiovascular defects in their mouse model
13 of severe SMA and although structural defects were rectified, heart function incorporating heart
14 rate, stroke volume and cardiac output remained significantly lower than WT mice, as did
15 lifespan (13). In the SMN Δ 7 mouse model, scAAV9 treatment resolved the bradycardia issues,
16 but "cardiac output" remained similar to untreated mice, probably as a result of "stroke
17 volume" remaining decreased following scAAV9 treatment (12). In addition, contractility
18 remained lower than WTs following treatment. Another study using the SMN Δ 7 SMA mouse
19 model used the histone deacetylase inhibitor, trichostatin A, which is known to improve the
20 phenotype of SMA mice. Although heart function improved, these mice did not survive as well
21 as the WT mice (1015). Typically, levels of lamin A/C in mouse cardiomyocytes, desmin in
22 rat heart tissues and the elastin component of connective tissues decline with age (102-104),
23 although in male F344/BN hybrid rats, desmin levels were found to increase in aging skeletal
24 muscle (105). In future studies, it will therefore be important to characterise the temporal
25 regulation of the proteins investigated throughout the disease time-course in the *Smn*^{2B/-} mouse
26 model, with and without AAV-9 mediated *SMN1* replacement, and to establish whether
27 restoring levels of these proteins would have an impact on cardiac function of the mouse model.
28
29 SMN may be essential for heart development prior to birth and thus scAAV9 treatment may
30 not correct key development milestones involving SMN. Additionally, other factors such as
31 lung and metabolic function or scoliosis may contribute to continued impairment of heart
32 function in SMA. Prior to the introduction of treatments, such as, nusinersen and risdiplam
33
34
35
36
37
38
39
40
41
42
43
44
45
46
47
48
49
50
51
52
53
54
55
56
57
58
59
60

1
2
3 which modify *SMN2* gene regulation to increase functional SMN expression, the impact on
4 concomitant health issues in SMA patients following respiratory assistance, and thus extended
5 life expectancy, has been previously highlighted (10) and included development of heart
6 arrhythmia (bradycardia).
7
8
9

10
11
12
13
14 In conclusion, accumulating evidence suggests that cardiac assessment in the long-term care
15 of SMA patients is warranted. We only investigated three of the dysregulated proteins
16 identified from mass spectrometry analysis in the *Smn*^{2B/-} mouse model, but there are many
17 more that warrant further investigation, especially those pertinent to heart function. AAV9-
18 *SMN1* gene therapy only corrected one of the proteins investigated, and although severe
19 symptoms may be rare in SMA, subtle differences in cardiac performance in combination with
20 current treatments increasing longevity in these patients, may impact cardiac health in future
21 years. Thus, additional cardiac therapies may prove useful in optimising treatment regimens
22 for SMA patients.
23
24
25
26
27
28
29
30
31
32
33
34
35
36
37

38 **Materials & Methods & Materials**

39 **SMA mouse models**

40
41
42 The *Smn*^{2B/-} and Taiwanese (original strain from Jackson Laboratories, No. 005058) mouse
43 models were housed at Keele and Edinburgh Universities, respectively. As previously
44 described (23106), the less-severe *Smn*^{2B/-} mouse model is maintained on a pure C57BL/6
45 genetic background with creation of the 2B mutation via a 3-nucleotide substitution within the
46 exon splicing enhancer of exon 7 (24107,25108). The severe Taiwanese mouse model is
47 heterozygous for the *SMN2* transgene on a *Smn* null background (*Smn*^{-/-}; *SMN2*^{tg/+}) (26109).
48
49 Tissues were harvested at a symptomatic time point of post-natal day (P) 18 and P8 for the
50 *Smn*^{2B/-} and Taiwanese models, respectively, in addition to age-matched WT mice. All
51
52
53
54
55
56
57
58
59
60

1
2
3 experimental procedures on Taiwanese mice were authorized and approved by the University
4 of Edinburgh Animal Welfare Ethical Review Body (AWERB) and UK Home Office (Project
5 Licence 60/4569) in accordance with the Animals (Scientific Procedures) Act 1986. For the
6
7
8 *Smn*^{2B/-} mice, experimental procedures were authorized and approved by the Keele University
9
10
11 ~~Animal Welfare Ethical Review Body (AWERB)~~ and UK Home Office (Project Licence
12
13
14 P99AB3B95) in accordance with the Animals (Scientific Procedures) Act 1986.
15
16
17
18

19 **Protein extraction and preparation for quantitative proteomic analysis**

20
21 Total protein extracts were prepared as previously described ([27110](#)) from the hearts of P18
22
23 *Smn*^{2B/-} and age-matched WT animals (both n = 3) and isobaric tags for relative and absolute
24
25 quantitation (iTRAQ) quantitative mass spectrometry analysis were added. Briefly, proteins
26
27 were digested with trypsin, then peptides tagged with iTRAQTM reagents as described in the
28
29 iTRAQ kit protocol and sample groups assigned as follows: 116-P18 WT and 117-P18 *Smn*^{2B/-}.
30
31
32

33 **High pH reverse-phase liquid chromatography fractionation and liquid** 34 35 **chromatography–tandem mass spectrometry analysis**

36
37 Fractionation and mass spectrometry analysis were carried out as previously described (15). In
38
39 brief, the iTRAQ-labelled peptides were combined, concentrated, resuspended in buffer A (10
40
41 mm ammonium formate [NH₄HCO₂], 2% acetonitrile [MeCN], pH 10.0) then fractionated
42
43 using high pH reverse-phase liquid chromatography (C18 column). Following rinsing of the
44
45 column with 96% buffer A until the optical density returned to baseline, a gradient was run
46
47 from 4% to 28% of buffer B (10 mm NH₄HCO₂, 90% MeCN, pH 10.0) for 30 min followed
48
49 by another from 28–50% buffer B for 6 min. Buffer B at 80% was used to rinse the column for
50
51 5 min and the column then re-equilibrated with 4% buffer B for 11 min. Fractions (0.5 ml)
52
53 were collected every 30 s and their UV chromatograms analysed. Fractions with similar peptide
54
55
56
57
58
59
60

1
2
3 concentrations were combined resulting in 12 fractions which were vacuum dried then
4
5 resuspended in 30 μ l of 0.1% formic acid.
6
7

8
9
10 For the mass spectrometry analysis, one-third of each fraction was analysed by mass
11 spectrometry. Following separation of the peptides via liquid chromatography, peptides were
12 loaded with buffer A (2% MeCN, 0.05% TFA in ultrapure water) and bound to an Acclaim
13 PepMap100 AQ6 trap (100 μ m \times 2 cm) (Thermo Fisher Scientific) which was then washed for
14 10 min with buffer A. The analytical solvent system consisted of buffer A and buffer B (98%
15 MeCN, 0.1% FA in ultrapure water) at 300 nl/min flow rate. To elute the peptides the following
16 gradient was utilized: linear 2–20% of buffer B over 90 min, linear 20–40% of buffer B for 30
17 min, linear 40–98% of buffer B for 10 min, isocratic 98% of buffer B for 5 min, linear 98–2%
18 of buffer B for 2.5 min and isocratic 2% buffer B for 12.5 min. Eluent was sprayed with a
19 NANOSpray II source (electrospray ionization) into the TripleTOF 5600+ tandem mass
20 spectrometer (AB Sciex) under the control of Analyst® TF software (AB Sciex). The mass
21 spectrometer was operated as previously described (15) and the raw mass spectrometry data
22 files analyzed by ProteinPilot software, version 5.0.1.0 (Applied Biosystems) in addition to the
23 Paragon™ database search and Pro Group™ algorithm using the UniProtKB/Swiss-Prot
24 FASTA database. Paragon search analysis parameters for sample were: type “iTRAQ4plex
25 (Peptide Labeled),” cysteine alkylation “MMTS,” digestion “trypsin,” instrument “TripleTOF”
26 and species “Mouse” with processing parameters described as “quantitative,” “bias correction,”
27 “background correction,” “thorough ID” and “biological modifications.” A protein threshold
28 of >5 was used in the Pro Group algorithm to calculate the relative protein expression with the
29 generation of an error factor and *p*-value, and Proteomics System Performance Evaluation
30 Pipeline used to determine false discovery rate. The mass spectrometry proteomic data can be
31 accessed at the following DOI: 10.6084/m9.figshare.23256374
32
33
34
35
36
37
38
39
40
41
42
43
44
45
46
47
48
49
50
51
52
53
54
55
56
57
58
59
60

Bioinformatics analysis

Data that met the criteria for differential expression in the *Smn*^{2B/-} mice were analysed using Database for Annotation, Visualization and Integrated Discovery (DAVID) Functional Annotation Bioinformatics 2021 (28111,29112) and Ingenuity Pathway Analysis software (IPA; QIAGEN Inc., <https://www.qiagenbioinformatics.com/products/ingenuity-pathway-analysis>) (1139). Proteins were deemed differentially **expressed-abundant** in the *Smn*^{2B/-} mice in comparison to age-matched WT mice after the following filtering criteria were applied and proteins removed if; (i) they were identified from just one peptide, (ii) had expression changes of less than 25% (SMA vs WT) or (iii) had *p*-values of >0.05 assigned to their expression changes. Only terms with at least three annotated proteins and a *p*-value of ≤0.05 were noted for the DAVID analysis.

SMN replacement in *Smn*^{2B/-} mice via viral vector treatment

For SMN replacement, AAV9 vectors were used from two sources, RY (single stranded AAV9_ *eGFP* and AAV9_ *Co-hSMNI*) (3128) and BS (self-complementary scAAV9-*GFP* and scAAV9-*SMNI*) (329) and administered through the facial vein at P0 (5E10 vg/pup-7E10 vg/pup). The vector sourced from RY uses a codon-optimised cDNA transgene which has been developed to enhance levels of the functional SMN protein produced both *in vitro* and *in vivo* (3128) whilst the vector from BS used standard cloning procedures as previously described (33114). Following CO₂ anaesthesia and exsanguination, heart tissues were harvested from the following groups at the symptomatic time-point of P18: untreated WT mice (n=4), untreated *Smn*^{2B/-} mice (n=6), *Smn*^{2B/-} mice treated with the vector plus GFP (RY, n=5; BS, n=4) and *Smn*^{2B/-} mice treated with the vector plus *SMNI* (RY, n=5; BS, n=5).

Protein extraction and western blotting

All extraction steps were carried out on ice and as previously described (34115). Heart tissues were diced then homogenized with pellet pestles in 2× modified RIPA buffer (2% NP-40, 0.5% Deoxycholic acid, 2 mM EDTA, 300 mM NaCl and 100 mM Tris-HCl (pH 7.4)) plus protease inhibitor cocktail at 1:100 (Sigma-Aldrich; P8340), left on ice for 5 min then sonicated briefly at 5 microns for 10 s. This process was repeated an additional two times. The samples were centrifugated at 13,000 RPM (MSE, Heathfield, UK; MSB010.CX2.5 Micro Centaur) for 5 min at 4°C and protein concentration determined via the BCA protein assay (Pierce™, 23227). The concentration of the protein extracts was adjusted to approximately 2mg/ml, and they were heated in 2× SDS sample buffer (4% SDS, 10% 2-mercaptoethanol, 20% glycerol, 0.125 M Tris-HCl (pH 6.8) and bromophenol blue) for 3 min at 95 °C prior to loading onto 4-12% Bis-Tris polyacrylamide gels (Life Technologies, Warrington, UK) for SDS-PAGE (Biorad, Hercules, CA, USA). A horizontal slice of the gel was excised and stained with Coomassie blue as an internal loading control for total protein, if necessary, protein concentrations were further adjusted to ensure even loading of the samples. The proteins in the remaining gel were transferred overnight via western blot onto a nitrocellulose membrane. Following blocking with 4% powdered milk, the membranes were incubated with primary monoclonal antibodies against: mouse anti-SMN (MANSMA12 2E6; 1:100 (35116)); rabbit anti-lamin A/C (Abcam; ab169532; 1:2000); rabbit anti-desmin (Abcam; ab227651; 1:1000) in dilution buffer (1% FBS, 1% horse serum (HS), 0.1% bovine serum albumin (BSA) in PBS with 0.05% Triton X-100) for 2 h at RT or O/N at 4°C. Membranes were then incubated with HRP-labelled rabbit anti-mouse Ig (DAKO, P0260) or goat anti-rabbit Ig (DAKO, P0488) at 0.25 ng/ml in dilution buffer for 1 h followed by either West Pico or West Femto (both ThermoFisher) and bands imaged with the ChemiDoc™ Touch Imaging Gel Image Documentation sSystem (Bio-Rad).

1
2
3 Using ImageJ Fiji software (v1.51) ([36117](#)) densitometry measurements of both antibody
4 reactive bands and Coomassie-stained gel bands were undertaken.
5
6
7

8 9 10 **Immunofluorescence microscopy**

11
12 Following excision, heart tissues [incorporating the left and right ventricles](#) were flash frozen
13 in liquid nitrogen and stored at -80°C then sectioned (7 µm) on a rotary cryostat, collected onto
14 polylysine-coated slides and stored at -20°C. Prior to staining, slides were brought to RT. All
15 subsequent steps were carried out at RT and PBS used for each wash step (3 x 5 min) whilst
16 blocking buffer (1% FBS, 1% HS, 0.1% BSA in PBS) was used for antibody dilution. Sections
17 were washed, then blocked for 30 min prior to being incubated either for 2 h at RT or O/N at
18 4°C with primary antibodies against mouse anti-SMN (MANSMA12 2E6; 1:4 ([35116](#))), rabbit
19 polyclonal anti-lamin A/C (NOVUS; NBP2-19324; 1:100), rabbit monoclonal anti-desmin
20 (Abcam; ab227651; 1:100), rabbit polyclonal anti-elasticin (Fisher Scientific; PA5-99418;
21 1:100) or mouse anti-alpha Actinin 2 (Gene Tex; GTX632361; 1:200). Following washing, 5
22 µg/ml of secondary antibody (Molecular Probes; goat anti-rabbit IgG ALEXA Flour 488;
23 A11034) was applied for 1 h. Sections were washed prior to being stained with 4',6-diamidino-
24 2-phenylindole (DAPI; D9542; 0.4 µg/mL) for 10 min, then washed, mounted and imaged with
25 a Leica TCS SP5 spectral confocal microscope (Leica Microsystems, Milton Keynes, UK).
26
27
28
29
30
31
32
33
34
35
36
37
38
39
40
41
42
43
44
45
46

47 Images generated were analysed via ImageJ. For lamin A, images obtained with the 63x
48 objective with an additional four-fold magnification were utilised, whereas images taken with
49 the 63x objective were used for desmin and elasticin analysis. For the lamin A sections, a
50 minimum of 100 cells were analysed whereas for desmin and elasticin a minimum of 200 cells
51 were analysed per condition. For each analysis the scale function was removed, so only the
52 pixels either staining for DAPI or the protein (lamin A, desmin and elasticin) were counted.
53
54
55
56
57
58
59
60

1
2
3 Using the threshold function ([37118](#)), the highlighted pixels were analysed, and protein
4 staining was corrected for cells present by dividing by the measure obtained for the positively
5 stained DAPI areas. The fold difference between the SMA mouse models and their relevant
6
7
8
9
10
11
12
13
14
15
16
17
18
19
20
21
22
23
24
25
26
27
28
29
30
31
32
33
34
35
36
37
38
39
40
41
42
43
44
45
46
47
48
49
50
51
52
53
54
55
56
57
58
59
60

WTs were then determined.

Histochemical staining of elastin

Heart tissue sections were also stained for elastin with the Miller's Elastic Van Gieson ([EVG](#))
Stain Kit (Atom Scientific Ltd; RRSK11-100) using the protocol provided. All wash steps were
carried out with tap water unless otherwise stated. Briefly, sections were washed then treated
with acidified potassium permanganate (0.5%) for 5 min. Following further washing the
sections were bleached with oxalic acid (1%) for 1 min, washed, then rinsed in 95% alcohol
and submerged in Miller's elastin stain for 3 h at RT. Sections were then rinsed with 95%
alcohol until the slides were clear, washed, and counterstained with filtered Van Gieson stain
for 2 min, then blotted, dehydrated, cleared and mounted.

Statistical analysis

Statistical analyses were carried out using GraphPad Prism version 9.0.0 ([121](#)) for Windows,
GraphPad Software, San Diego, California USA, www.graphpad.com. Data distribution was
assessed with the Shapiro–Wilk test and the unpaired two-tailed t-test and Mann-Whitney U
test applied to parametric and non-parametric data respectively. Western blot densitometry
measurements were assessed using an unpaired, one-tailed or two-tailed t-test with Welch's
correction (2-sample equal variance), depending on the null-hypothesis that was tested in each
case. Venn diagrams were generated via a web-based tool ([38119](#)). Data are presented as mean
± standard deviation with a *p*-value of ≤ 0.05 being considered as significant for all analyses.

Supplementary Material

Supplementary File (Word document containing Figures 1 and 2)

Supplementary Tables (Excel document containing supplementary Tables 1-4)

Data Availability Statement: The mass spectrometry proteomic data can be accessed for reviewing purposes at <https://figshare.com/s/72b949c0934737a15b51>

Following publication, the mass spectrometry proteomic data can be accessed at the following DOI: 10.6084/m9.figshare.23256374

Acknowledgements

The Authors would like to thank Philippe Colin, Aline Aebi, and Jean-Philippe Gaudry from the EPFL Bertarelli Gene Therapy Platform for their expert technical support in vector preparation.

Funding sources

This work was supported by Great Ormond Street Hospital Charity (GOSH) and SPARKS Children's Medical Research Charity (Grant No. V5018 to H.R.F.). M.B. acknowledges general financial support from SMA Angels Charity, SMA UK, Muscular Dystrophy UK, Action Medical Research, Academy of Medical Sciences and Association Française contre les Myopathies for SMA research in her laboratory. H.K.S. and T.H.G. acknowledge support from the Euan MacDonald Centre for Motor Neuron Disease Research and SMA Europe. E.M.C. was partially funded by a scholarship from Royal Holloway University of London. R.J.Y.-M. acknowledges general financial support from SMA UK (formerly The SMA Trust), through the UK SMA Research Consortium, for SMA research in his laboratory.

Conflicts of Interest Statement

1
2
3 THG has served on advisory boards for SMA Europe, LifeArc, Roche and Novartis.
4
5
6
7

8 **References**

- 9
10
11 1. Lefebvre, S., Bürglen, L., Reboullet, S., Clermont, O., Burlet, P., Viollet, L., Benichou,
12 B., Cruaud, C., Millasseau, P., Zeviani, M., *et al.* (1995) Identification and
13 characterization of a Spinal Muscular Atrophy-determining gene. *Cell*, **80**, 155–165.
14
15 *DOI: 10.1016/0092-8674(95)90460-3*
16
17
18
19
20 2. Rochette, C.F., Gilbert, N. and Simard, L.R. (2001) SMN gene duplication and the
21 emergence of the SMN2 gene occurred in distinct hominids: SMN2 is unique to Homo
22 sapiens. *Hum. Genet.*, **108**, 255–266. *DOI: 10.1007/s004390100473*
23
24
25
26
27 3. Lorson, C.L. and Androphy, E.J. (2000) An exonic enhancer is required for inclusion of
28 an essential exon in the SMA-determining gene SMN. *Hum. Mol. Genet.*, **9**, 259–265.
29
30 *DOI: 10.1093/hmg/9.2.259*
31
32
33
34
35 4. Feldkötter, M., Schwarzer, V., Wirth, R., Wienker, T.F. and Wirth, B. (2002)
36 Quantitative analyses of SMN1 and SMN2 based on real-time lightcycler PCR: Fast and
37 highly reliable carrier testing and prediction of severity of spinal muscular atrophy. *Am.*
38
39 *J. Hum. Genet.*, **70**, 358–368. *DOI: 10.1086/338627*
40
41
42
43
44
45 5. Ramdas, S. and Servais, L. (2020) New treatments in spinal muscular atrophy: an
46 overview of currently available data. *Expert Opin. Pharmacother.*, **21**, 307–315. *DOI:*
47
48 *10.1080/14656566.2019.1704732*
49
50
51
52 6. Simone, C., Ramirez, A., Bucchia, M., Rinchetti, P., Rideout, H., Papadimitriou, D., Re,
53 D.B. and Corti, S. (2016) Is Spinal Muscular Atrophy a disease of the motor neurons
54 only: pathogenesis and therapeutic implications? *Cell. Mol. Life Sci.*, **73**, 1003–1020.
55
56
57
58
59 *DOI: 10.1007/s00018-015-2106-9.*
60

- 1
2
3 7. Yeo, C.J.J. and Darras, B.T. (2020) Overturning the Paradigm of Spinal Muscular
4 Atrophy as Just a Motor Neuron Disease. *Pediatr. Neurol.*, **109**, 12–19. DOI:
5
6 *10.1016/j.pediatrneurol.2020.01.003*
7
8
- 9
10 8. Huang, J.-J., Jong, Y.-J., Huang, M.-Y., Chiang, C.-H. and Huang, T.-Y. (1996)
11 Electrocardiographic Findings in Children with Spinal Muscular Atrophy. *Jpn. Heart J.*,
12
13 **37**, 239–242. DOI: *10.1536/ihj.37.239*
14
15
- 16
17 9. Finsterer, J. and Stöllberger, C. (1999) Cardiac Involvement in Werdnig-Hoffmann's
18 Spinal Muscular Atrophy. *Cardiology*, **92**, 178–182. DOI: *10.1159/000006968*
19
20
- 21 10. Bach, J.R. (2007) Medical considerations of long-term survival of Werdnig-Hoffmann
22 disease. *Am. J. Phys. Med. Rehabil.*, **86**, 349–355. DOI:
23 *10.1097/PHM.0b013e31804b1d66*
24
25
- 26 11. Rudnik-Schöneborn, S., Heller, R., Berg, C., Betzler, C., Grimm, T., Eggermann, T.,
27 Eggermann, K., Wirth, R., Wirth, B. and Zerres, K. (2008) Congenital heart disease is a
28 feature of severe infantile spinal muscular atrophy. *J. Med. Genet.*, **45**, 635–638. DOI:
29 *10.1136/jmg.2008.057950*
30
31
- 32 12. Bevan, A.K., Hutchinson, K.R., Foust, K.D., Braun, L., McGovern, V.L., Schmelzer,
33 L., Ward, J.G., Petruska, J.C., Lucchesi, P.A., Burghes, A.H.M., *et al.* (2010) Early heart
34 failure in the SMN Δ 7 model of spinal muscular atrophy and correction by postnatal
35 scAAV9-SMN delivery. *Hum. Mol. Genet.*, **19**, 3895–3905. DOI: *10.1093/hmg/ddq300*
36
37
38
39
- 40 13. Shababi, M., Habibi, J., Ma, L., Glascock, J., Sowers, J.R. and Lorson, C.L. (2012)
41 Partial restoration of cardio-vascular defects in rescued severe model of Spinal Muscular
42 Atrophy. *J. Mol. Cell. Cardiol.*, **52**, 1074–1082. DOI: *10.1016/j.yjmcc.2012.01.005*
43
44
45
46
47
48
49
50
51
52
53
54
55
56
57
58
59
60

- 1
2
3
4
5
6
7
8
9
10
11
12
13
14
15
16
17
18
19
20
21
22
23
24
25
26
27
28
29
30
31
32
33
34
35
36
37
38
39
40
41
42
43
44
45
46
47
48
49
50
51
52
53
54
55
56
57
58
59
60
14. Maxwell, G.K., Szunyogova, E., Shorrock, H.K., Gillingwater, T.H. and Parson, S.H. (2018) Developmental and degenerative cardiac defects in the Taiwanese mouse model of severe spinal muscular atrophy. *J. Anat.*, **232**, 965–978. DOI: [10.1111/joa.12793](https://doi.org/10.1111/joa.12793)
 15. Šoltić, D., Shorrock, H.K., Allardyce, H., Wilson, E.L., Holt, I., Synowsky, S.A., Shirran, S.L., Parson, S.H., Gillingwater, T.H. and Fuller, H.R. (2019) Lamin A/C dysregulation contributes to cardiac pathology in a mouse model of severe spinal muscular atrophy. *Hum. Mol. Genet.*, **28**, 3515–3527. DOI: [10.1093/hmg/ddz195](https://doi.org/10.1093/hmg/ddz195)
 16. Djordjevic, S.A., Milic-Rasic, V., Brankovic, V., Kosac, A., Vukomanovic, G., Topalovic, M., Marinkovic, D., Mladenovic, J., Pavlovic, A.S., Bijelic, M., *et al.* (2021) Cardiac findings in pediatric patients with spinal muscular atrophy types 2 and 3. *Muscle Nerve*, **63**, 75–83. DOI: [10.1002/mus.27088](https://doi.org/10.1002/mus.27088)
 17. Lipnick, S.L., Agniel, D.M., Aggarwal, R., Makhortova, N.R., Finlayson, S.G., Brocato, A., Palmer, N., Darras, B.T., Kohane, I. and Rubin, L.L. (2019) Systemic nature of spinal muscular atrophy revealed by studying insurance claims. *PLoS One*, **14**, e0213680. DOI: [10.1371/journal.pone.0213680](https://doi.org/10.1371/journal.pone.0213680)
 18. Wijngaarde, C.A., Blank, A.C., Stam, M., Wadman, R.I., Van Den Berg, L.H. and Van Der Pol, W.L. (2017) Cardiac pathology in spinal muscular atrophy: a systematic review. *Orphanet J. Rare Dis.*, **12**, 67. DOI: [10.1186/s13023-017-0613-5](https://doi.org/10.1186/s13023-017-0613-5)
 19. Rajendra, T.K., Gonsalvez, G.B., Walker, M.P., Shpargel, K.B., Salz, H.K. and Matera, A.G. (2007) A *Drosophila melanogaster* model of spinal muscular atrophy reveals a function for SMN in striated muscle. *J. Cell Biol.*, **176**, 831–841. DOI: [10.1083/jcb.200610053](https://doi.org/10.1083/jcb.200610053)

- 1
2
3
4
5
6
7
8
9
10
11
12
13
14
15
16
17
18
19
20
21
22
23
24
25
26
27
28
29
30
31
32
33
34
35
36
37
38
39
40
41
42
43
44
45
46
47
48
49
50
51
52
53
54
55
56
57
58
59
60
20. Walker, M.P., Rajendra, T.K., Saieva, L., Fuentes, J.L., Pellizzoni, L. and Matera, A.G. (2008) SMN complex localizes to the sarcomeric Z-disc and is a proteolytic target of calpain. *Hum. Mol. Genet.*, **17**, 3399–3410. DOI: [10.1093/hmg/ddn234](https://doi.org/10.1093/hmg/ddn234)
 21. Deguise, M.O., Boyer, J.G., McFall, E.R., Yazdani, A., De Repentigny, Y. and Kothary, R. (2016) Differential induction of muscle atrophy pathways in two mouse models of spinal muscular atrophy. *Sci. Rep.*, **6**, 28846. DOI: [10.1038/srep28846](https://doi.org/10.1038/srep28846)
 22. Khayrullina, G., Moritz, K.E., Schooley, J.F., Fatima, N., Viollet, C., McCormack, N.M., Smyth, J.T., Doughty, M.L., Dalgard, C.L., Flagg, T.P., *et al.* (2020) SMN-deficiency disrupts SERCA2 expression and intracellular Ca²⁺ signaling in cardiomyocytes from SMA mice and patient-derived iPSCs. *Skelet. Muscle*, **10**, 16. DOI: [10.1186/s13395-020-00232-7](https://doi.org/10.1186/s13395-020-00232-7)
 23. [Mourelatos, Z., Dostie, J., Paushkin, S., Sharma, A., Charroux, B., Abel, L., Rappsilber, J., Mann, M. and Dreyfuss, G. \(2002\) miRNPs: A novel class of ribonucleoproteins containing numerous microRNAs. *Genes Dev.*, **16**, 720–728. DOI: \[10.1101/gad.974702\]\(https://doi.org/10.1101/gad.974702\)](#)
 24. [Ripolone, M., Ronchi, D., Violano, R., Vallejo, D., Fagiolari, G., Barca, E., Lucchini, V., Colombo, I., Villa, L., Berardinelli, A., *et al.* \(2015\) Impaired Muscle Mitochondrial Biogenesis and Myogenesis in Spinal Muscular Atrophy. *JAMA Neurol.*, **72**, 666–675. DOI: \[10.1001/jamaneurol.2015.0178\]\(https://doi.org/10.1001/jamaneurol.2015.0178\)](#)
 25. [Tsikitis, M., Galata, Z., Mavroidis, M., Psarras, S. and Capetanaki, Y. \(2018\) Intermediate filaments in cardiomyopathy. *Biophys. Rev.*, **10**, 1007–1031. DOI: \[10.1007/s12551-018-0443-2\]\(https://doi.org/10.1007/s12551-018-0443-2\)](#)
 26. [Rudnik-Schöneborn, S., Botzenhart, E., Eggermann, T., Senderek, J., Schoser, B.G.H., Schröder, R., Wehnert, M., Wirth, B. and Zerres, K. \(2007\) Mutations of the LMNA](#)

- gene can mimic autosomal dominant proximal spinal muscular atrophy. *Neurogenetics*, **8**, 137–142. DOI: [10.1007/s10048-006-0070-0](https://doi.org/10.1007/s10048-006-0070-0)
27. Iwahara, N., Hisahara, S., Hayashi, T., Kawamata, J. and Shimohama, S. (2015) A novel *lamin A/C* gene mutation causing spinal muscular atrophy phenotype with cardiac involvement: Report of one case. *BMC Neurol.*, **15**, 13. DOI: [10.1186/s12883-015-0269-5](https://doi.org/10.1186/s12883-015-0269-5)
28. Nafchi, N.A.M., Chilcott, E.M., Brown, S., Fuller, H.R., Bowerman, M. and Yáñez-Muñoz, R.J. (2023) Enhanced expression of the human *Survival motor neuron 1* gene from a codon-optimised cDNA transgene *in vitro* and *in vivo*. *Gene Ther.*, Epub ahead of print. PMID: 37322133. DOI: [10.1038/s41434-023-00406-0](https://doi.org/10.1038/s41434-023-00406-0).
29. Deguise, M.-O., Beauvais, A., Schneider B.L. and Kothary, R. (2020) Blood flow to the spleen is altered in a mouse model of Spinal Muscular Atrophy. *J. Neuromuscul. Dis.*, **7**, 315–322. DOI: [10.3233/JND-200493](https://doi.org/10.3233/JND-200493)
30. Harada, T., Swift, J., Irianto, J., Shin, J.-W., Spinler, K.R., Athirasala, A., Diegmiller, R., Dingal, P.C.D.P., Ivanovska, I.L. and Discher, D.E. (2014) Nuclear lamin stiffness is a barrier to 3D migration, but softness can limit survival. *J. Cell Biol.*, **204**, 669–682. DOI: [10.1083/jcb.201308029](https://doi.org/10.1083/jcb.201308029)
31. Swift, J., Ivanovska, I.L., Buxboim, A., Harada, T., Dingal, P.C.D.P., Pinter, J., Pajerowski, J.D., Spinler, K.R., Shin, J.-W., Tewari, M., *et al.* (2013) Nuclear Lamin-A Scales with Tissue Stiffness and Enhances Matrix-Directed Differentiation. *Science*, **341**, 1240104. DOI: [10.1126/science.1240104](https://doi.org/10.1126/science.1240104)
32. Borbély, A., Van Der Velden, J., Papp, Z., Bronzwaer, J.G.F., Edes, I., Stienen, G.J.M. and Paulus, W.J. (2005) Cardiomyocyte stiffness in diastolic heart failure. *Circulation*, **111**, 774–781. DOI: [10.1161/01.CIR.0000155257.33485.6D](https://doi.org/10.1161/01.CIR.0000155257.33485.6D)

- 1
2
3
4
5
6
7
8
9
10
11
12
13
14
15
16
17
18
19
20
21
22
23
24
25
26
27
28
29
30
31
32
33
34
35
36
37
38
39
40
41
42
43
44
45
46
47
48
49
50
51
52
53
54
55
56
57
58
59
60
33. [Røe, Å.T., Aronsen, J.M., Skårdal, K., Hamdani, N., Linke, W.A., Danielsen, H.E., Sejersted, O.M., Sjaastad, I. and Louch, W.E. \(2017\) Increased passive stiffness promotes diastolic dysfunction despite improved Ca²⁺ handling during left ventricular concentric hypertrophy. *Cardiovasc. Res.*, **113**, 1161–1172. DOI: \[10.1093/cvr/cvx087\]\(#\)](#)
34. [Chaytow, H., Huang, Y.-T., Gillingwater, T.H. and Faller, K.M.E. \(2018\) The role of survival motor neuron protein \(SMN\) in protein homeostasis. *Cell. Mol. Life Sci.*, **75**, 3877–3894. DOI: \[10.1007/s00018-018-2849-1\]\(#\)](#)
35. [Bernabò, P., Tebaldi, T., Groen, E.J.N., Lane, F.M., Perenthaler, E., Mattedi, F., Newbery, H.J., Zhou, H., Zuccotti, P., Potrich, V., et al. \(2017\) In Vivo Translatome Profiling in Spinal Muscular Atrophy Reveals a Role for SMN Protein in Ribosome Biology. *Cell Rep*, **21**, 953–965. DOI: \[10.1016/j.celrep.2017.10.010\]\(#\)](#)
36. [Fallini, C., Donlin-Asp, P.G., Rouanet, J.P., Bassell, G.J. and Rossoll, W. \(2016\) Deficiency of the survival of motor neuron protein impairs mRNA localization and local translation in the growth cone of motor neurons. *J. Neurosci.*, **36**, 3811–3820. DOI: \[10.1523/JNEUROSCI.2396-15.2016\]\(#\)](#)
37. [Kye, M.J., Niederst, E.D., Wertz, M.H., Gonçalves, I. do C.G., Akten, B., Dover, K.Z., Peters, M., Riessland, M., Neveu, P., Wirth, B., et al. \(2014\) SMN regulates axonal local translation via miR-183/mTOR pathway. *Hum. Mol. Genet.*, **23**, 6318–6331. DOI: \[10.1093/hmg/ddu350\]\(#\)](#)
38. [van Bergeijk, J., Rydel-Könecke, K., Grothe, C. and Claus, P. \(2007\) The spinal muscular atrophy gene product regulates neurite outgrowth: importance of the C terminus. *FASEB J.*, **21**, 1492–1502. DOI: \[10.1096/fj.06-7136com\]\(#\)](#)

- 1
2
3
4
5
6
7
8
9
10
11
12
13
14
15
16
17
18
19
20
21
22
23
24
25
26
27
28
29
30
31
32
33
34
35
36
37
38
39
40
41
42
43
44
45
46
47
48
49
50
51
52
53
54
55
56
57
58
59
60
39. [Acsadi, G., Lee, I., Li, X., Khaidakov, M., Pecinova, A., Parker, G.C. and Hüttemann, M. \(2009\) Mitochondrial dysfunction in a neural cell model of spinal muscular atrophy. *J. Neurosci. Res.*, **87**, 2748–2756. DOI: \[10.1002/jnr.22106\]\(#\)](#)
40. [Miller, N., Shi, H., Zelikovich, A.S. and Ma, Y.-C. \(2016\) Motor neuron mitochondrial dysfunction in spinal muscular atrophy. *Hum. Mol. Genet.*, **25**, 3395–3406. DOI: \[10.1093/hmg/ddw262\]\(#\)](#)
41. [Thelen, M.P., Wirth, B. and Kye, M.J. \(2020\) Mitochondrial defects in the respiratory complex I contribute to impaired translational initiation via ROS and energy homeostasis in SMA motor neurons. *Acta Neuropathol. Commun.*, **8**, 223. DOI: \[10.1186/s40478-020-01101-6\]\(#\)](#)
42. [Towbin, J.A. and Bowles, N.E. \(2006\) Dilated cardiomyopathy: A tale of cytoskeletal proteins and beyond. *J. Cardiovasc. Electrophysiol.*, **17**, 919–926. DOI: \[10.1111/j.1540-8167.2006.00530.x\]\(#\)](#)
43. [Davies, B.S.J., Fong, L.G., Yang, S.H., Coffinier, C. and Young, S.G. \(2009\) The posttranslational processing of prelamin A and disease. *Annu. Rev. Genomics Hum. Genet.*, **10**, 153–174. DOI: \[10.1146/annurev-genom-082908-150150\]\(#\)](#)
44. [Carmosino, M., Torretta, S., Procino, G., Gerbino, A., Forleo, C., Favale, S. and Svelto, M. \(2014\) Role of nuclear Lamin A/C in cardiomyocyte functions. *Biol. Cell*, **106**, 346–358. DOI: \[10.1111/boc.201400033\]\(#\)](#)
45. [Gruenbaum, Y. and Foisner, R. \(2015\) Lamins: Nuclear intermediate filament proteins with fundamental functions in nuclear mechanics and genome regulation. *Annu. Rev. Biochem.*, **84**, 131–164. DOI: \[10.1146/annurev-biochem-060614-034115\]\(#\)](#)

- 1
2
3
4
5
6
7
8
9
10
11
12
13
14
15
16
17
18
19
20
21
22
23
24
25
26
27
28
29
30
31
32
33
34
35
36
37
38
39
40
41
42
43
44
45
46
47
48
49
50
51
52
53
54
55
56
57
58
59
60
46. [Šoltić, D. and Fuller, H.R. \(2020\) Molecular Crosstalk Between Non-SMN-Related and SMN-Related Spinal Muscular Atrophy. *Neurosci. Insights*, **15**, 2633105520914301. DOI: 10.1177/2633105520914301](#)
47. [Mutsaers, C.A., Lamont, D.J., Hunter, G., Wishart, T.M. and Gillingwater, T.H. \(2013\) Label-free proteomics identifies Calreticulin and GRP75/Mortalin as peripherally accessible protein biomarkers for spinal muscular atrophy. *Genome Med.*, **5**, 95. DOI: 10.1186/gm498](#)
48. [Aghamaleky Sarvestany, A., Hunter, G., Tavendale, A., Lamont, D.J., Llaverro Hurtado, M., Graham, L.C., Wishart, T.M. and Gillingwater, T.H. \(2014\) Label-free quantitative proteomic profiling identifies disruption of ubiquitin homeostasis as a key driver of Schwann cell defects in spinal muscular atrophy. *J. Proteome Res.*, **13**, 4546–4557. DOI: 10.1021/pr500492j](#)
49. [Fuller, H.R., Gillingwater, T.H. and Wishart, T.M. \(2016\) Commonality amid diversity: Multi-study proteomic identification of conserved disease mechanisms in spinal muscular atrophy. *Neuromuscul. Disord.*, **26**, 560–569. DOI: 10.1016/j.nmd.2016.06.004](#)
50. [Captur, G., Arbustini, E., Bonne, G., Syrris, P., Mills, K., Wahbi, K., Mohiddin, S.A., McKenna, W.J., Pettit, S., Ho, C.Y., *et al.* \(2018\) Lamin and the heart. *Heart*, **104**, 468–479. DOI: 10.1136/heartjnl-2017-312338](#)
51. [Fatkin, D., MacRae, C., Sasaki, T., Wolff, M.R., Porcu, M., Frenneaux, M., Atherton, J., Vidaillet, H.J., Spudich, S., de Girolami, U., *et al.* \(1999\) Missense Mutations in the Rod Domain of the Lamin A/C Gene As Causes of Dilated Cardiomyopathy and Conduction-System Disease. *N. Engl. J. Med.*, **341**, 1715–1724. DOI: 10.1056/NEJM199912023412302](#)

- 1
2
3
4
5
6
7
8
9
10
11
12
13
14
15
16
17
18
19
20
21
22
23
24
25
26
27
28
29
30
31
32
33
34
35
36
37
38
39
40
41
42
43
44
45
46
47
48
49
50
51
52
53
54
55
56
57
58
59
60
52. [Van Berlo, J.H., De Voogt, W.G., Van Der Kooi, A.J., Van Tintelen, J.P., Bonne, G., Yaou, R.B., Duboc, D., Rossenbacker, T., Heidebüchel, H., De Visser, M., et al. \(2005\) Meta-analysis of clinical characteristics of 299 carriers of LMNA gene mutations: Do lamin A/C mutations portend a high risk of sudden death? *J. Mol. Med.*, **83**, 79–83. DOI: \[10.1007/s00109-004-0589-1\]\(#\)](#)
53. [van Rijsingen, I.A.W., Nannenbergh, E.A., Arbustini, E., Elliott, P.M., Mogensen, J., Hermans-van Ast, J.F., van der Kooi, A.J., van Tintelen, J.P., van den Berg, M.P., Grasso, M., et al. \(2013\) Gender-specific differences in major cardiac events and mortality in lamin A/C mutation carriers. *Eur. J. Heart Fail.*, **15**, 376–384. DOI: \[10.1093/eurjhf/hfs191\]\(#\)](#)
54. [Cattin, M.E., Muchir, A. and Bonne, G. \(2013\) ‘State-of-the-heart’ of cardiac laminopathies. *Curr. Opin. Cardiol.*, **28**, 297–304. DOI: \[10.1097/HCO.0b013e32835f0c79\]\(#\)](#)
55. [Brayson, D. and Shanahan, C.M. \(2017\) Current insights into LMNA cardiomyopathies: Existing models and missing LINC. *Nucleus*, **8**, 17–33. DOI: \[10.1080/19491034.2016.1260798\]\(#\)](#)
56. [Storey, E.C. and Fuller, H.R. \(2022\) Genotype-Phenotype Correlations in Human Diseases Caused by Mutations of LINC Complex-Associated Genes: A Systematic Review and Meta-Summary. *Cells*, **11**.4065. DOI: \[10.3390/cells11244065\]\(#\)](#)
57. [Battey, E., Stroud, M.J. and Ochala, J. \(2020\) Using nuclear envelope mutations to explore age-related skeletal muscle weakness. *Clin. Sci.*, **134**, 2177–2187. DOI: \[10.1042/CS20190066\]\(#\)](#)
58. [Cho, S., Vashisth, M., Abbas, A., Majkut, S., Vogel, K., Xia, Y., Ivanovska, I.L., Irianto, J., Tewari, M., Zhu, K., et al. \(2019\) Mechanosensing by the lamina protects against](#)

- 1
2
3 nuclear rupture, DNA damage, and cell cycle arrest. *Dev. Cell*, **49**, 920–935. DOI:
4 [10.1016/j.devcel.2019.04.020](https://doi.org/10.1016/j.devcel.2019.04.020)
5
6
7
8
9 59. Buxboim, A., Swift, J., Irianto, J., Spinler, K.R., Dingal, P.C.D.P., Athirasala, A., Kao,
10 Y.-R.C., Cho, S., Harada, T., Shin, J.-W., *et al.* (2014) Matrix elasticity regulates lamin-
11 A,C phosphorylation and turnover with feedback to actomyosin. *Curr. Biol.*, **24**, 1909–
12 1917. DOI: [10.1016/j.cub.2014.07.001](https://doi.org/10.1016/j.cub.2014.07.001)
13
14
15
16
17
18 60. Uzer, G., Rubin, C.T. and Rubin, J. (2016) Cell mechanosensitivity is enabled by the
19 LINC nuclear complex. *Curr. Mol. Biol. Rep.*, **2**, 36–47. DOI: [10.1007/s40610-016-](https://doi.org/10.1007/s40610-016-0032-8)
20 [0032-8](https://doi.org/10.1007/s40610-016-0032-8)
21
22
23
24
25
26 61. Pradhan, R., Ranade, D. and Sengupta, K. (2018) Emerin modulates spatial organization
27 of chromosome territories in cells on softer matrices. *Nucleic Acids Res.*, **46**, 5561–5586.
28 DOI: [10.1093/nar/gky288](https://doi.org/10.1093/nar/gky288)
29
30
31
32
33
34 62. Lammerding, J., Schulze, P.C., Takahashi, T., Kozlov, S., Sullivan, T., Kamm, R.D.,
35 Stewart, C.L. and Lee, R.T. (2004) Lamin A/C deficiency causes defective nuclear
36 mechanics and mechanotransduction. *J. Clin. Invest.*, **113**, 370–378. DOI:
37 [10.1172/JCI200419670](https://doi.org/10.1172/JCI200419670)
38
39
40
41
42
43 63. Lanzicher, T., Martinelli, V., Puzzi, L., Del Favero, G., Codan, B., Long, C.S., Mestroni,
44 L., Taylor, M.R.G. and Sbaizero, O. (2015) The cardiomyopathy lamin A/C D192G
45 mutation disrupts whole-cell biomechanics in cardiomyocytes as measured by atomic
46 force microscopy loading-unloading curve analysis. *Sci. Rep.*, **5**, 13388. DOI:
47 [10.1038/srep13388](https://doi.org/10.1038/srep13388)
48
49
50
51
52
53
54
55 64. Nikolova, V., Leimena, C., McMahon, A.C., Tan, J.C., Chandar, S., Jogia, D., Kesteven,
56 S.H., Michalicek, J., Otway, R., Verheyen, F., *et al.* (2004) Defects in nuclear structure
57
58
59
60

- 1
2
3 and function promote dilated cardiomyopathy in lamin A/C-deficient mice. *J. Clin.*
4
5 *Invest.*, **113**, 357–369. DOI: [10.1172/JCI200419448](https://doi.org/10.1172/JCI200419448)
6
7
8
9 65. Ramos, F.J., Chen, S.C., Garelick, M.G., Dai, D.-F., Liao, C.-Y., Schreiber, K.H.,
10 MacKay, V.L., An, E.H., Strong, R., Ladiges, W.C., *et al.* (2012) Rapamycin reverses
11 elevated mTORC1 signaling in lamin A/C-deficient mice, rescues cardiac and skeletal
12 muscle function, and extends survival. *Sci. Transl. Med.*, **4**, 144ra103. DOI:
13 [10.1126/scitranslmed.3003802](https://doi.org/10.1126/scitranslmed.3003802)
14
15
16
17
18
19
20 66. Cahill, T.J., Ashrafian, H. and Watkins, H. (2013) Genetic cardiomyopathies causing
21 heart failure. *Circ. Res.*, **113**, 660–675. DOI: [10.1161/CIRCRESAHA.113.300282](https://doi.org/10.1161/CIRCRESAHA.113.300282)
22
23
24
25
26 67. Soussi-Yanicostas, N., Ben Hamida, C., Bejaoui, K., Hentati, F., Ben Hamida, M. and
27 Butler-Browne, G.S. (1992) Evolution of muscle specific proteins in Werdnig-
28 Hoffman's disease. *J. Neurol. Sci.*, **109**, 111–120. DOI: [10.1016/0022-510x\(92\)90103-](https://doi.org/10.1016/0022-510x(92)90103-r)
29 *r*
30
31
32
33
34
35
36 68. Capetanaki, Y., Bloch, R.J., Kouloumenta, A., Mavroidis, M. and Psarras, S. (2007)
37 Muscle intermediate filaments and their links to membranes and membranous
38 organelles. *Exp. Cell Res.*, **313**, 2063–2076. DOI: [10.1016/j.yexcr.2007.03.033](https://doi.org/10.1016/j.yexcr.2007.03.033)
39
40
41
42
43
44 69. Heffler, J., Shah, P.P., Robison, P., Phyo, S., Veliz, K., Uchida, K., Bogush, A.,
45 Rhoades, J., Jain, R. and Prosser, B.L. (2020) A Balance Between Intermediate
46 Filaments and Microtubules Maintains Nuclear Architecture in the Cardiomyocyte.
47 *Circ. Res.*, **126**, e10–e26. DOI: [10.1161/CIRCRESAHA.119.315582](https://doi.org/10.1161/CIRCRESAHA.119.315582)
48
49
50
51
52
53 70. Granger, B.L. and Lazarides, E. (1978) The existence of an insoluble Z disc scaffold in
54 chicken skeletal muscle. *Cell*, **15**, 1253–1268. DOI: [10.1016/0092-8674\(78\)90051-x](https://doi.org/10.1016/0092-8674(78)90051-x)
55
56
57
58
59
60

- 1
2
3
4
5
6
7
8
9
10
11
12
13
14
15
16
17
18
19
20
21
22
23
24
25
26
27
28
29
30
31
32
33
34
35
36
37
38
39
40
41
42
43
44
45
46
47
48
49
50
51
52
53
54
55
56
57
58
59
60
71. [Hijikata, T., Murakami, T., Imamura, M., Fujimaki, N. and Ishikawa, H. \(1999\) Plectin is a linker of intermediate filaments to Z-discs in skeletal muscle fibers. *J. Cell Sci.*, **112**, 867–876. DOI: 10.1242/jcs.112.6.867](#)
72. [Maggi, L., Mavroidis, M., Psarras, S., Capetanaki, Y. and Lattanzi, G. \(2021\) Skeletal and cardiac muscle disorders caused by mutations in genes encoding intermediate filament proteins. *Int. J. Mol. Sci.*, **22**, 4256. DOI: 10.3390/ijms22084256](#)
73. [Jaka, O., Casas-Fraile, L., López De Munain, A. and Sáenz, A. \(2015\) Costamere proteins and their involvement in myopathic processes. *Expert Rev. Mol. Med.*, **17**, e12. DOI: 10.1017/erm.2015.9](#)
74. [Bär, H., Strelkov, S. V., Sjöberg, G., Aebi, U. and Herrmann, H. \(2004\) The biology of desmin filaments: How do mutations affect their structure, assembly, and organisation? *J. Struct. Biol.*, **148**, 137–152. DOI: 10.1016/j.jsb.2004.04.003](#)
75. [Milner, D.J., Weitzer, G., Tran, D., Bradley, A. and Capetanaki, Y. \(1996\) Disruption of muscle architecture and myocardial degeneration in mice lacking desmin. *J. Cell Biol.*, **134**, 1255–1270. DOI: 10.1083/jcb.134.5.1255](#)
76. [Li, Z., Mericskay, M., Agbulut, O., Butler-Browne, G., Carlsson, L., Thornell, L.-E., Babinet, C. and Paulin, D. \(1997\) Desmin is essential for the tensile strength and integrity of myofibrils but not for myogenic commitment, differentiation, and fusion of skeletal muscle. *J. Cell Biol.*, **139**, 129–144. DOI: 10.1083/jcb.139.1.129](#)
77. [Lovering, R.M., O'Neill, A., Muriel, J.M., Prosser, B.L., Strong, J. and Bloch, R.J. \(2011\) Physiology, structure, and susceptibility to injury of skeletal muscle in mice lacking keratin 19-based and desmin-based intermediate filaments. *Am. J. Physiol. Cell Physiol.*, **300**, C803–C813. DOI: 10.1152/ajpcell.00394.2010](#)

- 1
2
3
4
5
6
7
8
9
10
11
12
13
14
15
16
17
18
19
20
21
22
23
24
25
26
27
28
29
30
31
32
33
34
35
36
37
38
39
40
41
42
43
44
45
46
47
48
49
50
51
52
53
54
55
56
57
58
59
60
78. Meyer, G.A. and Lieber, R.L. (2012) Skeletal muscle fibrosis develops in response to desmin deletion. *Am. J. Physiol. Cell Physiol.*, **302**, C1609–C1620. DOI: [10.1152/ajpcell.00441.2011](https://doi.org/10.1152/ajpcell.00441.2011)
79. Carlsson, L. and Thornell, L.-E. (2001) Desmin-related myopathies in mice and man. *Acta Physiol. Scand.*, **171**, 341–348. DOI: [10.1046/j.1365-201X.2001.00837.x](https://doi.org/10.1046/j.1365-201X.2001.00837.x)
80. Anderson, J., Li, Z. and Goubel, F. (2001) Passive stiffness is increased in soleus muscle of desmin knockout mouse. *Muscle Nerve*, **24**, 1090–1092. DOI: [10.1002/mus.1115](https://doi.org/10.1002/mus.1115)
81. Münch, J. and Abdelilah-Seyfried, S. (2021) Sensing and Responding of Cardiomyocytes to Changes of Tissue Stiffness in the Diseased Heart. *Front. Cell Dev. Biol.*, **9**, 642840. DOI: [10.3389/fcell.2021.642840](https://doi.org/10.3389/fcell.2021.642840)
82. Parker, K.K. and Ingber, D.E. (2007) Extracellular matrix, mechanotransduction and structural hierarchies in heart tissue engineering. *Phil. Trans. R. Soc. B*, **362**, 1267–1279. DOI: [10.1098/rstb.2007.2114](https://doi.org/10.1098/rstb.2007.2114)
83. Farquharson, C. and Robins, S.P. (1989) The distribution of elastin in developing and adult rat organs using immunocytochemical techniques. *J. Anat.*, **165**, 225–36.
84. Montero, P., Flandes-Iparraguirre, M., Musquiz, S., Pérez Araluce, M., Plano, D., Sanmartín, C., Orive, G., Gavira, J.J., Prosper, F. and Mazo, M.M. (2020) Cells, Materials, and Fabrication Processes for Cardiac Tissue Engineering. *Front. Bioeng. Biotechnol.*, **8**, 955. DOI: [10.3389/fbioe.2020.00955](https://doi.org/10.3389/fbioe.2020.00955)
85. Li, S.-H., Sun, Z., Guo, L., Han, M., Wood, M.F.G., Ghosh, N., Vitkin, I.A., Weisel, R.D. and Li, R.-K. (2012) Elastin overexpression by cell-based gene therapy preserves matrix and prevents cardiac dilation. *J. Cell Mol. Med.*, **16**, 2429–2439. DOI: [10.1111/j.1582-4934.2012.01560.x](https://doi.org/10.1111/j.1582-4934.2012.01560.x)

- 1
2
3
4
5
6
7
8
9
10
11
12
13
14
15
16
17
18
19
20
21
22
23
24
25
26
27
28
29
30
31
32
33
34
35
36
37
38
39
40
41
42
43
44
45
46
47
48
49
50
51
52
53
54
55
56
57
58
59
60
86. [Cocciolone, A.J., Hawes, J.Z., Staiculescu, M.C., Johnson, E.O., Murshed, M. and Wagenseil, J.E. \(2018\) Elastin, arterial mechanics, and cardiovascular disease. *Am. J. Physiol. Heart Circ. Physiol.*, **315**, H189–H205. DOI: \[10.1152/ajpheart.00087.2018\]\(#\)](#)
87. [Engler, A.J., Carag-Krieger, C., Johnson, C.P., Raab, M., Tang, H.-Y., Speicher, D.W., Sanger, J.W., Sanger, J.M. and Discher, D.E. \(2008\) Embryonic cardiomyocytes beat best on a matrix with heart-like elasticity: scar-like rigidity inhibits beating. *J. Cell Sci.*, **121**, 3794–3802. DOI: \[10.1242/jcs.029678\]\(#\)](#)
88. [Sato, S., Ashraf, M., Millard, R.W., Fujiwara, H. and Schwartz, A. \(1983\) Connective tissue changes in early ischemia of porcine myocardium: An ultrastructural study. *J. Mol. Cell Cardiol.*, **15**, 261–275. DOI: \[10.1016/0022-2828\\(83\\)90281-x\]\(#\)](#)
89. [Sugayama, S.M.M., Moisés, R.L., Wagénfur, J., Ikari, N.M., Abe, K.T., Leone, C., Da Silva, C.A.A., Ferrari Chauffaille, M.de L.L. and Kim, C.A. \(2003\) Williams-Beuren syndrome. Cardiovascular abnormalities in 20 patients diagnosed with fluorescence in situ hybridization. *Arq. Bras. Cardiol.*, **81**, 468–473. DOI: \[10.1590/S0066-782X2003001300003\]\(#\)](#)
90. [Hou, C., Zheng, J., Liu, W., Xie, L., Sun, X., Zhang, Y., Xu, M., Li, Y. and Xiao, T. \(2021\) Identification and characterization of a novel ELN mutation in congenital heart disease with pulmonary artery stenosis. *Sci. Rep.*, **11**, 14154. DOI: \[10.1038/s41598-021-93736-1\]\(#\)](#)
91. [Shi, X., Zhang, S., Liu, Y., Brazile, B., Cooley, J., Butler, J.R., McMahan, S.R., Perez, K.L., Xu, J., Eastep, T., et al. \(2023\) Spatial distribution and network morphology of epicardial, endocardial, interstitial, and Purkinje cell-associated elastin fibers in porcine left ventricle. *Bioact. Mater.*, **19**, 348–359. DOI: \[10.1016/j.bioactmat.2022.04.019\]\(#\)](#)

- 1
2
3
4
5
6
7
8
9
10
11
12
13
14
15
16
17
18
19
20
21
22
23
24
25
26
27
28
29
30
31
32
33
34
35
36
37
38
39
40
41
42
43
44
45
46
47
48
49
50
51
52
53
54
55
56
57
58
59
60
92. [Fomovsky, G.M., Thomopoulos, S. and Holmes, J.W. \(2010\) Contribution of extracellular matrix to the mechanical properties of the heart. *J. Mol. Cell Cardiol.*, **48**, 490–496. DOI: \[10.1016/j.yjmcc.2009.08.003\]\(#\)](#)
93. [Boyden, P.A., Dun, W. and Robinson, R.B. \(2016\) Cardiac Purkinje fibers and Arrhythmias; The GK Moe Award Lecture 2015. *Heart Rhythm*, **13**, 1172–1181. DOI: \[10.1016/j.hrthm.2016.01.011\]\(#\)](#)
94. [Tanaka, H., Nishi, S., Nuruki, K. and Tanaka, N. \(1977\) Myocardial ultrastructural changes in Kugelberg-Welander syndrome. *Br. Heart J.*, **39**, 1390–1393. DOI: \[10.1136/hrt.39.12.1390\]\(#\)](#)
95. [Dawood, A.F., Alzamil, N.M., Hewett, P.W., Momenah, M.A., Dallak, M., Kamar, S.S., Abdel Kader, D.H., Yassin, H., Haidara, M.A., Maarouf, A., *et al.* \(2022\) Metformin Protects against Diabetic Cardiomyopathy: An Association between Desmin–Sarcomere Injury and the iNOS/mTOR/TIMP-1 Fibrosis Axis. *Biomedicines*, **10**, 984. DOI: \[10.3390/biomedicines10050984\]\(#\)](#)
96. [Palmisano, M.G., Bremner, S.N., Hornberger, T.A., Meyer, G.A., Domenighetti, A.A., Shah, S.B., Kiss, B., Kellermayer, M., Ryan, A.F. and Lieber, R.L. \(2015\) Skeletal muscle intermediate filaments form a stress-transmitting and stress-signaling network. *J. Cell Sci.*, **128**, 219–224. DOI: \[10.1242/jcs.142463\]\(#\)](#)
97. [Berciano, M.T., Castillo-Iglesias, M.S., Val-Bernal, J.F., Lafarga, V., Rodriguez-Rey, J.C., Lafarga, M. and Tapia, O. \(2020\) Mislocalization of SMN from the I-band and M-band in human skeletal myofibers in spinal muscular atrophy associates with primary structural alterations of the sarcomere. *Cell Tissue Res.*, **381**, 461–478. DOI: \[10.1007/s00441-020-03236-3\]\(#\)](#)

- 1
2
3
4
5
6
7
8
9
10
11
12
13
14
15
16
17
18
19
20
21
22
23
24
25
26
27
28
29
30
31
32
33
34
35
36
37
38
39
40
41
42
43
44
45
46
47
48
49
50
51
52
53
54
55
56
57
58
59
60
98. [Liu, H.-X., Jing, Y.-X., Wang, J.-J., Yang, Y.-P., Wang, Y.-X., Li, H.-R., Song, L., Li, A.-H., Cui, H.-L. and Jing, Y. \(2020\) Expression patterns of intermediate filament proteins desmin and lamin A in the developing conduction system of early human embryonic hearts. *J. Anat.*, **236**, 540–548. DOI: \[10.1111/joa.13108\]\(#\)](#)
99. [Brodsky, G.L., Muntoni, F., Miocic, S., Sinagra, G., Sewry, C.A. and Mestroni, L. \(2000\) Lamin A/C gene mutation associated with dilated cardiomyopathy with variable skeletal muscle involvement. *Circulation*, **101**, 473–476. DOI: \[10.1161/01.cir.101.5.473\]\(#\)](#)
100. [Lindgren, M., Robertson, J., Adiels, M., Schaufelberger, M., Åberg, M., Torén, K., Waern, M., Åberg, N.D. and Rosengren, A. \(2020\) Elevated resting heart rate in adolescent men and risk of heart failure and cardiomyopathy. *ESC Heart Fail.*, **7**, 1178–1185. DOI: \[10.1002/ehf2.12726\]\(#\)](#)
101. [Heier, C.R., Satta, R., Lutz, C. and Didonato, C.J. \(2010\) Arrhythmia and cardiac defects are a feature of spinal muscular atrophy model mice. *Hum. Mol. Genet.*, **19**, 3906–3918. DOI: \[10.1093/hmg/ddq330\]\(#\)](#)
102. [Afilalo, J., Sebag, I.A., Chalifour, L.E., Rivas, D., Akter, R., Sharma, K. and Duque, G. \(2007\) Age-related changes in lamin A/C expression in cardiomyocytes. *Am. J. Physiol. Heart Circ. Physiol.*, **293**, H1451-H1456. DOI: \[10.1152/ajpheart.01194.2006\]\(#\)](#)
103. [Lieber, S.C., Qiu, H., Chen, L., Shen, Y.-T., Hong, C., Hunter, W.C., Aubry, N., Vatner, S.F. and Vatner, D.E. \(2008\) Cardiac dysfunction in aging conscious rats: altered cardiac cytoskeletal proteins as a potential mechanism. *Am. J. Physiol. Heart Circ. Physiol.*, **295**, H860-H866. DOI: \[10.1152/ajpheart.00146.2008\]\(#\)](#)
104. [Sarbacher, C.A. and Halper, J.T. \(2019\) Connective tissue and age-related diseases. *Subcell. Biochem.*, **91**, 281-310. DOI: \[10.1007/978-981-13-3681-2_11\]\(#\)](#)

- 1
2
3
4
5
6
7
8
9
10
11
12
13
14
15
16
17
18
19
20
21
22
23
24
25
26
27
28
29
30
31
32
33
34
35
36
37
38
39
40
41
42
43
44
45
46
47
48
49
50
51
52
53
54
55
56
57
58
59
60
- [105. Russ, D.W. and Grandy, J.S. \(2011\) Increased desmin expression in hindlimb muscles of aging rats. *J. Cachexia Sarcopenia Muscle*, **2**, 175-180. DOI: \[10.1007/s13539-011-0033-7\]\(#\)](#)
- [23106. Bowerman, M., Murray, L.M., Beauvais, A., Pinheiro, B. and Kothary, R. \(2012\) A critical smn threshold in mice dictates onset of an intermediate spinal muscular atrophy phenotype associated with a distinct neuromuscular junction pathology. *Neuromuscul. Disord.*, **22**, 263–276. DOI: \[10.1016/j.nmd.2011.09.007\]\(#\)](#)
- [24107. DiDonato, C.J., Lorson, C.L., De Repentigny, Y., Simard, L., Chartrand, C., Androphy, E.J. and Kothary, R. \(2001\) Regulation of murine survival motor neuron \(Smn\) protein levels by modifying Smn exon 7 splicing. *Hum. Mol. Genet.*, **10**, 2727–2736. DOI: \[10.1093/hmg/10.23.2727\]\(#\)](#)
- [25108. Hammond, S.M., Gogliotti, R.G., Rao, V., Beauvais, A., Kothary, R. and DiDonato, C.J. \(2010\) Mouse survival motor neuron alleles that mimic SMN2 splicing and are inducible rescue embryonic lethality early in development but not late. *PLoS One*, **5**, e15887. DOI: \[10.1371/journal.pone.0015887\]\(#\)](#)
- [26109. Hsieh-Li, H.M., Chang, J.-G., Jong, Y.-J., Wu, M.-H., Wang, N.M., Tsai, C.H. and Li, H. \(2000\) A mouse model for spinal muscular atrophy. *Nat. Genet.*, **24**, 66–70. DOI: \[10.1038/71709\]\(#\)](#)
- [27110. Fuller, H.R., Hurtado, M.L., Wishart, T.M. and Gates, M.A. \(2014\) The rat striatum responds to nigro-striatal degeneration via the increased expression of proteins associated with growth and regeneration of neuronal circuitry. *Proteome Sci.*, **12**, 20. DOI: \[10.1186/1477-5956-12-20\]\(#\)](#)

- 1
2
3 **28111**. Huang, D.W., Sherman, B.T. and Lempicki, R.A. (2009) Systematic and integrative
4 analysis of large gene lists using DAVID bioinformatics resources. *Nat. Protoc.*, **4**, 44–
5
6 57. DOI: [10.1038/nprot.2008.211](https://doi.org/10.1038/nprot.2008.211)
7
8
9
10 **29112**. Huang, D.W., Sherman, B.T. and Lempicki, R.A. (2009) Bioinformatics enrichment
11 tools: Paths toward the comprehensive functional analysis of large gene lists. *Nucleic*
12 *Acids Res.*, **37**, 1–13. DOI: [10.1093/nar/gkn923](https://doi.org/10.1093/nar/gkn923)
13
14
15
16
17
18 **1130**. Krämer, A., Green, J., Pollard, J. and Tugendreich, S. (2014) Causal analysis approaches
19 in Ingenuity Pathway Analysis. *Bioinformatics*, **30**, 523–530. DOI:
20 [10.1093/bioinformatics/btt703](https://doi.org/10.1093/bioinformatics/btt703)
21
22
23
24
25
26 ~~31. Nafehi, N.A.M., Chilcott, E.M., Brown, S., Fuller, H.R., Bowerman, M. and Yáñez-~~
27 ~~Muñoz, R.J. (2023) Enhanced expression of the human *Survival motor neuron 1* gene~~
28 ~~from a codon-optimised cDNA transgene *in vitro* and *in vivo*. *Gene Ther.*, **In press**.~~
29
30
31
32
33
34 ~~32. Deguise, M.-O., Beauvais, A., Schneider B.L. and Kothary, R. (2020) Blood flow to the~~
35 ~~spleen is altered in a mouse model of Spinal Muscular Atrophy. *J. Neuromuscul. Dis.*,~~
36 ~~**7**, 315–322. DOI: [10.3233/JND-200493](https://doi.org/10.3233/JND-200493)~~
37
38
39
40
41 **33114**. Blessing, D., Vachey, G., Pythoud, C., Rey, M., Padrun, V., Wurm, F.M., Schneider,
42 B.L. and Déglon, N. (2018) Scalable Production of AAV9 Vectors in Orbitally Shaken
43 HEK293 Cells. *Mol. Ther. Methods Clin. Dev.*, **13**, 14–26. DOI:
44 [10.1016/j.omtm.2018.11.004](https://doi.org/10.1016/j.omtm.2018.11.004)
45
46
47
48
49
50
51 **34115**. Šoltić, D., Bowerman, M., Stock, J., Shorrock, H.K., Gillingwater, T.H. and Fuller,
52 H.R. (2018) Multi-Study Proteomic and Bioinformatic Identification of Molecular
53 Overlap between Amyotrophic Lateral Sclerosis (ALS) and Spinal Muscular Atrophy
54 (SMA). *Brain Sci.*, **8**, 212. DOI: [10.3390/brainsci8120212](https://doi.org/10.3390/brainsci8120212)
55
56
57
58
59
60

- 1
2
3 **35116.** Young, P.J., Le, T.T., Thi Man, N., Burghes, A.H.M. and Morris, G.E. (2000) The
4 relationship between SMN, the spinal muscular atrophy protein, and nuclear coiled
5 bodies in differentiated tissues and cultured cells. *Exp. Cell Res.*, **256**, 365–374. DOI:
6 [10.1006/excr.2000.4858](https://doi.org/10.1006/excr.2000.4858)
7
8
9
10
11
12
13 **36117.** Abràmoff, M.D., Magalhães, P.J. and Ram, S.J. (2004) Image processing with imageJ.
14 *Biophotonics Intern.ational*, **11**, 36–41. DOI: [10.1201/9781420005615.ax4](https://doi.org/10.1201/9781420005615.ax4)
15
16
17
18
19 **37118.** Jensen, E.C. (2013) Quantitative Analysis of Histological Staining and Fluorescence
20 Using ImageJ. *Anat. Rec.*, **296**, 378–381. DOI: [10.1002/ar.22641](https://doi.org/10.1002/ar.22641)
21
22
23
24 **38119.** Heberle, H., Meirelles, G.V., da Silva, F.R., Telles, G.P. and Minghim, R. (2015)
25 InteractiVenn: A web-based tool for the analysis of sets through Venn diagrams. *BMC*
26 *Bioinformatics*, **16**, 169. DOI: [10.1186/s12859-015-0611-3](https://doi.org/10.1186/s12859-015-0611-3)
27
28
29
30
31 ~~39. Mourelatos, Z., Dostie, J., Paushkin, S., Sharma, A., Charroux, B., Abel, L., Rappsilber,~~
32 ~~J., Mann, M. and Dreyfuss, G. (2002) miRNPs: A novel class of ribonucleoproteins~~
33 ~~containing numerous microRNAs. *Genes Dev.*, **16**, 720–728. DOI: [10.1101/gad.974702](https://doi.org/10.1101/gad.974702)~~
34
35
36
37
38
39 ~~409. Ripolone, M., Ronchi, D., Violano, R., Vallejo, D., Fagiolari, G., Barca, E., Lucchini,~~
40 ~~V., Colombo, I., Villa, L., Berardinelli, A., et al. (2015) Impaired Muscle Mitochondrial~~
41 ~~Biogenesis and Myogenesis in Spinal Muscular Atrophy. *JAMA Neurol.*, **72**, 666–675.~~
42 ~~DOI: [10.1001/jamaneurol.2015.0178](https://doi.org/10.1001/jamaneurol.2015.0178)~~
43
44
45
46
47
48
49 ~~41. Tsikitis, M., Galata, Z., Mavroidis, M., Psarras, S. and Capetanaki, Y. (2018)~~
50 ~~Intermediate filaments in cardiomyopathy. *Biophys. Rev.*, **10**, 1007–1031. DOI:~~
51 ~~[10.1007/s12551-018-0443-2](https://doi.org/10.1007/s12551-018-0443-2)~~
52
53
54
55
56 ~~42. Rudnik-Schöneborn, S., Botzenhart, E., Eggermann, T., Senderek, J., Schoser, B.G.H.,~~
57 ~~Schröder, R., Wehnert, M., Wirth, B. and Zerres, K. (2007) Mutations of the LMNA~~
58
59
60

- gene can mimic autosomal dominant proximal spinal muscular atrophy. *Neurogenetics*, **8**, 137–142. DOI: 10.1007/s10048-006-0070-0
43. Iwahara, N., Hisahara, S., Hayashi, T., Kawamata, J. and Shimohama, S. (2015) A novel *lamin A/C* gene mutation causing spinal muscular atrophy phenotype with cardiac involvement: Report of one case. *BMC Neurol.*, **15**, 13. DOI: 10.1186/s12883-015-0269-5
44. Harada, T., Swift, J., Irianto, J., Shin, J.-W., Spinler, K.R., Athirasala, A., Diegmiller, R., Dingal, P.C.D.P., Ivanovska, I.L. and Discher, D.E. (2014) Nuclear lamin stiffness is a barrier to 3D migration, but softness can limit survival. *J. Cell Biol.*, **204**, 669–682. DOI: 10.1083/jcb.201308029
45. Swift, J., Ivanovska, I.L., Buxboim, A., Harada, T., Dingal, P.C.D.P., Pinter, J., Pajerowski, J.D., Spinler, K.R., Shin, J.-W., Tewari, M., *et al.* (2013) Nuclear Lamin-A Scales with Tissue Stiffness and Enhances Matrix Directed Differentiation. *Science*, **341**, 1240104. DOI: 10.1126/science.1240104
46. Borbély, A., Van Der Velden, J., Papp, Z., Bronzwaer, J.G.F., Edes, I., Stienen, G.J.M. and Paulus, W.J. (2005) Cardiomyocyte stiffness in diastolic heart failure. *Circulation*, **111**, 774–781. DOI: 10.1161/01.CIR.0000155257.33485.6D
47. Røe, Å.T., Aronsen, J.M., Skårdal, K., Hamdani, N., Linke, W.A., Danielsen, H.E., Sejersted, O.M., Sjaastad, I. and Louch, W.E. (2017) Increased passive stiffness promotes diastolic dysfunction despite improved Ca²⁺ handling during left ventricular concentric hypertrophy. *Cardiovasc. Res.*, **113**, 1161–1172. DOI: 10.1093/evr/evx087
48. Chaytow, H., Huang, Y.-T., Gillingwater, T.H. and Faller, K.M.E. (2018) The role of survival motor neuron protein (SMN) in protein homeostasis. *Cell. Mol. Life Sci.*, **75**, 3877–3894. DOI: 10.1007/s00018-018-2849-1

- 1
2
3
4
5
6
7
8
9
10
11
12
13
14
15
16
17
18
19
20
21
22
23
24
25
26
27
28
29
30
31
32
33
34
35
36
37
38
39
40
41
42
43
44
45
46
47
48
49
50
51
52
53
54
55
56
57
58
59
60
49. Bernabò, P., Tebaldi, T., Groen, E.J.N., Lane, F.M., Perenthaler, E., Mattedi, F., Newbery, H.J., Zhou, H., Zuccotti, P., Potrich, V., *et al.* (2017) In Vivo Translatome Profiling in Spinal Muscular Atrophy Reveals a Role for SMN Protein in Ribosome Biology. *Cell Rep*, **21**, 953–965. DOI: [10.1016/j.celrep.2017.10.010](https://doi.org/10.1016/j.celrep.2017.10.010)
50. Fallini, C., Donlin-Asp, P.G., Rouanet, J.P., Bassell, G.J. and Rossoll, W. (2016) Deficiency of the survival of motor neuron protein impairs mRNA localization and local translation in the growth cone of motor neurons. *J. Neurosci.*, **36**, 3811–3820. DOI: [10.1523/JNEUROSCI.2396-15.2016](https://doi.org/10.1523/JNEUROSCI.2396-15.2016)
51. Kye, M.J., Niederst, E.D., Wertz, M.H., Gonçalves, I. do C.G., Akten, B., Dover, K.Z., Peters, M., Riessland, M., Neveu, P., Wirth, B., *et al.* (2014) SMN regulates axonal local translation via miR-183/mTOR pathway. *Hum. Mol. Genet.*, **23**, 6318–6331. DOI: [10.1093/hmg/ddu350](https://doi.org/10.1093/hmg/ddu350)
52. van Bergeijk, J., Rydel-Könecke, K., Grothe, C. and Claus, P. (2007) The spinal muscular atrophy gene product regulates neurite outgrowth: importance of the C terminus. *FASEB J.*, **21**, 1492–1502. DOI: [10.1096/fj.06-7136com](https://doi.org/10.1096/fj.06-7136com)
53. Acsadi, G., Lee, I., Li, X., Khaidakov, M., Pecinova, A., Parker, G.C. and Hüttemann, M. (2009) Mitochondrial dysfunction in a neural cell model of spinal muscular atrophy. *J. Neurosci. Res.*, **87**, 2748–2756. DOI: [10.1002/jnr.22106](https://doi.org/10.1002/jnr.22106)
54. Miller, N., Shi, H., Zelikovich, A.S. and Ma, Y.-C. (2016) Motor neuron mitochondrial dysfunction in spinal muscular atrophy. *Hum. Mol. Genet.*, **25**, 3395–3406. DOI: [10.1093/hmg/ddw262](https://doi.org/10.1093/hmg/ddw262)
55. Thelen, M.P., Wirth, B. and Kye, M.J. (2020) Mitochondrial defects in the respiratory complex I contribute to impaired translational initiation via ROS and energy

- 1
2
3 homeostasis in SMA motor neurons. *Acta Neuropathol. Commun.*, **8**, 223. DOI:
4 10.1186/s40478-020-01101-6
5
6
7
8
9 56.—Towbin, J.A. and Bowles, N.E. (2006) Dilated cardiomyopathy: A tale of cytoskeletal
10 proteins and beyond. *J. Cardiovasc. Electrophysiol.*, **17**, 919–926. DOI: 10.1111/j.1540-
11 8167.2006.00530.x
12
13
14
15
16 57.—Davies, B.S.J., Fong, L.G., Yang, S.H., Coffinier, C. and Young, S.G. (2009) The
17 posttranslational processing of prelamin A and disease. *Annu. Rev. Genomics Hum.*
18 *Genet.*, **10**, 153–174. DOI: 10.1146/annurev-genom-082908-150150
19
20
21
22
23
24 58.—Carmosino, M., Torretta, S., Procino, G., Gerbino, A., Forleo, C., Favale, S. and Svelto,
25 M. (2014) Role of nuclear Lamin A/C in cardiomyocyte functions. *Biol. Cell*, **106**, 346–
26 358. DOI: 10.1111/boc.201400033
27
28
29
30
31 59.—Gruenbaum, Y. and Foisner, R. (2015) Lamins: Nuclear intermediate filament proteins
32 with fundamental functions in nuclear mechanics and genome regulation. *Annu. Rev.*
33 *Biochem.*, **84**, 131–164. DOI: 10.1146/annurev-biochem-060614-034115
34
35
36
37
38
39 60.—Šoltić, D. and Fuller, H.R. (2020) Molecular Crosstalk Between Non-SMN-Related and
40 SMN-Related Spinal Muscular Atrophy. *Neurosci. Insights*, **15**, 2633105520914301.
41 DOI: 10.1177/2633105520914301
42
43
44
45
46 61.—Mutsaers, C.A., Lamont, D.J., Hunter, G., Wishart, T.M. and Gillingwater, T.H. (2013)
47 Label-free proteomics identifies Calreticulin and GRP75/Mortalin as peripherally
48 accessible protein biomarkers for spinal muscular atrophy. *Genome Med.*, **5**, 95. DOI:
49 10.1186/gm498
50
51
52
53
54
55
56 62.—Aghamaleky Sarvestany, A., Hunter, G., Tavendale, A., Lamont, D.J., Llaverro-Hurtado,
57 M., Graham, L.C., Wishart, T.M. and Gillingwater, T.H. (2014) Label-free quantitative
58
59
60

- 1
2
3 proteomic profiling identifies disruption of ubiquitin homeostasis as a key driver of
4 Schwann cell defects in spinal muscular atrophy. *J. Proteome Res.*, **13**, 4546–4557.
5
6 DOI: [10.1021/pr500492j](https://doi.org/10.1021/pr500492j)
7
8
9
10
11 63. Fuller, H.R., Gillingwater, T.H. and Wishart, T.M. (2016) Commonality amid diversity:
12 Multi-study proteomic identification of conserved disease mechanisms in spinal
13 muscular atrophy. *Neuromuscul. Disord.*, **26**, 560–569. DOI:
14 [10.1016/j.nmd.2016.06.004](https://doi.org/10.1016/j.nmd.2016.06.004)
15
16
17
18
19
20
21 64. Captur, G., Arbustini, E., Bonne, G., Syrris, P., Mills, K., Wahbi, K., Mohiddin, S.A.,
22 McKenna, W.J., Pettit, S., Ho, C.Y., *et al.* (2018) Lamin and the heart. *Heart*, **104**, 468–
23 479. DOI: [10.1136/heartjnl-2017-312338](https://doi.org/10.1136/heartjnl-2017-312338)
24
25
26
27
28
29 65. Fatkin, D., MacRae, C., Sasaki, T., Wolff, M.R., Porcu, M., Frenneaux, M., Atherton,
30 J., Vidaillet, H.J., Spudich, S., de Girolami, U., *et al.* (1999) Missense Mutations in the
31 Rod Domain of the Lamin A/C Gene As Causes of Dilated Cardiomyopathy and
32 Conduction System Disease. *N. Engl. J. Med.*, **341**, 1715–1724. DOI:
33 [10.1056/NEJM199912023412302](https://doi.org/10.1056/NEJM199912023412302)
34
35
36
37
38
39
40
41 66. Van Berlo, J.H., De Voogt, W.G., Van Der Kooi, A.J., Van Tintelen, J.P., Bonne, G.,
42 Yaou, R.B., Duboc, D., Rossenbacker, T., Heidbüchel, H., De Visser, M., *et al.* (2005)
43 Meta-analysis of clinical characteristics of 299 carriers of LMNA gene mutations: Do
44 lamin A/C mutations portend a high risk of sudden death? *J. Mol. Med.*, **83**, 79–83. DOI:
45 [10.1007/s00109-004-0589-1](https://doi.org/10.1007/s00109-004-0589-1)
46
47
48
49
50
51
52
53 67. van Rijsingen, I.A.W., Nannenbergh, E.A., Arbustini, E., Elliott, P.M., Mogensen, J.,
54 Hermans van Ast, J.F., van der Kooi, A.J., van Tintelen, J.P., van den Berg, M.P.,
55 Grasso, M., *et al.* (2013) Gender-specific differences in major cardiac events and
56
57
58
59
60

- 1
2
3 mortality in lamin A/C mutation carriers. *Eur. J. Heart Fail.*, **15**, 376–384. DOI:
4 [10.1093/eurjhf/hfs191](https://doi.org/10.1093/eurjhf/hfs191)
5
6
7
8
9 68. Cattin, M.E., Muchir, A. and Bonne, G. (2013) ‘State of the heart’ of cardiac
10 laminopathies. *Curr. Opin. Cardiol.*, **28**, 297–304. DOI:
11 [10.1097/HCO.0b013e32835f0e79](https://doi.org/10.1097/HCO.0b013e32835f0e79)
12
13
14
15
16 69. Brayson, D. and Shanahan, C.M. (2017) Current insights into LMNA cardiomyopathies:
17 Existing models and missing LINC. *Nucleus*, **8**, 17–33. DOI:
18 [10.1080/19491034.2016.1260798](https://doi.org/10.1080/19491034.2016.1260798)
19
20
21
22
23
24 70. Storey, E.C. and Fuller, H.R. (2022) Genotype-Phenotype Correlations in Human
25 Diseases Caused by Mutations of LINC Complex Associated Genes: A Systematic
26 Review and Meta-Summary. *Cells*, **11**, 4065. DOI: [10.3390/cells11244065](https://doi.org/10.3390/cells11244065)
27
28
29
30
31
32 71. Battey, E., Stroud, M.J. and Ochala, J. (2020) Using nuclear envelope mutations to
33 explore age-related skeletal muscle weakness. *Clin. Sci.*, **134**, 2177–2187. DOI:
34 [10.1042/CS20190066](https://doi.org/10.1042/CS20190066)
35
36
37
38
39 72. Cho, S., Vashisth, M., Abbas, A., Majkut, S., Vogel, K., Xia, Y., Ivanovska, I.L., Irianto,
40 J., Tewari, M., Zhu, K., *et al.* (2019) Mechanosensing by the lamina protects against
41 nuclear rupture, DNA damage, and cell cycle arrest. *Dev. Cell*, **49**, 920–935. DOI:
42 [10.1016/j.devcel.2019.04.020](https://doi.org/10.1016/j.devcel.2019.04.020)
43
44
45
46
47
48
49 73. Buxboim, A., Swift, J., Irianto, J., Spinler, K.R., Dingal, P.C.D.P., Athirasala, A., Kao,
50 Y.-R.C., Cho, S., Harada, T., Shin, J.-W., *et al.* (2014) Matrix elasticity regulates lamin-
51 A,C phosphorylation and turnover with feedback to actomyosin. *Curr. Biol.*, **24**, 1909–
52 1917. DOI: [10.1016/j.cub.2014.07.001](https://doi.org/10.1016/j.cub.2014.07.001)
53
54
55
56
57
58
59
60

- 1
2
3
4
5
6
7
8
9
10
11
12
13
14
15
16
17
18
19
20
21
22
23
24
25
26
27
28
29
30
31
32
33
34
35
36
37
38
39
40
41
42
43
44
45
46
47
48
49
50
51
52
53
54
55
56
57
58
59
60
74. Uzer, G., Rubin, C.T. and Rubin, J. (2016) Cell mechanosensitivity is enabled by the LINC nuclear complex. *Curr. Mol. Biol. Rep.*, **2**, 36–47. DOI: 10.1007/s40610-016-0032-8
75. Pradhan, R., Ranade, D. and Sengupta, K. (2018) Emerin modulates spatial organization of chromosome territories in cells on softer matrices. *Nucleic Acids Res.*, **46**, 5561–5586. DOI: 10.1093/nar/gky288
76. Lammerding, J., Schulze, P.C., Takahashi, T., Kozlov, S., Sullivan, T., Kamm, R.D., Stewart, C.L. and Lee, R.T. (2004) Lamin A/C deficiency causes defective nuclear mechanics and mechanotransduction. *J. Clin. Invest.*, **113**, 370–378. DOI: 10.1172/JCI200419670
77. Lanzicher, T., Martinelli, V., Puzzi, L., Del Favero, G., Codan, B., Long, C.S., Mestroni, L., Taylor, M.R.G. and Sbaizero, O. (2015) The cardiomyopathy lamin A/C D192G mutation disrupts whole-cell biomechanics in cardiomyocytes as measured by atomic force microscopy loading-unloading curve analysis. *Sci. Rep.*, **5**, 13388. DOI: 10.1038/srep13388
78. Nikolova, V., Leimena, C., McMahon, A.C., Tan, J.C., Chandar, S., Jogia, D., Kesteven, S.H., Michaliecek, J., Otway, R., Verheyen, F., *et al.* (2004) Defects in nuclear structure and function promote dilated cardiomyopathy in lamin A/C-deficient mice. *J. Clin. Invest.*, **113**, 357–369. DOI: 10.1172/JCI200419448
79. Ramos, F.J., Chen, S.C., Garelick, M.G., Dai, D.F., Liao, C.Y., Schreiber, K.H., MacKay, V.L., An, E.H., Strong, R., Ladiges, W.C., *et al.* (2012) Rapamycin reverses elevated mTORC1 signaling in lamin A/C-deficient mice, rescues cardiac and skeletal muscle function, and extends survival. *Sci. Transl. Med.*, **4**, 144ra103. DOI: 10.1126/scitranslmed.3003802

- 1
2
3
4
5
6
7
8
9
10
11
12
13
14
15
16
17
18
19
20
21
22
23
24
25
26
27
28
29
30
31
32
33
34
35
36
37
38
39
40
41
42
43
44
45
46
47
48
49
50
51
52
53
54
55
56
57
58
59
60
809. ~~Cahill, T.J., Ashrafian, H. and Watkins, H. (2013) Genetic cardiomyopathies causing heart failure. *Circ. Res.*, **113**, 660–675. DOI: 10.1161/CIRCRESAHA.113.300282~~
81. ~~Soussi-Yanicostas, N., Ben Hamida, C., Bejaoui, K., Hentati, F., Ben Hamida, M. and Butler-Browne, G.S. (1992) Evolution of muscle specific proteins in Werdnig-Hoffman's disease. *J. Neurol. Sci.*, **109**, 111–120. DOI: 10.1016/0022-510x(92)90103-#~~
82. ~~Capetanaki, Y., Bloch, R.J., Kouloumenta, A., Mavroidis, M. and Psarras, S. (2007) Muscle intermediate filaments and their links to membranes and membranous organelles. *Exp. Cell Res.*, **313**, 2063–2076. DOI: 10.1016/j.yexer.2007.03.033~~
83. ~~Heffler, J., Shah, P.P., Robison, P., Phyto, S., Veliz, K., Uchida, K., Bogush, A., Rhoades, J., Jain, R. and Prosser, B.L. (2020) A Balance Between Intermediate Filaments and Microtubules Maintains Nuclear Architecture in the Cardiomyocyte. *Circ. Res.*, **126**, e10–e26. DOI: 10.1161/CIRCRESAHA.119.315582~~
84. ~~Granger, B.L. and Lazarides, E. (1978) The existence of an insoluble Z-disc scaffold in chicken skeletal muscle. *Cell*, **15**, 1253–1268. DOI: 10.1016/0092-8674(78)90051-x~~
85. ~~Hijikata, T., Murakami, T., Imamura, M., Fujimaki, N. and Ishikawa, H. (1999) Plectin is a linker of intermediate filaments to Z-discs in skeletal muscle fibers. *J. Cell Sci.*, **112**, 867–876. DOI: 10.1242/jcs.112.6.867~~
86. ~~Maggi, L., Mavroidis, M., Psarras, S., Capetanaki, Y. and Lattanzi, G. (2021) Skeletal and cardiac muscle disorders caused by mutations in genes encoding intermediate filament proteins. *Int. J. Mol. Sci.*, **22**, 4256. DOI: 10.3390/ijms22084256~~

- 1
2
3 87. Jaka, O., Casas-Fraile, L., López-De Munain, A. and Sáenz, A. (2015) Costamere
4 proteins and their involvement in myopathic processes. *Expert Rev. Mol. Med.*, **17**, e12.
5
6 *DOI: 10.1017/erm.2015.9*
7
8
9
10 88. Bär, H., Strelkov, S. V., Sjöberg, G., Aebi, U. and Herrmann, H. (2004) The biology of
11 desmin filaments: How do mutations affect their structure, assembly, and organisation?
12
13 *J. Struct. Biol.*, **148**, 137–152. *DOI: 10.1016/j.jsb.2004.04.003*
14
15
16
17
18 89. Milner, D.J., Weitzer, G., Tran, D., Bradley, A. and Capetanaki, Y. (1996) Disruption
19 of muscle architecture and myocardial degeneration in mice lacking desmin. *J. Cell*
20 *Biol.*, **134**, 1255–1270. *DOI: 10.1083/jcb.134.5.1255*
21
22
23
24
25
26 90. Li, Z., Merieskay, M., Agbulut, O., Butler-Browne, G., Carlsson, L., Thornell, L. E.,
27 Babinet, C. and Paulin, D. (1997) Desmin is essential for the tensile strength and
28 integrity of myofibrils but not for myogenic commitment, differentiation, and fusion of
29 skeletal muscle. *J. Cell Biol.*, **139**, 129–144. *DOI: 10.1083/jcb.139.1.129*
30
31
32
33
34
35
36 91. Lovering, R.M., O'Neill, A., Muriel, J.M., Prosser, B.L., Strong, J. and Bloch, R.J.
37 (2011) Physiology, structure, and susceptibility to injury of skeletal muscle in mice
38 lacking keratin 19-based and desmin-based intermediate filaments. *Am. J. Physiol. Cell*
39 *Physiol.*, **300**, C803–C813. *DOI: 10.1152/ajpcell.00394.2010*
40
41
42
43
44
45
46 92. Meyer, G.A. and Lieber, R.L. (2012) Skeletal muscle fibrosis develops in response to
47 desmin deletion. *Am. J. Physiol. Cell Physiol.*, **302**, C1609–C1620. *DOI:*
48 *10.1152/ajpcell.00441.2011*
49
50
51
52
53 93. Carlsson, L. and Thornell, L. E. (2001) Desmin-related myopathies in mice and man.
54 *Acta Physiol. Scand.*, **171**, 341–348. *DOI: 10.1046/j.1365-201X.2001.00837.x*
55
56
57
58
59
60

- 1
2
3 94. Anderson, J., Li, Z. and Goubel, F. (2001) Passive stiffness is increased in soleus muscle
4 of desmin knockout mouse. *Muscle Nerve*, **24**, 1090–1092. DOI: 10.1002/mus.1115
5
6
7
8
9 95. Münch, J. and Abdelilah-Seyfried, S. (2021) Sensing and Responding of
10 Cardiomyocytes to Changes of Tissue Stiffness in the Diseased Heart. *Front. Cell Dev.*
11 *Biol.*, **9**, 642840. DOI: 10.3389/fcell.2021.642840
12
13
14
15
16 96. Parker, K.K. and Ingber, D.E. (2007) Extracellular matrix, mechanotransduction and
17 structural hierarchies in heart tissue engineering. *Phil. Trans. R. Soc. B*, **362**, 1267–1279.
18 DOI: 10.1098/rstb.2007.2114
19
20
21
22
23 97. Farquharson, C. and Robins, S.P. (1989) The distribution of elastin in developing and
24 adult rat organs using immunocytochemical techniques. *J. Anat.*, **165**, 225–36.
25
26
27
28
29 98. Montero, P., Flandes-Iparraguirre, M., Musquiz, S., Pérez Araluce, M., Plano, D.,
30 Sanmartín, C., Orive, G., Gavira, J.J., Prosper, F. and Mazo, M.M. (2020) Cells,
31 Materials, and Fabrication Processes for Cardiac Tissue Engineering. *Front. Bioeng.*
32 *Biotechnol.*, **8**, 955. DOI: 10.3389/fbioe.2020.00955
33
34
35
36
37
38
39 99. Li, S. H., Sun, Z., Guo, L., Han, M., Wood, M.F.G., Ghosh, N., Vitkin, I.A., Weisel,
40 R.D. and Li, R. K. (2012) Elastin overexpression by cell-based gene therapy preserves
41 matrix and prevents cardiac dilation. *J. Cell Mol. Med.*, **16**, 2429–2439. DOI:
42 10.1111/j.1582-4934.2012.01560.x
43
44
45
46
47
48
49 100. Cocciolone, A.J., Hawes, J.Z., Staiculescu, M.C., Johnson, E.O., Murshed, M. and
50 Wagenseil, J.E. (2018) Elastin, arterial mechanics, and cardiovascular disease. *Am. J.*
51 *Physiol. Heart Circ. Physiol.*, **315**, H189–H205. DOI: 10.1152/ajpheart.00087.2018
52
53
54
55
56 101. Engler, A.J., Carag-Krieger, C., Johnson, C.P., Raab, M., Tang, H. Y., Speicher, D.W.,
57 Sanger, J.W., Sanger, J.M. and Discher, D.E. (2008) Embryonic cardiomyocytes beat
58
59
60

- 1
2
3 best on a matrix with heart-like elasticity: scar-like rigidity inhibits beating. *J. Cell Sci.*,
4
5 **121**, 3794–3802. DOI: 10.1242/jcs.029678
6
7
8
9 102. Sato, S., Ashraf, M., Millard, R.W., Fujiwara, H. and Schwartz, A. (1983) Connective
10
11 tissue changes in early ischemia of porcine myocardium: An ultrastructural study. *J.*
12
13 *Mol. Cell Cardiol.*, **15**, 261–275. DOI: 10.1016/0022-2828(83)90281-x
14
15
16 103. Sugayama, S.M.M., Moisés, R.L., Wagênfur, J., Ikari, N.M., Abe, K.T., Leone, C., Da
17
18 Silva, C.A.A., Ferrari-Chauffaille, M.de L.L. and Kim, C.A. (2003) Williams-Beuren
19
20 syndrome. Cardiovascular abnormalities in 20 patients diagnosed with fluorescence in
21
22 situ hybridization. *Arq. Bras. Cardiol.*, **81**, 468–473. DOI: 10.1590/S0066-
23
24 782X2003001300003
25
26
27
28 104. Hou, C., Zheng, J., Liu, W., Xie, L., Sun, X., Zhang, Y., Xu, M., Li, Y. and Xiao, T.
29
30 (2021) Identification and characterization of a novel ELN mutation in congenital heart
31
32 disease with pulmonary artery stenosis. *Sci. Rep.*, **11**, 14154. DOI: 10.1038/s41598-021-
33
34 93736-1
35
36
37
38 105. Shi, X., Zhang, S., Liu, Y., Brazile, B., Cooley, J., Butler, J.R., McMahan, S.R., Perez,
39
40 K.L., Xu, J., Eastep, T., *et al.* (2023) Spatial distribution and network morphology of
41
42 epicardial, endocardial, interstitial, and Purkinje cell-associated elastin fibers in porcine
43
44 left ventricle. *Bioact. Mater.*, **19**, 348–359. DOI: 10.1016/j.bioactmat.2022.04.019
45
46
47
48 106. Fomovsky, G.M., Thomopoulos, S. and Holmes, J.W. (2010) Contribution of
49
50 extracellular matrix to the mechanical properties of the heart. *J. Mol. Cell Cardiol.*, **48**,
51
52 490–496. DOI: 10.1016/j.yjmcc.2009.08.003
53
54
55
56 107. Boyden, P.A., Dun, W. and Robinson, R.B. (2016) Cardiac Purkinje fibers and
57
58 Arrhythmias; The GK Moe Award Lecture 2015. *Heart Rhythm*, **13**, 1172–1181. DOI:
59
60 10.1016/j.hrthm.2016.01.011

- 1
2
3
4
5
6
7
8
9
10
11
12
13
14
15
16
17
18
19
20
21
22
23
24
25
26
27
28
29
30
31
32
33
34
35
36
37
38
39
40
41
42
43
44
45
46
47
48
49
50
51
52
53
54
55
56
57
58
59
60
108. Tanaka, H., Nishi, S., Nuruki, K. and Tanaka, N. (1977) Myocardial ultrastructural changes in Kugelberg-Welander syndrome. *Br. Heart J.*, **39**, 1390–1393. DOI: [10.1136/hrt.39.12.1390](https://doi.org/10.1136/hrt.39.12.1390)
109. Dawood, A.F., Alzamil, N.M., Hewett, P.W., Momenah, M.A., Dallak, M., Kamar, S.S., Abdel Kader, D.H., Yassin, H., Haidara, M.A., Maarouf, A., *et al.* (2022) Metformin Protects against Diabetic Cardiomyopathy: An Association between Desmin–Sarcomere Injury and the iNOS/mTOR/TIMP-1 Fibrosis Axis. *Biomedicines*, **10**, 984. DOI: [10.3390/biomedicines10050984](https://doi.org/10.3390/biomedicines10050984)
110. Palmisano, M.G., Bremner, S.N., Hornberger, T.A., Meyer, G.A., Domenighetti, A.A., Shah, S.B., Kiss, B., Kellermayer, M., Ryan, A.F. and Lieber, R.L. (2015) Skeletal muscle intermediate filaments form a stress-transmitting and stress-signaling network. *J. Cell Sci.*, **128**, 219–224. DOI: [10.1242/jcs.142463](https://doi.org/10.1242/jcs.142463)
111. Berciano, M.T., Castillo-Iglesias, M.S., Val-Bernal, J.F., Lafarga, V., Rodriguez-Rey, J.C., Lafarga, M. and Tapia, O. (2020) Mislocalization of SMN from the I-band and M-band in human skeletal myofibers in spinal muscular atrophy associates with primary structural alterations of the sarcomere. *Cell Tissue Res.*, **381**, 461–478. DOI: [10.1007/s00441-020-03236-3](https://doi.org/10.1007/s00441-020-03236-3)
112. Liu, H.-X., Jing, Y.-X., Wang, J.-J., Yang, Y.-P., Wang, Y.-X., Li, H.-R., Song, L., Li, A.-H., Cui, H.-L. and Jing, Y. (2020) Expression patterns of intermediate filament proteins desmin and lamin A in the developing conduction system of early human embryonic hearts. *J. Anat.*, **236**, 540–548. DOI: [10.1111/joa.13108](https://doi.org/10.1111/joa.13108)
113. Brodsky, G.L., Muntoni, F., Mioic, S., Sinagra, G., Sewry, C.A. and Mestroni, L. (2000) Lamin A/C gene mutation associated with dilated cardiomyopathy with variable

skeletal muscle involvement. *Circulation*, **101**, 473–476. DOI: 10.1161/01.cir.101.5.473

114. Lindgren, M., Robertson, J., Adiels, M., Schaufelberger, M., Åberg, M., Torén, K., Waern, M., Åberg, N.D. and Rosengren, A. (2020) Elevated resting heart rate in adolescent men and risk of heart failure and cardiomyopathy. *ESC Heart Fail.*, **7**, 1178–1185. DOI: 10.1002/ehf2.12726

115. Heier, C.R., Satta, R., Lutz, C. and Didonato, C.J. (2010) Arrhythmia and cardiac defects are a feature of spinal muscular atrophy model mice. *Hum. Mol. Genet.*, **19**, 3906–3918. DOI: 10.1093/hmg/ddq330

Figures & Legends to Figures

Figure 1. Summary and bioinformatics analysis of the proteomic profiles of heart tissues differentially expressed-abundant in the *Smn*^{2B/-} and Taiwanese mice models of SMA compared to age-matched WT mice. (A) Venn diagram showing an overlap of 50 proteins identified as significantly up- or down-regulated in both *Smn*^{2B/-} and Taiwanese mouse models of SMA (an unused ProtScore (conf) > 0.05, detected by ≥2 unique peptides, and a statistically significant (p≤0.05) fold change of ≥1.25 or ≤0.8). (B) Heat map illustrating the size of fold-change in proteins found to be dysregulated in both mice models of SMA. Two-way comparisons generated in IPA® in which the following were ranked by -log(p-value) for each SMA mouse model: (C) Disease & disorders, physiological system development & function; (D) Molecular & cellular functions and (E) Canonical pathways. (F) Schematic illustrating the cellular components impacted by the significantly dysregulated proteins of the *Smn*^{2B/-} mouse model of SMA as determined following DAVID analysis. Image created with BioRender.com.

1
2
3 **Figure 2. Levels and distribution of SMN in heart tissues from *Smn*^{2B/-} mice following**
4 **AAV9-mediated *SMNI* delivery at P0. (A)** Representative western blots of SMN levels in
5 heart tissues from untreated *Smn*^{2B/-} mice, *Smn*^{2B/-} mice following AAV9-mediated treatment
6 with and without *SMNI* from two sources plus a corresponding age-matched WT mouse (P18).
7 The bar graph represents average SMN levels expressed relative to the corresponding WT
8 mouse. **(B)** Representative [immunofluorescent images \(IMFs\)](#) for SMN staining within heart
9 tissues from untreated *Smn*^{2B/-} mice and *Smn*^{2B/-} mice following treatment with AAV9-mediated
10 *SMNI* from two sources. ****p*<0.001. Scale bars represent 75 μm.

11
12
13
14
15
16
17
18
19
20
21
22
23
24 **Figure 3. Levels and distribution of lamin A/C in heart tissues from *Smn*^{2B/-} mice**
25 **following AAV9-mediated *SMNI* delivery at P0. (A)** Representative western blots of lamin
26 A/C levels in heart tissues from WT mice (P18), untreated *Smn*^{2B/-} mice and *Smn*^{2B/-} mice
27 following AAV9-mediated treatment with *SMNI* from two sources. The bar graph represents
28 average lamin A/C levels expressed relative to WT mice. **(B)** Representative western blots of
29 lamin A/C levels in heart tissues from untreated *Smn*^{2B/-} mice and *Smn*^{2B/-} mice following
30 AAV9-mediated treatment without *SMNI* (vehicle control) from two different vector sources.
31 The bar graph represents average lamin A/C levels expressed relative to untreated *Smn*^{2B/-} mice.
32 **(C)** Representative IMFs for lamin A/C staining within heart tissues from WT mice (P18),
33 untreated *Smn*^{2B/-} mice and *Smn*^{2B/-} mice following AAV9-mediated treatment with *SMNI* from
34 two vector sources. Corresponding bar graph reflects the area of cells stained for lamin A/C
35 corrected for number of cells present (DAPI stain) as determined by ImageJ analysis and
36 expressed relative to corresponding WT mice. Dashed line represents the average lamin A/C
37 levels in WT mice and error bars represent the standard deviation from the mean. **(D)** Images
38 demonstrating dual staining of sarcomeres with alpha-actinin 2 (red) and lamin A/C (green) in
39
40
41
42
43
44
45
46
47
48
49
50
51
52
53
54
55
56
57
58
59
60

1
2
3 WT mice. * $p < 0.05$; ** $p < 0.01$. Scale bars represent 25 μm except the lower panel of (D) where
4 they represent 5 μm . Δ represents a combined sample not included in the analysis.
5
6
7
8
9

10 **Figure 4. Levels and distribution of desmin in heart tissues from *Smn*^{2B/-} mice following**
11 **AAV9-mediated *SMNI* delivery at P0. (A)** Representative western blots of desmin levels in
12 heart tissues from WT mice (P18), untreated *Smn*^{2B/-} mice and *Smn*^{2B/-} mice following AAV9-
13 mediated treatment with *SMNI* from two sources. The bar graph represents average desmin
14 levels expressed relative to WT mice. **(B)** Representative western blots of desmin levels in
15 heart tissues from untreated *Smn*^{2B/-} mice and *Smn*^{2B/-} mice following AAV9-mediated
16 treatment without *SMNI* (vehicle control) from two different vector sources. The bar graph
17 represents average desmin levels expressed relative to untreated *Smn*^{2B/-} mice. **(C)**
18 Representative IMFs for desmin staining within heart tissues from WT mice (P18), untreated
19 *Smn*^{2B/-} mice and *Smn*^{2B/-} mice following AAV9-mediated treatment with *SMNI* from two
20 vector sources. Zoomed images to highlight the reduction in desmin positive striations in
21 untreated *Smn*^{2B/-} mice in comparison to WT mice and AAV9-mediated *SMNI* treated *Smn*^{2B/-}
22 mice. Corresponding bar graph reflects the area of cells stained for desmin corrected for
23 number of cells present (DAPI stain) as determined by ImageJ analysis and expressed relative
24 to corresponding WT mice. Dashed line represents the average desmin levels in WT mice and
25 error bars represent the standard deviation from the mean. * $p < 0.05$; ** $p < 0.01$; *** $p < 0.001$.
26 Scale bars represent 75 μm (panels a-d), 25 μm (panels e-g) and 10 μm (panel h).
27
28
29
30
31
32
33
34
35
36
37
38
39
40
41
42
43
44
45
46
47
48
49
50

51 **Figure 5. Levels and distribution of elastin in heart tissues from *Smn*^{2B/-} mice following**
52 **AAV9-mediated *SMNI* delivery at P0. (Panels a-d)** Representative heart sections stained
53 with Miller's Elastin van Gieson from WT mice (P18), untreated *Smn*^{2B/-} mice and *Smn*^{2B/-} mice
54 following AAV9-mediated treatment with *SMNI* from two different vector sources. Elastic
55
56
57
58
59
60

1
2
3 fibres (blue/black); mature collagen (red); other tissues such as muscle and red blood cells
4 (yellow). **(Panels e-l)** Representative IMFs for elastin staining within heart tissues from WT
5 mice (P18), untreated *Smn*^{2B/-} mice and *Smn*^{2B/-} mice following AAV9-mediated treatment with
6 *SMN1* from two vector sources. Corresponding bar graph reflects the area of cells stained for
7 elastin corrected for number of cells present (DAPI stain) as determined by ImageJ analysis
8 and expressed relative to corresponding WT mice. Dashed line represents the average elastin
9 levels in WT mice and error bars represent the standard deviation from the mean. ****p*<0.001.
10 Black scale bars represent 10 μm (panels a-d). White scale bars represent 75 μm (panels e-h)
11 and 10 μm (panels i-l).

Abbreviations

26 AWERB Animal Welfare Ethical Review Body

27 DAVID Database for Annotation, Visualization and Integrated Discovery

28 ECM Extracellular matrix

29 Gems Gemini of the coiled bodies

30 IMF Immunofluorescent image

31 IPA Ingenuity Pathway Analysis

32 iPSCs Induced pluripotent stem cells

33 iTRAQ Isobaric tags for relative and absolute quantitation

34 P Post-natal day

35 SMA Spinal muscular atrophy

36 SMN Survival motor neuron

37 WT Wild type

1
2
3 **AAV9-mediated *SMN* gene therapy rescues cardiac desmin but**
4
5
6 **not lamin A/C and elastin dysregulation in *Smn*^{2B/-} spinal**
7
8
9 **muscular atrophy mice**
10
11
12
13

14 Sharon J. Brown^{1,2}, Darija Šoltić^{1,2}, Silvia A. Synowsky³, Sally L. Shirran³, Ellie Chilcott⁴,
15 Hannah K. Shorrocks⁵, Thomas H. Gillingwater⁵, Rafael J. Yáñez-Muñoz⁴, Bernard
16 Schneider^{6,7}, Melissa Bowerman^{2,8} and Heidi R. Fuller^{1,2*}
17
18
19
20
21
22

23 ¹School of Pharmacy and Bioengineering, Keele University, ST5 5BG, UK; ²Wolfson Centre
24 for Inherited Neuromuscular Disease, TORCH Building, RJA Orthopaedic Hospital,
25 Oswestry SY10 7AG, UK; ³BSRC Mass Spectrometry and Proteomics Facility, University of
26 St Andrews, St Andrews KY16 9ST, UK; ⁴AGCTlab.org, Centre of Gene and Cell Therapy,
27 Centre for Biomedical Sciences, Department of Biological Sciences, School of Life Sciences
28 and the Environment, Royal Holloway University of London, Egham Hill, Egham, Surrey
29 TW20 0EX, UK; ⁵Edinburgh Medical School: Biomedical Sciences, University of Edinburgh,
30 UK; Euan MacDonald Centre for Motor Neurone Disease Research, University of Edinburgh,
31 Edinburgh EH8 9XD, UK; ⁶Bertarelli Platform for Gene Therapy, Ecole Polytechnique
32 Fédérale de Lausanne (EPFL), Geneva, Switzerland; ⁷Brain Mind Institute, Ecole
33 Polytechnique Fédérale de Lausanne (EPFL), 1015 Lausanne, Switzerland; ⁸School of
34 Medicine, Keele University, ST5 5BG, UK.
35
36
37
38
39
40
41
42
43
44
45
46
47
48
49

50
51 *Corresponding author email: h.r.fuller@keele.ac.uk
52

53 Postal Address: Wolfson Centre for Inherited Neuromuscular Disease, TORCH Building,
54 RJA Orthopaedic Hospital, Oswestry SY10 7AG, UK
55
56

57 Telephone: +44(0)1782734546
58
59
60

Abstract

Structural, functional and molecular cardiac defects have been reported in spinal muscular atrophy (SMA) patients and mouse models. Previous quantitative proteomics analyses demonstrated widespread molecular defects in the severe Taiwanese SMA mouse model. Whether such changes are conserved across different mouse models, including less severe forms of the disease, has yet to be established. Here, using the same high-resolution proteomics approach in the less-severe *Smn*^{2B/-} SMA mouse model, 277 proteins were found to be differentially abundant at a symptomatic timepoint (post-natal day (P) 18), 50 of which were similarly dysregulated in severe Taiwanese SMA mice. Bioinformatics analysis linked many of the differentially abundant proteins to cardiovascular development and function, with intermediate filaments highlighted as an enriched cellular compartment in both datasets. Lamin A/C was increased in cardiac tissue whilst another intermediate filament protein, desmin, was reduced. The extracellular matrix (ECM) protein, elastin, was also robustly decreased in the heart of *Smn*^{2B/-} mice. AAV9-*SMN1*-mediated gene therapy rectified low levels of survival motor neuron (SMN) protein and restored desmin levels in heart tissues of *Smn*^{2B/-} mice. In contrast AAV9-*SMN1* therapy failed to correct lamin A/C or elastin levels. Intermediate filament proteins and the ECM have key roles in cardiac function and their dysregulation may explain cardiac impairment in SMA, especially since mutations in genes encoding these proteins cause other diseases with cardiac aberration. Cardiac pathology may need to be considered in the long-term care of SMA patients, as it is unclear whether currently available treatments can fully rescue peripheral pathology in SMA.

Introduction

Spinal muscular atrophy (SMA) arises from insufficient levels of survival motor neuron (SMN) protein due to a homozygous mutation/deletion in the *SMN1* gene (1). Although humans possess the *SMN2* gene (2), this generates only a limited amount of functional SMN (~10%) with the majority (~90%) being an unstable, truncated form of the protein (3). SMA patients present with a range of clinical phenotypes with varying severity, which generally, but not always, have an inverse relationship with *SMN2* copy number (4). Recent advances in SMA treatments aim to increase the levels of full-length SMN by either upregulating the *SMN2* gene or by delivering the *SMN1* gene directly to the cells via a viral vector (5). Neither treatment option is fully effective and evidence is emerging of new patient phenotypes with long-term treatment outcomes remaining unknown (5).

Although SMA is typically considered a motor neuron disease, the ubiquitous nature of SMN production has prompted research into the effects of reduced levels of SMN in peripheral tissues and organs, in both patients and animal models of SMA. Evidence demonstrating that SMA is a multisystem disease has been accruing (6,7) and impairment of cardiac function in mouse models of SMA and in SMA patients described (8–15). Examples of cardiac dysfunction include observations of bradycardia, dilated cardiomyopathy, and decreased contractility in *SMN Δ 7* mice (12), and electrocardiogram abnormalities and thickened myocardium in patients with milder forms of SMA (9,16); whilst a retrospective study of patients with SMA Type I identified ~24% of patients with severe symptomatic bradycardia (10). Congenital heart defects, such as septal defects, in severe Type I patients (11) and in the severe Taiwanese SMA mouse model (14) have also been noted. A study in which the incidence of health insurance claims in Type I to III patients pre-SMA diagnosis were compared to control patients found valve disorders, cardiomyopathies, septal defects and premature beats to be increased (17).

1
2
3 Furthermore, a systematic review of more than 70 studies in which 264 SMA patients were
4 identified with cardiac pathology found a tendency for structural abnormalities to occur in the
5
6 more severe form of SMA (Type I) whilst in patients with less severe SMA, cardiac rhythm
7
8 disturbances were more common (18).
9
10

11
12
13 SMN protein is found in both the cytoplasm and nucleus of cells, and typically associated with
14
15 structures called Gemini of the coiled bodies (Gems) in the nucleus. There is also evidence that
16
17 SMN localises to structural components such as the sarcomere in striated muscle fibres (19)
18
19 and the Z-disc in mice cardiac myofibrils (20), but its function in cardiac muscle remains
20
21 unknown. Most studies have focussed on the more severe form of SMA, including our previous
22
23 quantitative proteomics study in which we demonstrated widespread molecular defects in heart
24
25 tissue from the severe Taiwanese SMA mouse model compared to healthy controls (15). In
26
27 particular, a robust increase in the intermediate filament protein, lamin A/C, was observed,
28
29 which we hypothesised may contribute to the impairment of cardiac function by causing
30
31 nuclear stiffness in the cardiomyocytes.
32
33
34
35
36
37
38
39

40 A recent study that focussed on the FoxO family of transcription factors in heart tissues from
41
42 the less-severe *Smn*^{2B/-} SMA mouse model, found no significant pathology related to these
43
44 factors or their downstream targets of proteosomal and autophagosomal degradation (21), but
45
46 the full extent of molecular consequences and their implications remain unknown for this less-
47
48 severe SMA mouse model. A recent transcriptome study of cardiomyocytes isolated from a
49
50 severe SMA mouse model and cardiomyocytes generated from induced pluripotent stem cells
51
52 (iPSCs) derived from an SMA Type II patient, however, found that SMN deficiency disrupts
53
54 muscle cell and fibre development, muscle function and Ca²⁺ handling (22). Cell studies are
55
56 extremely useful, but cell isolation and subsequent culture changes the physiological stresses
57
58
59
60

1
2
3 that they are exposed to in comparison to those experienced *in vivo*. Thus, we undertook a
4 quantitative proteomic comparison of heart tissues from the less-severe *Smn*^{2B/-} SMA mouse
5 model and age-matched wild-type (WT) mice and compared these findings with those
6 identified in our previous study of heart tissues from the severe Taiwanese SMA mouse model
7
8
9
10
11
12 (15).
13
14
15

16
17 We report evidence of widespread protein dysregulation in *Smn*^{2B/-} mouse hearts compared to
18 age-matched WT mice, some of which was common to the Taiwanese SMA mouse model. In
19 agreement with our previous findings from the Taiwanese model (15), the intermediate
20 filament protein, lamin A/C, was increased in expression in hearts from the less-severe *Smn*^{2B/-}
21 SMA mouse model, whereas desmin, another intermediate filament protein, was found to be
22 decreased in heart tissues in both mouse models. The extracellular matrix (ECM) protein,
23 elastin, was also significantly decreased in the heart tissues of the *Smn*^{2B/-} mouse. Whilst
24 AAV9-mediated *SMN1* delivery restored desmin levels in the *Smn*^{2B/-} SMA mouse model to
25 those seen in WT mice, this treatment did not rescue the increased levels of lamin A/C or the
26 decreased levels of elastin, even though levels of SMN were significantly enhanced when a
27 codon-optimised transgene was administered. Together these findings suggest that post-natal
28 AAV9-mediated *SMN1* delivery may not rectify all the dysregulated proteins found in the
29 *Smn*^{2B/-} mouse model of SMA, and since these proteins have the potential to detrimentally
30 impact heart function, additional cardiac monitoring may prove useful in the long-term care of
31 SMA patients.
32
33
34
35
36
37
38
39
40
41
42
43
44
45
46
47
48
49
50
51
52
53

54 **Results**

55 **Quantitative proteomics analysis of heart tissue from a mouse model of less-severe SMA** 56 **reveals widespread molecular defects** 57 58 59 60

1
2
3 To determine the molecular consequences of SMN depletion in heart tissue from the less-severe
4 *Smn*^{2B/-} SMA mouse model, a relative quantitation proteomic comparison against age-matched
5
6 WT mouse hearts was undertaken using iTRAQ™ mass spectrometry analysis at the
7
8 symptomatic time-point of P18. This approach identified 3105 proteins in total (Supplementary
9
10 Table 1) after removing proteins identified from 1 or more peptides and those which matched
11
12 to the decoy search (i.e., prefixed with “REVERSED...”). Of these, 2479 were identified with
13
14 a 5% local false-discovery rate. From these, 277 proteins met the specified criteria (an unused
15
16 ProtScore (conf) > 0.05, detected by ≥2 unique peptides, and a statistically significant (p≤0.05)
17
18 fold change of ≥1.25 or ≤0.8) for differential expression in the *Smn*^{2B/-} mouse heart compared
19
20 to age-matched WT hearts, of which 156 proteins were increased and 121 were decreased in
21
22 expression in SMA mouse hearts (Supplementary Table 2).
23
24
25
26
27
28
29
30

31 To guide the direction of further studies, we were interested to understand whether any of the
32
33 differentially abundant proteins identified in heart tissue from the less-severe *Smn*^{2B/-} SMA
34
35 mouse model were conserved with those identified previously from the severe Taiwanese SMA
36
37 mouse model (15). The iTRAQ data pertaining to the Taiwanese model were derived in the
38
39 same experiment as the *Smn*^{2B/-} data reported here, but only the Taiwanese section of the data
40
41 was published previously (15). Compared to their respective age-matched WT mice (i.e., P18
42
43 for the *Smn*^{2B/-} & P8 for the Taiwanese), and using the same criteria (p≤0.05, fold change of
44
45 ≥1.25 or ≤0.8, >1 unique peptide), 50 proteins were found to be commonly dysregulated in
46
47 both mouse models of SMA (Supplementary Table 3). Of these, 30 were up-regulated and 20
48
49 down-regulated with statistical significance in both models (Figure 1A) with a similar fold-
50
51 change in most dysregulated proteins (Figure 1B).
52
53
54
55
56
57
58
59
60

1
2
3 The list of differentially abundant proteins from both mouse models was also compared using
4 the comparison analysis function of the curated bioinformatics platform, Ingenuity Pathway
5 Analysis (IPA®). This two-way comparison in which the enriched terms were ranked by
6 absolute p -value, demonstrated a similar enrichment of terms for “diseases & disorders,
7 physiological system development & function” after removal of cancer related terms. In
8 particular, “abnormal morphology” and “dilated cardiomyopathy” were highly enriched in both
9 mouse models (*Smn*^{2B/-} mouse model, p -value range 3.72×10^{-19} to 2.65×10^{-7} ; Taiwanese
10 mouse model, p -value range 9.52×10^{-24} to 4.69×10^{-8}) (Figure 1C). Similarly, for “molecular
11 & cellular functions”, terms relating to “translation, synthesis and metabolism of proteins” and
12 “cell & organismal death” were significantly enriched among the differentially abundant
13 proteins common to both mouse models (*Smn*^{2B/-} mouse model, p -value range 5.01×10^{-40} to
14 2.65×10^{-7} ; Taiwanese mouse model, p -value range 9.52×10^{-24} to 4.69×10^{-8}) (Figure 1D).
15 Various canonical pathways already linked to SMA such as “EIF2 signaling” (23) and
16 “mitochondrial dysfunction” (24) were also enriched in the *Smn*^{2B/-} and Taiwanese mouse
17 models (Figure 1E). In addition, the “dilated cardiomyopathy signaling pathway” was
18 significantly enriched in both models (*Smn*^{2B/-} mouse model, $p=6.52 \times 10^{-11}$, z -score = 1.043;
19 Taiwanese mouse model, $p=2.72 \times 10^{-18}$, z -score = -0.667).

20
21
22
23
24
25
26
27
28
29
30
31
32
33
34
35
36
37
38
39
40
41
42
43
44
45 Using the Database for Annotation, Visualization and Integrated Discovery (DAVID)
46 bioinformatics tool, the cellular components with which the significantly dysregulated proteins
47 in the *Smn*^{2B/-} mouse model were associated was ascertained (Figure 1F and Supplementary
48 Table 4A). Of particular interest were those cellular components pertinent to cardiomyocyte
49 function including the Z-disk (12 proteins; $p=4.7 \times 10^{-6}$), the costamere (6 proteins; $p=5.4 \times 10^{-6}$),
50 focal adhesion (12 proteins; $p=7.9 \times 10^{-5}$) and adherens junction (10 proteins; $p=3.2 \times 10^{-4}$),
51 the sarcolemma (9 proteins; $p=5.4 \times 10^{-4}$), the intercalated disc (6 proteins; $p=1.4 \times 10^{-3}$), and
52
53
54
55
56
57
58
59
60

1
2
3 intermediate filaments (6 proteins; $p=2.5 \times 10^{-2}$). When the 50 proteins significantly
4
5 dysregulated in both the *Smn*^{2B/-} and Taiwanese SMA mouse models were considered in the
6
7 DAVID analysis, “intermediate filament” (3 proteins; $p=4.8 \times 10^{-2}$) remained an enriched
8
9 cellular component term (Supplementary Table 4B).
10
11
12
13

14 **The intermediate filament proteins, lamin A/C and desmin, are differentially abundant** 15 **in heart tissue from two mouse models of SMA** 16 17

18
19 The finding that intermediate filament proteins are differentially abundant in both SMA mouse
20
21 models is of particular interest with regards to heart conditions. Mutations affecting both lamin
22
23 and desmin (type V and type III intermediate filament proteins, respectively), commonly give
24
25 rise to conditions associated with cardiomyopathy and heart failure (25). Of additional
26
27 relevance is that mutations in *LMNA* -the lamin A/C gene- have been attributed to adult-onset
28
29 conditions with an SMA-like phenotype (26,27). Lamin A was identified by iTRAQ as being
30
31 increased in both the Taiwanese (15) and *Smn*^{2B/-} SMA mouse models (Supplementary Table
32
33 1) (albeit it just missed the criteria for differential expression in the *Smn*^{2B/-} with $p=0.056$).
34
35 Desmin, on the other hand, was decreased in expression in both the Taiwanese (15) and *Smn*^{2B/-}
36
37 SMA mouse models, but only met the criteria for differential expression when peptides
38
39 quantified with 99% confidence were used to calculate the ratio, resulting in $p=0.049$.
40
41
42
43
44
45
46

47 To gain further insights into the involvement of these intermediate filament proteins in SMA,
48
49 we verified the differential expression of lamin A/C and desmin in heart tissue from the *Smn*^{2B/-}
50
51 and Taiwanese SMA mice. Quantitative western blotting confirmed a 1.94-fold and 2.06-fold
52
53 increase in lamin A and C expression, respectively, in heart tissue extracts from *Smn*^{2B/-} mice
54
55 compared to age-matched WT mice ($p=0.014$ and $p=0.030$, respectively) (Supplementary File
56
57 Figure 1A). Immunohistochemistry analysis also confirmed increased lamin A
58
59
60

1
2
3 immunoreactivity in heart tissues from the *Smn*^{2B/-} mouse model compared to those from WT
4 mice (1.74-fold increase, $p=0.007$; Supplementary File Figure 1B). This aligned with our
5
6 previous findings (15) where lamin A/C levels were increased in heart tissue from the severe
7
8 Taiwanese SMA mouse model. Immunohistochemistry analysis of *Smn*^{2B/-} mouse heart
9
10 sections revealed few lamin A/C positive cells in the ventricle lumen (Supplementary File
11
12 Figure 1C), in line with our previous observation from the Taiwanese SMA mouse model (15).
13
14 Although we cannot rule out a minor contribution, this result confirms that the increased lamin
15
16 A/C levels cannot be solely attributed to circulating blood cells. For reference, SMN levels in
17
18 heart tissue extracts from the *Smn*^{2B/-} mice were reduced to 0.08-fold ($p=0.007$) of that found
19
20 in WT mice (Supplementary File Figure 1A).
21
22
23
24
25
26
27
28
29

30 Decreased desmin expression was also confirmed in both mouse models of SMA by western
31 blotting, with levels being reduced in the *Smn*^{2B/-} mice compared to age-matched (P18) WT
32 mice to 0.73-fold ($p=0.033$) and in the Taiwanese mice compared to age-matched (P8) WT
33 mice to 0.76-fold ($p=0.007$) (Supplementary File Figure 2A). These findings were corroborated
34
35 by immunohistochemistry analysis (Supplementary File Figure 2B) with desmin
36
37 immunoreactivity in *Smn*^{2B/-} mice showing a decrease to 0.41-fold ($p=0.033$) compared to WT
38
39 (P18) mice and desmin staining in Taiwanese mice demonstrating a decrease to 0.26-fold
40
41 ($p=0.019$) compared to (P8) WT mice (Supplementary File Figure 2C).
42
43
44
45
46
47
48
49

50 **AAV9-mediated *SMNI* delivery to increase SMN expression in the hearts of *Smn*^{2B/-} SMA** 51 **mice**

52
53 To establish the impact of currently approved gene therapy treatments, which are designed to
54
55 increase SMN levels in SMA patients, on a peripheral tissue such as the heart, we examined
56
57 the extent to which AAV9-mediated *SMNI* treatment restored expression levels of lamin A/C
58
59
60

1
2
3 and desmin towards control mice. For these experiments, we chose to focus only on the less-
4
5 severe *Smn*^{2B/-} SMA model as these mice have a longer pre-symptomatic period compared to
6
7 the Taiwanese mouse model allowing for a better understanding of developmental defects
8
9 secondary to motor neuron loss. In addition, to validate our findings further, two distinct
10
11 vectors that have previously been used in *Smn*^{2B/-} mice were utilised (28,29), in particular the
12
13 one vector results in enhanced expression of the *SMN1* gene (28). SMN levels were confirmed
14
15 by quantitative western blotting to be significantly increased in extracts of heart tissues from
16
17 *Smn*^{2B/-} mice following AAV9-mediated *SMN1* replacement (Figure 2). As expected (28),
18
19 delivery of the optimised cDNA transgene AAV9_*Co-hSMN1* resulted in enhanced levels of
20
21 SMN (169-fold; $p=0.0002$) compared to untreated *Smn*^{2B/-} mice with increased levels of SMN
22
23 beyond that expected in WT mice (~13.50-fold). Although the scAAV9-*SMN1*-mediated
24
25 delivery also resulted in an SMN increase (2.4-fold; $p=0.0003$) compared to untreated *Smn*^{2B/-}
26
27 mice, SMN levels remained below that found in WT mice (~0.32-fold) (Figure 2A). There was
28
29 no statistically significant difference in SMN expression levels between untreated *Smn*^{2B/-} mice
30
31 and vehicle controls (i.e., AAV9_*eGFP* (2.1-fold; $p=0.14$); scAAV9-*GFP* (1.8-fold; $p=0.08$)
32
33 (Figure 2A). Immunohistochemistry analysis of heart tissues from *Smn*^{2B/-} mice revealed
34
35 increased SMN immunoreactivity following SMN replacement, particularly in those treated
36
37 with AAV9_*Co-hSMN1* (Figure 2B).
38
39
40
41
42
43
44
45
46

47 **AAV9-mediated *SMN1* delivery restores desmin expression but does not correct** 48 49 **increased lamin A/C expression in the hearts of *Smn*^{2B/-} SMA mice**

50
51 Quantitative western blotting and immunohistochemistry analysis revealed that AAV9-
52
53 mediated *SMN1* treatment did not correct the increased production of lamin A/C in *Smn*^{2B/-}
54
55 mouse hearts. On western blots, lamin A expression levels following delivery of AAV9_*Co-*
56
57 *hSMN1* were 0.80-fold ($p=0.36$) compared to untreated *Smn*^{2B/-} mice and 1.56-fold ($p=0.04$)
58
59
60

1
2
3 compared to WT mice. Following scAAV9-*SMN1*-mediated delivery lamin A levels were 0.96-
4 fold ($p=0.44$) compared to untreated *Smn*^{2B/-} mice and 1.56-fold ($p=0.003$) compared to WT
5 mice (Figure 3A). Similarly, lamin C expression levels following delivery of AAV9_*Co-*
6 *hSMN1* were 0.77-fold ($p=0.26$) compared to untreated *Smn*^{2B/-} mice and 1.39-fold ($p=0.13$)
7 compared to WT mice and following scAAV9-*SMN1*-mediated delivery were 0.96-fold
8 ($p=0.50$) compared to untreated *Smn*^{2B/-} mice and 1.54-fold ($p=0.004$) compared to WT mice
9 (Figure 3A). There was no statistically significant difference in lamin A and C expression levels
10 between untreated *Smn*^{2B/-} mice and vehicle controls (i.e., AAV9_*eGFP* (1.06-fold ($p=0.46$))
11 for lamin A and 1.21-fold ($p=0.06$) for lamin C); scAAV9-*GFP* (0.96-fold ($p=0.59$) for lamin
12 A and 0.84-fold ($p=0.06$) for lamin C) (Figure 3B).

13
14
15
16
17
18
19
20
21
22
23
24
25
26
27
28
29 In heart sections from WT mice, lamin A/C immunoreactivity was largely confined to the
30 nuclear membrane, as expected, with a small proportion being localised to the sarcomere as
31 confirmed by double-label immunohistochemistry with alpha-actinin 2, a sarcomere marker
32 (Figure 3C & 3D). In heart sections from the *Smn*^{2B/-} mice, lamin A/C was significantly
33 increased in expression at the nuclear membrane alongside a strikingly increased distribution
34 of lamin A/C at the sarcomeres (Figure 3C). When quantified across each section, lamin A/C
35 immunoreactivity in heart tissues from *Smn*^{2B/-} mice showed a significant increase in lamin A/C
36 expression compared to age-matched (P18) WT mice (3.29 ± 1.13 -fold; $p=0.004$; Figure 3C),
37 and after treatment with AAV9_*Co-hSMN1* or scAAV9-*SMN1* lamin A/C levels in *Smn*^{2B/-}
38 mice remained increased compared to the untreated *Smn*^{2B/-} mice (3.66 ± 0.70 -fold ($p=0.54$)
39 and 4.25 ± 0.45 -fold ($p=0.13$), respectively (Figure 3C).

40
41
42
43
44
45
46
47
48
49
50
51
52
53
54
55
56
57
58
59
60
Western blot and immunohistochemistry analysis revealed that AAV9-mediated *SMN1*
treatment did, however, restore the decreased expression of desmin in *Smn*^{2B/-} mouse hearts

1
2
3 towards WT levels. From western blots, desmin expression levels following delivery of
4 AAV9_*Co-hSMNI* were 1.74-fold ($p=0.0095$) compared to untreated *Smn*^{2B/-} mice and 1.06-
5
6 fold ($p=0.44$) compared to WT mice and following scAAV9-*SMNI*-mediated delivery were
7
8 1.84-fold ($p=0.04$) compared to untreated *Smn*^{2B/-} mice and 1.31-fold ($p=0.13$) compared to
9
10 WT mice (Figure 4A). There was no statistically significant difference in desmin expression
11
12 levels between untreated *Smn*^{2B/-} mice and vehicle controls (i.e., AAV9_*eGFP*) (0.99-fold
13
14 ($p=0.88$)) and scAAV9-*GFP* (1.16-fold ($p=0.19$)) (Figure 4B). Desmin immunoreactivity in
15
16 heart sections from WT mice was typically present at the Z-disc (Figure 4C). Desmin
17
18 immunoreactivity in heart sections from the *Smn*^{2B/-} mice was clearly reduced (Figure 4C, high
19
20 magnification images), although some striations could still be seen, the staining appearing to
21
22 be variable in intensity and disorganised. Quantification of desmin immunoreactivity across
23
24 each heart section from the *Smn*^{2B/-} mice found desmin expression to be significantly decreased
25
26 compared to age-matched (P18) WT mice (0.61 ± 0.12 -fold ($p<0.001$)) (Figure 4C), but
27
28 treatment with AAV9_*Co-hSMNI* or scAAV9-*SMNI* confirmed that desmin levels in *Smn*^{2B/-}
29
30 mice were increased compared to the untreated *Smn*^{2B/-} mice (1.75 ± 0.19 -fold ($p<0.0001$) and
31
32 1.28 ± 0.22 -fold ($p=0.035$)), respectively (Figure 4C).
33
34
35
36
37
38
39
40
41

42 **Decreased elastin expression in *Smn*^{2B/-} mouse heart is also refractory to AAV9-mediated** 43 ***SMNI* delivery**

44
45
46 Lamin A/C is a significant regulator of cell stability and dynamics (30), and its expression
47
48 correlates with the stiffness of tissue (31). Increased rigidity of cardiomyocytes enhances
49
50 passive tension *in vitro* and *in vivo*, resulting in functional heart defects (32,33). To gain
51
52 insights into the wider impact of increased lamin A/C levels on the contractile apparatus of
53
54 cardiomyocytes and overall stiffness of heart tissues in the *Smn*^{2B/-} SMA mouse model, we
55
56 examined the levels of elastin, a protein essential for the elastic properties of many tissues.
57
58
59
60

1
2
3 Elastin was identified by iTRAQ analysis to be significantly reduced to 0.01-fold ($p=0.003$) in
4 heart tissue from the *Smn*^{2B/-} SMA mouse model compared to WT. This finding was confirmed
5
6 qualitatively by immunohistochemical analysis of van Gieson staining (i.e., a modified Miller's
7
8 stain which differentially stains elastin from collagen and muscle), and quantitatively by
9
10 higher-power immunofluorescence analysis (0.30 ± 0.14 -fold ($p<0.00001$) in *Smn*^{2B/-} vs WT)
11
12 (Figure 5). Elastin levels in *Smn*^{2B/-} mice following treatment with either AAV9_*Co-hSMNI* or
13
14 scAAV9-*SMNI* remained comparable to those observed in untreated *Smn*^{2B/-} mice (0.37 ± 0.16 -
15
16 fold ($p=0.41$), and 0.30 ± 0.13 -fold ($p=0.24$)) of WT levels respectively) (Figure 5).
17
18
19
20
21
22
23

24 Discussion

25
26 Over the last two decades, evidence has built to suggest that in severe forms of SMA, structural
27
28 and functional abnormalities in heart tissues exist (14,18,22), whilst in patients with less severe
29
30 types, a potentially milder impairment of cardiac function is suggested (9,16). The aim of this
31
32 study was to conduct a proteomic comparison of heart tissues from the less-severe *Smn*^{2B/-} SMA
33
34 mouse model and age-matched wild-type (WT) mice and compare these findings with those
35
36 identified in our previous study of heart tissues from the severe Taiwanese SMA mouse model
37
38 (15) to determine whether a conserved response to reduced SMN levels is evident. We also
39
40 investigated whether dysregulated proteins with a known role in heart function are impacted
41
42 and whether their levels could be rescued by increasing SMN levels in the less-severe *Smn*^{2B/-}
43
44 mouse model.
45
46
47
48
49
50

51 In each SMA mouse model, hundreds of proteins were found to be dysregulated compared to
52
53 age-matched WT mice. Bioinformatics analysis revealed a highly significant enrichment of
54
55 terms relating to “abnormal morphology” and “dilated cardiomyopathy” in reference to
56
57 “diseases & disorders, physiological system development & function” in both dysregulated
58
59
60

1
2
3 datasets. Previously, cardiac defects such as thinning of the interventricular septum and
4
5 cardiomyocyte disorganisation have been noted in the severe Taiwanese SMA mouse model
6
7 (14) as have atrial or ventricular septal defects (11) and thickened myocardium (9) in patients
8
9 with SMA type I. Out of 42 SMA type II and III patients, one patient had mitral valve prolapse,
10
11 7 had sinus tachycardia, and more than half had an elevated minimum 24-hour heart rate (16).
12
13 When “molecular and cellular functions” were considered, terms relating to the “translation,
14
15 synthesis and metabolism of proteins”, and “cell and organismal death” were highly significant.
16
17 Most of these terms are typically associated with SMA, in particular, SMN is known to be key
18
19 for protein homeostasis (34). Both *in vitro* and *in vivo* studies provide support for impaired
20
21 translation in SMA (35,36) and a comprehensive study involving rat primary neuron culture,
22
23 fibroblasts from SMA Type I patients and neurons from a severe mouse model of SMA (*Smn*^{-/-};
24
25 *SMN2*^{tg0}) demonstrated reduced *de novo* protein synthesis linked to mTOR signalling (37).
26
27 In an earlier study, microfilament metabolism was found to be impacted by reduced levels of
28
29 SMN (38), and with evidence building for a role of mitochondrial dysfunction in SMA (24,39–
30
31 41), all these factors may contribute to altered protein metabolism. Most of the significantly
32
33 enriched “canonical pathways” common to both mouse models have also been implicated in
34
35 SMA, such as EIF2 signaling (23), mitochondrial dysfunction (24) and mTOR signaling (37),
36
37 but of particular interest was the significant enrichment of “dilated cardiomyopathy” and the
38
39 “dilated cardiomyopathy signaling pathway” in both mouse models of SMA.
40
41
42
43
44
45
46
47
48

49 While differentially abundant proteins from the *Smn*^{2B/-} dataset were associated with several
50
51 cellular components pertinent to cardiomyocyte function, the only cellular component to be
52
53 significantly enriched among proteins common to both mouse models was intermediate
54
55 filaments. Genetic mutations of the intermediate filaments lamin A/C and desmin are known
56
57 contributors of cardiomyopathies and heart failure (25,42). Both proteins form networks within
58
59
60

1
2
3 the cardiomyocyte and help maintain intra- and intercellular structure, with lamin A/C at the
4 nuclear envelope (43) and desmin within the cytoplasm. In addition, lamin and desmin have
5 important functions in nucleo-cytoskeletal coupling and mechano-transduction, gene
6 regulation, metabolism, mitochondrial homeostasis and cardiomyocyte differentiation and
7 survival (43–45), all of which are necessary for a fully functioning heart.
8
9
10
11
12
13
14
15
16

17 As previously confirmed in the Taiwanese mouse model of severe SMA (15), levels of lamin
18 A/C were significantly increased in heart tissues from the *Smn*^{2B/-} mouse model of less-severe
19 SMA. Increased levels of lamin A/C were localised to the nuclear envelope and to the
20 sarcomere of *Smn*^{2B/-} mouse hearts, and further support the concept that appropriate lamin A/C
21 production is SMN-dependent (15,27,46). Previously, increased lamin A/C levels have been
22 described in muscle (47) and Schwann cells from SMA mice (48) and in motor neurons
23 obtained from Type I SMA patients (49). In terms of impact on heart conditions and
24 development of dilated cardiomyopathy, impairment of the lamin A/C gene is a well-known
25 factor (50) and results in conduction problems, arrhythmias, atrioventricular block and sudden
26 cardiac death (51–55) with at least 260 *LMNA* mutations having been linked to cardiac diseases
27 (56). In several studies, *LMNA* mutations have also resulted in an SMA-like phenotype with
28 cardiac involvement (26,27).
29
30
31
32
33
34
35
36
37
38
39
40
41
42
43
44
45
46

47 An increase in lamin A/C may result in a “stiffer” nucleus which will alter the biomechanics
48 of the cardiomyocyte, and thus the heart tissue, and may be in response to increased stiffness
49 of the heart tissue (31). Conditions where increased accumulation of lamin A at the nuclear
50 envelope is known to occur are Hutchinson-Gilford progeria syndrome and restrictive
51 dermatopathy. Both conditions arise from improper post-translational processing of prelamin A,
52 the former from an *LMNA* mutation which results in a mutant farnesylated prelamin A
53
54
55
56
57
58
59
60

1
2
3 (progerin) whilst the latter is due to reduced levels of ZMPSTE24, the enzyme necessary for
4 processing prelamin A (57). Although not verified by immuno techniques in the current study,
5
6 ZMPSTE24 was significantly increased in the mass spectrometry data from both SMA mouse
7
8 models which may imply dysregulation of lamin A processing. In the current study, lamin A
9
10 was also prevalent at the sarcomere, especially in *Smn*^{2B/-} mice where it co-localised with alpha-
11
12 actinin 2. This may indicate an increase in unprocessed lamin A in SMA, as previously
13
14 prelamin A was identified at the sarcomere along with alpha-actinin 2 (55). Since it has been
15
16 suggested that prelamin A may be toxic and could promote dilated cardiomyopathy (55),
17
18 further investigations into understanding whether lamin A processing is defective in SMA may
19
20 prove useful. Additionally, the phosphorylation status of lamin A in SMA is worthy of
21
22 investigation as this may have implications for the regulation of lamin A levels since hypo-
23
24 phosphorylation renders lamin A more stable and less likely to be degraded (58) and has
25
26 occurred in mesenchymal stem cells when subjected to increased tissue stiffness (59).
27
28
29
30
31
32
33
34

35 Lamin A/C is the main provider of nuclear membrane mechanical strength and is key to
36
37 transmitting mechanical force from the ECM to the nucleus (60,61). Deficiency or mutations
38
39 in lamin A/C can cause mechano-transduction impairment (62) or impact whole-cell
40
41 biomechanical properties (63). In a lamin A-deficient mouse model, the desmin network was
42
43 disrupted and detached from the nuclear surface (64), suggesting defective force transmission
44
45 due to loss of lamin interactions with desmin and subsequent loss of cytoskeletal tension. In
46
47 another study of lamin A-deficient mice, desmin accumulation was increased in both muscle
48
49 and cardiac tissues (65). It may prove useful to consider whether the reverse is true in SMA
50
51 cardiomyocytes whereby decreased levels of desmin result in increased lamin A or *vice versa*.
52
53
54
55
56
57
58
59
60

1
2
3 Desmin is located throughout the cardiomyocyte and assists in transmitting force across the
4
5 ECM, sarcomere and cytoskeleton (66), and has been implicated in SMA (67). In combination
6
7 with microtubules and microfilaments, desmin helps to maintain the cytoskeleton structure and
8
9 organisation of sub-cellular organelles (68) and is thought to provide cardiomyocyte nuclei
10
11 with tension (69). Structurally, desmin links individual myofibrils at the Z-discs (70,71),
12
13 connects Z-discs to the intercalated disc (72), forms part of the desmosomes, and is linked to
14
15 the costamere enabling adhesion to the ECM (73). Overall, desmin is key to the functioning of
16
17 sarcomeres in efficient syncytia. Mutations often result in loss of sarcomere integrity and
18
19 myofibrillar structure (74) and depletion causes muscle architecture disruption (75), which is
20
21 not impacted during embryogenesis and myofibrillar assembly but affects muscle regeneration
22
23 resulting in weaker mice in a desmin knock-out model (76). In other studies, lack of desmin
24
25 impacted contractile function (77) and increased fibrosis (78) with muscle fibres lacking
26
27 desmin being more susceptible to physical damage (79) and desmin loss causing increased
28
29 passive stiffness in muscle (80).
30
31
32
33
34
35
36
37

38 Mechano-sensing within cardiomyocytes is a “two-way” system, with the nucleus being an
39
40 important mechanosensory organelle in the cell and intimately connected to the cytoskeleton,
41
42 and the latter in turn to the ECM. For optimal heart performance, both electrical and mechanical
43
44 stimuli are required with cardiomyocytes being subjected to cyclic contraction as the heart
45
46 beats (81). Cardiomyocytes also experience passive mechanical stimuli such as that exerted by
47
48 the cardiac ECM. The cardiac ECM is a combination of elastin bundles, collagen and
49
50 interconnected basement membranes (82), with intra- and extracellular components
51
52 contributing to overall myocardial stiffness (81). Although collagen is the main extracellular
53
54 protein in myocardial tissue, elastin, which is found in the epicardium, endomysium and
55
56 structures such as arteries, atria and ventricles of the heart (83), provides elasticity upon
57
58
59
60

1
2
3 mechanical demand (84). Elastin is a structural glycoprotein and an essential component of
4
5 myocardial stiffness (85), so any alterations in its levels will impact heart function. Typically,
6
7 elastin is very stable with a considerably low turnover rate, with degradation or damage
8
9 indicating pathological remodelling of the tissue and cardiovascular disease (86). Reduced
10
11 levels of elastin, as found in this study, will increase the heart tissue's passive stiffness,
12
13 potentially reducing cardiac function, since cardiomyocytes cultured on a stiff, fibrotic-like
14
15 matrix fail to beat properly (87). Typically, following myocardial infarction/ischaemia, elastin
16
17 levels will decrease (88), promoting ECM remodelling which further increases the stiffness of
18
19 the cardiac tissue and impairment of cardiac function (85). In Williams-Beuren syndrome,
20
21 impairment of the elastin *ELN* gene results in 4 out of 5 patients having cardiovascular
22
23 abnormalities (89), with mutations also resulting in congenital heart disease (90). Elastin fibres
24
25 are crucial for the proper functioning of Purkinje's fibres (91) and blood vessels (92), and
26
27 impairment can cause arrhythmias (93) or altered blood flow respectively, again impacting
28
29 heart function.
30
31
32
33
34
35
36
37

38 Two AAV9-mediated *SMN1* treatments were used in this study, both of which have previously
39
40 been used in *Smn^{2B/-}* mice (28,29), but the novel codon-optimised cDNA transgene
41
42 demonstrated significantly enhanced expression of the human *SMN1* gene in *Smn^{2B/-}* mice
43
44 hearts. Both treatments restored desmin levels to that of WT mice, but lamin A/C levels
45
46 remained elevated and elastin levels decreased even though the codon-optimised cDNA
47
48 transgene generated SMN levels more than 10-fold greater than those found in WT mice. The
49
50 lack of effect of increased SMN levels on lamin A in this study may be due to several reasons:
51
52 (i) lamin A is independent of SMN levels; (ii) the impact of low SMN levels on lamin A is
53
54 greatest during embryonic development so post-natal treatment is too late; (iii) cardiac
55
56 remodelling is influencing lamin A levels; and/or (iv) dysregulation of proteins responsible for
57
58
59
60

1
2
3 post-translation processing or regulating the stability of lamin A are not independent of SMN
4 levels. In contrast, desmin levels were increased by both AAV9-mediated *SMNI* treatments,
5
6 indicating a direct relationship between these two proteins. Previously, abnormalities in the Z-
7
8 bands of a patient with SMA were identified (94). Since low levels of desmin appeared to be
9
10 associated with sarcomere damage in a rat model of diabetes mellitus (95) and alpha-actinin
11
12 staining showed disrupted sarcomere/costamere/z-disc striations in desmin-null mice (96), it is
13
14 coherent that the improved levels of desmin in the AAV9-treated *Smn*^{2B/-} mice result in
15
16 improved sarcomere structure, although higher resolution microscopy is required to confirm
17
18 this. Interestingly, SMN has been found to be localised to the I- and M-bands of sarcomeres in
19
20 normal human skeletal fibres (97) and the Z-disc in mice (20) which suggests that sarcomeric
21
22 SMN may directly or indirectly interact with the cytoskeleton and thus be involved in
23
24 sarcomere structure (97), or its maintenance (20). In addition, during heart development,
25
26 desmin and lamin A are abundant in the cardiac conduction systems; desmin preferentially in
27
28 the myocardium of the central conduction system and lamin A more localised to the peripheral
29
30 conduction system, then progressively to the central conduction system (98). It may be possible
31
32 that AAV9-mediated treatment does not rectify lamin A/C levels due to inherent problems with
33
34 the central conduction system that are established prior to treatment being administered.
35
36 Additionally, abnormalities in conduction usually occur before dilated cardiomyopathy
37
38 development (99) with elevated heart rate being associated with cardiomyopathy in late
39
40 adolescence and increased heart failure risk (100). In desmin mutant mice, distribution of lamin
41
42 A/C was nucleoplasmic whilst in WT mice, lamin A/C was mostly at the nuclear periphery
43
44 (72). Since AAV9-mediated treatment restored desmin levels, lamin A/C's nuclear distribution
45
46 may improve over time.
47
48
49
50
51
52
53
54
55
56
57
58
59
60

1
2
3 Other researchers have found the outcome of AAV9 treatment in SMA to be variable. A study
4
5 focussed on fibrosis, remodelling, vascular integrity and oxidative stress in two mouse models
6
7 of differing severity only found a partial rescue of cardiovascular defects in their mouse model
8
9 of severe SMA and although structural defects were rectified, heart function incorporating heart
10
11 rate, stroke volume and cardiac output remained significantly lower than WT mice, as did
12
13 lifespan (13). In the SMN Δ 7 mouse model, scAAV9 treatment resolved the bradycardia issues,
14
15 but “cardiac output” remained similar to untreated mice, probably as a result of “stroke
16
17 volume” remaining decreased following scAAV9 treatment (12). In addition, contractility
18
19 remained lower than WTs following treatment. Another study using the SMN Δ 7 SMA mouse
20
21 model used the histone deacetylase inhibitor, trichostatin A, which is known to improve the
22
23 phenotype of SMA mice. Although heart function improved, these mice did not survive as well
24
25 as the WT mice (101). Typically, levels of lamin A/C in mouse cardiomyocytes, desmin in rat
26
27 heart tissues and the elastin component of connective tissues decline with age (102-104),
28
29 although in male F344/BN hybrid rats, desmin levels were found to increase in aging skeletal
30
31 muscle (105). In future studies, it will therefore be important to characterise the temporal
32
33 regulation of the proteins investigated throughout the disease time-course in the *Smn*^{2B/-} mouse
34
35 model, with and without AAV-9 mediated *SMN1* replacement, and to establish whether
36
37 restoring levels of these proteins would have an impact on cardiac function of the mouse model.
38
39 SMN may be essential for heart development prior to birth and thus scAAV9 treatment may
40
41 not correct key development milestones involving SMN. Additionally, other factors such as
42
43 lung and metabolic function or scoliosis may contribute to continued impairment of heart
44
45 function in SMA. Prior to the introduction of treatments, such as, nusinersen and risdiplam
46
47 which modify *SMN2* gene regulation to increase functional SMN expression, the impact on
48
49 concomitant health issues in SMA patients following respiratory assistance, and thus extended
50
51
52
53
54
55
56
57
58
59
60

1
2
3 life expectancy, has been previously highlighted (10) and included development of heart
4
5 arrhythmia (bradycardia).
6
7
8
9

10 In conclusion, accumulating evidence suggests that cardiac assessment in the long-term care
11
12 of SMA patients is warranted. We only investigated three of the dysregulated proteins
13
14 identified from mass spectrometry analysis in the *Smn*^{2B/-} mouse model, but there are many
15
16 more that warrant further investigation, especially those pertinent to heart function. AAV9-
17
18 *SMN1* gene therapy only corrected one of the proteins investigated, and although severe
19
20 symptoms may be rare in SMA, subtle differences in cardiac performance in combination with
21
22 current treatments increasing longevity in these patients, may impact cardiac health in future
23
24 years. Thus, additional cardiac therapies may prove useful in optimising treatment regimens
25
26 for SMA patients.
27
28
29
30
31
32

33 **Materials & Methods**

34 **SMA mouse models**

35
36 The *Smn*^{2B/-} and Taiwanese (original strain from Jackson Laboratories, No. 005058) mouse
37
38 models were housed at Keele and Edinburgh Universities, respectively. As previously
39
40 described (106), the less-severe *Smn*^{2B/-} mouse model is maintained on a pure C57BL/6 genetic
41
42 background with creation of the 2B mutation via a 3-nucleotide substitution within the exon
43
44 splicing enhancer of exon 7 (107,108). The severe Taiwanese mouse model is heterozygous
45
46 for the *SMN2* transgene on a *Smn* null background (*Smn*^{-/-}; *SMN2*^{tg/+}) (109). Tissues were
47
48 harvested at a symptomatic time point of post-natal day (P) 18 and P8 for the *Smn*^{2B/-} and
49
50 Taiwanese models, respectively, in addition to age-matched WT mice. All experimental
51
52 procedures on Taiwanese mice were authorized and approved by the University of Edinburgh
53
54 Animal Welfare Ethical Review Body (AWERB) and UK Home Office (Project Licence
55
56
57
58
59
60

1
2
3 60/4569) in accordance with the Animals (Scientific Procedures) Act 1986. For the *Smn*^{2B/-}
4 mice, experimental procedures were authorized and approved by the Keele University AWERB
5 and UK Home Office (Project Licence P99AB3B95) in accordance with the Animals
6 (Scientific Procedures) Act 1986.
7
8
9
10
11
12
13
14

15 **Protein extraction and preparation for quantitative proteomic analysis**

16
17 Total protein extracts were prepared as previously described (110) from the hearts of P18
18 *Smn*^{2B/-} and age-matched WT animals (both n = 3) and isobaric tags for relative and absolute
19 quantitation (iTRAQ) quantitative mass spectrometry analysis were added. Briefly, proteins
20 were digested with trypsin, then peptides tagged with iTRAQTM reagents as described in the
21 iTRAQ kit protocol and sample groups assigned as follows: 116-P18 WT and 117-P18 *Smn*^{2B/-}.
22
23
24
25
26
27

28 **High pH reverse-phase liquid chromatography fractionation and liquid** 29 **chromatography–tandem mass spectrometry analysis** 30 31

32
33 Fractionation and mass spectrometry analysis were carried out as previously described (15). In
34 brief, the iTRAQ-labelled peptides were combined, concentrated, resuspended in buffer A (10
35 mm ammonium formate [NH₄HCO₂], 2% acetonitrile [MeCN], pH 10.0) then fractionated
36 using high pH reverse-phase liquid chromatography (C18 column). Following rinsing of the
37 column with 96% buffer A until the optical density returned to baseline, a gradient was run
38 from 4% to 28% of buffer B (10 mm NH₄HCO₂, 90% MeCN, pH 10.0) for 30 min followed
39 by another from 28–50% buffer B for 6 min. Buffer B at 80% was used to rinse the column for
40 5 min and the column then re-equilibrated with 4% buffer B for 11 min. Fractions (0.5 ml)
41 were collected every 30 s and their UV chromatograms analysed. Fractions with similar peptide
42 concentrations were combined resulting in 12 fractions which were vacuum dried then
43 resuspended in 30 µl of 0.1% formic acid.
44
45
46
47
48
49
50
51
52
53
54
55
56
57
58
59
60

1
2
3 For the mass spectrometry analysis, one-third of each fraction was analysed by mass
4 spectrometry. Following separation of the peptides via liquid chromatography, peptides were
5
6 loaded with buffer A (2% MeCN, 0.05% TFA in ultrapure water) and bound to an Acclaim
7
8 PepMap100 AQ6 trap (100 μm \times 2 cm) (Thermo Fisher Scientific) which was then washed for
9
10 10 min with buffer A. The analytical solvent system consisted of buffer A and buffer B (98%
11
12 MeCN, 0.1% FA in ultrapure water) at 300 nl/min flow rate. To elute the peptides the following
13
14 gradient was utilized: linear 2–20% of buffer B over 90 min, linear 20–40% of buffer B for 30
15
16 min, linear 40–98% of buffer B for 10 min, isocratic 98% of buffer B for 5 min, linear 98–2%
17
18 of buffer B for 2.5 min and isocratic 2% buffer B for 12.5 min. Eluent was sprayed with a
19
20 NANOSpray II source (electrospray ionization) into the TripleTOF 5600+ tandem mass
21
22 spectrometer (AB Sciex) under the control of Analyst® TF software (AB Sciex). The mass
23
24 spectrometer was operated as previously described (15) and the raw mass spectrometry data
25
26 files analyzed by ProteinPilot software, version 5.0.1.0 (Applied Biosystems) in addition to the
27
28 Paragon™ database search and Pro Group™ algorithm using the UniProtKB/Swiss-Prot
29
30 FASTA database. Paragon search analysis parameters for sample were: type “iTRAQ4plex
31
32 (Peptide Labeled),” cysteine alkylation “MMTS,” digestion “trypsin,” instrument “TripleTOF”
33
34 and species “Mouse” with processing parameters described as “quantitative,” “bias correction,”
35
36 “background correction,” “thorough ID” and “biological modifications.” A protein threshold
37
38 of >5 was used in the Pro Group algorithm to calculate the relative protein expression with the
39
40 generation of an error factor and *p*-value, and Proteomics System Performance Evaluation
41
42 Pipeline used to determine false discovery rate. The mass spectrometry proteomic data can be
43
44 accessed at the following DOI: 10.6084/m9.figshare.23256374
45
46
47
48
49
50
51
52
53
54
55

56 **Bioinformatics analysis**

57
58
59
60

1
2
3 Data that met the criteria for differential expression in the *Smn*^{2B/-} mice were analysed using
4 Database for Annotation, Visualization and Integrated Discovery (DAVID) Functional
5 Annotation Bioinformatics 2021 (111,112) and Ingenuity Pathway Analysis software (IPA;
6 QIAGEN Inc., <https://www.qiagenbioinformatics.com/products/ingenuity-pathway-analysis>)
7 (113). Proteins were deemed differentially abundant in the *Smn*^{2B/-} mice in comparison to age-
8 matched WT mice after the following filtering criteria were applied and proteins removed if;
9 (i) they were identified from just one peptide, (ii) had expression changes of less than 25%
10 (SMA vs WT) or (iii) had *p*-values of >0.05 assigned to their expression changes. Only terms
11 with at least three annotated proteins and a *p*-value of ≤0.05 were noted for the DAVID
12 analysis.
13
14
15
16
17
18
19
20
21
22
23
24
25
26
27
28

29 **SMN replacement in *Smn*^{2B/-} mice via viral vector treatment**

30 For SMN replacement, AAV9 vectors were used from two sources, RY (single stranded
31 AAV9_*eGFP* and AAV9_*Co-hSMN1*) (28) and BS (self-complementary scAAV9-*GFP* and
32 scAAV9-*SMN1*) (29) and administered through the facial vein at P0 (5E10 vg/pup-7E10
33 vg/pup). The vector sourced from RY uses a codon-optimised cDNA transgene which has been
34 developed to enhance levels of the functional SMN protein produced both *in vitro* and *in vivo*
35 (28) whilst the vector from BS used standard cloning procedures as previously described (114).
36 Following CO₂ anaesthesia and exsanguination, heart tissues were harvested from the
37 following groups at the symptomatic time-point of P18: untreated WT mice (n=4), untreated
38 *Smn*^{2B/-} mice (n=6), *Smn*^{2B/-} mice treated with the vector plus GFP (RY, n=5; BS, n=4) and
39 *Smn*^{2B/-} mice treated with the vector plus *SMN1* (RY, n=5; BS, n=5).
40
41
42
43
44
45
46
47
48
49
50
51
52
53
54
55

56 **Protein extraction and western blotting**

1
2
3 All extraction steps were carried out on ice and as previously described (115). Heart tissues
4 were diced then homogenized with pellet pestles in 2× modified RIPA buffer (2% NP-40, 0.5%
5 Deoxycholic acid, 2 mM EDTA, 300 mM NaCl and 100 mM Tris-HCl (pH 7.4)) plus protease
6 inhibitor cocktail at 1:100 (Sigma-Aldrich; P8340), left on ice for 5 min then sonicated briefly
7 at 5 microns for 10 s. This process was repeated an additional two times. The samples were
8 centrifugated at 13,000 RPM (MSE, Heathfield, UK; MSB010.CX2.5 Micro Centaur) for 5
9 min at 4°C and protein concentration determined via the BCA protein assay (Pierce™, 23227).
10 The concentration of the protein extracts was adjusted to approximately 2mg/ml, and they were
11 heated in 2× SDS sample buffer (4% SDS, 10% 2-mercaptoethanol, 20% glycerol, 0.125 M
12 Tris-HCl (pH 6.8) and bromophenol blue) for 3 min at 95 °C prior to loading onto 4-12% Bis-
13 Tris polyacrylamide gels (Life Technologies, Warrington, UK) for SDS-PAGE (Biorad,
14 Hercules, CA, USA). A horizontal slice of the gel was excised and stained with Coomassie
15 blue as an internal loading control for total protein, if necessary, protein concentrations were
16 further adjusted to ensure even loading of the samples. The proteins in the remaining gel were
17 transferred overnight via western blot onto a nitrocellulose membrane. Following blocking
18 with 4% powdered milk, the membranes were incubated with primary monoclonal antibodies
19 against: mouse anti-SMN (MANSMA12 2E6; 1:100 (116)); rabbit anti-lamin A/C (Abcam;
20 ab169532; 1:2000); rabbit anti-desmin (Abcam; ab227651; 1:1000) in dilution buffer (1% FBS,
21 1% horse serum (HS), 0.1% bovine serum albumin (BSA) in PBS with 0.05% Triton X-100)
22 for 2 h at RT or O/N at 4°C. Membranes were then incubated with HRP-labelled rabbit anti-
23 mouse Ig (DAKO, P0260) or goat anti-rabbit Ig (DAKO, P0488) at 0.25 ng/ml in dilution
24 buffer for 1 h followed by either West Pico or West Femto (both ThermoFisher) and bands
25 imaged with the ChemiDoc™ Touch Imaging System (Bio-Rad). Using ImageJ Fiji software
26 (v1.51) (117) densitometry measurements of both antibody reactive bands and Coomassie-
27 stained gel bands were undertaken.
28
29
30
31
32
33
34
35
36
37
38
39
40
41
42
43
44
45
46
47
48
49
50
51
52
53
54
55
56
57
58
59
60

Immunofluorescence microscopy

Following excision, heart tissues incorporating the left and right ventricles were flash frozen in liquid nitrogen and stored at -80°C then sectioned ($7\ \mu\text{m}$) on a rotary cryostat, collected onto polylysine-coated slides and stored at -20°C . Prior to staining, slides were brought to RT. All subsequent steps were carried out at RT and PBS used for each wash step (3 x 5 min) whilst blocking buffer (1% FBS, 1% HS, 0.1% BSA in PBS) was used for antibody dilution. Sections were washed, then blocked for 30 min prior to being incubated either for 2 h at RT or O/N at 4°C with primary antibodies against mouse anti-SMN (MANSMA12 2E6; 1:4 (116)), rabbit polyclonal anti-lamin A/C (NOVUS; NBP2-19324; 1:100), rabbit monoclonal anti-desmin (Abcam; ab227651; 1:100), rabbit polyclonal anti-elastin (Fisher Scientific; PA5-99418; 1:100) or mouse anti-alpha Actinin 2 (Gene Tex; GTX632361; 1:200). Following washing, $5\ \mu\text{g}/\text{ml}$ of secondary antibody (Molecular Probes; goat anti-rabbit IgG ALEXA Flour 488; A11034) was applied for 1 h. Sections were washed prior to being stained with 4',6-diamidino-2-phenylindole (DAPI; D9542; $0.4\ \mu\text{g}/\text{mL}$) for 10 min, then washed, mounted and imaged with a Leica TCS SP5 spectral confocal microscope (Leica Microsystems, Milton Keynes, UK).

Images generated were analysed via ImageJ. For lamin A, images obtained with the 63x objective with an additional four-fold magnification were utilised, whereas images taken with the 63x objective were used for desmin and elastin analysis. For the lamin A sections, a minimum of 100 cells were analysed whereas for desmin and elastin a minimum of 200 cells were analysed per condition. For each analysis the scale function was removed, so only the pixels either staining for DAPI or the protein (lamin A, desmin and elastin) were counted. Using the threshold function (118), the highlighted pixels were analysed, and protein staining was corrected for cells present by dividing by the measure obtained for the positively stained

1
2
3 DAPI areas. The fold difference between the SMA mouse models and their relevant WTs were
4
5 then determined.
6
7
8
9

10 **Histochemical staining of elastin**

11
12 Heart tissue sections were also stained for elastin with the Miller's Elastic Van Gieson Stain
13
14 Kit (Atom Scientific Ltd; RRSK11-100) using the protocol provided. All wash steps were
15
16 carried out with tap water unless otherwise stated. Briefly, sections were washed then treated
17
18 with acidified potassium permanganate (0.5%) for 5 min. Following further washing the
19
20 sections were bleached with oxalic acid (1%) for 1 min, washed, then rinsed in 95% alcohol
21
22 and submerged in Miller's elastin stain for 3 h at RT. Sections were then rinsed with 95%
23
24 alcohol until the slides were clear, washed, and counterstained with filtered Van Gieson stain
25
26 for 2 min, then blotted, dehydrated, cleared and mounted.
27
28
29
30
31
32

33 **Statistical analysis**

34
35 Statistical analyses were carried out using GraphPad Prism version 9.0.0 for Windows,
36
37 GraphPad Software, San Diego, California USA, www.graphpad.com. Data distribution was
38
39 assessed with the Shapiro–Wilk test and the unpaired two-tailed t-test and Mann-Whitney U
40
41 test applied to parametric and non-parametric data respectively. Western blot densitometry
42
43 measurements were assessed using an unpaired, one-tailed or two-tailed t-test with Welch's
44
45 correction (2-sample equal variance), depending on the null-hypothesis that was tested in each
46
47 case. Venn diagrams were generated via a web-based tool (119). Data are presented as mean ±
48
49 standard deviation with a *p*-value of ≤0.05 being considered as significant for all analyses.
50
51
52
53
54
55

56 **Supplementary Material**

57
58 Supplementary File (Word document containing Figures 1 and 2)
59
60

1
2
3 Supplementary Tables (Excel document containing supplementary Tables 1-4)
4
5
6
7

8 **Data Availability Statement:** The mass spectrometry proteomic data can be accessed for
9 reviewing purposes at <https://figshare.com/s/72b949c0934737a15b51>
10
11

12 Following publication, the mass spectrometry proteomic data can be accessed at the following
13 DOI: 10.6084/m9.figshare.23256374
14
15
16
17
18

19 **Acknowledgements**

20
21 The Authors would like to thank Philippe Colin, Aline Aebi, and Jean-Philippe Gaudry from
22 the EPFL Bertarelli Gene Therapy Platform for their expert technical support in vector
23 preparation.
24
25
26
27

28 This work was supported by Great Ormond Street Hospital Charity (GOSH) and SPARKS
29 Children's Medical Research Charity (Grant No. V5018 to H.R.F.). M.B. acknowledges
30 general financial support from SMA Angels Charity, SMA UK, Muscular Dystrophy UK,
31 Action Medical Research, Academy of Medical Sciences and Association Française contre les
32 Myopathies for SMA research in her laboratory. H.K.S. and T.H.G. acknowledge support from
33 the Euan MacDonald Centre for Motor Neuron Disease Research and SMA Europe. E.M.C.
34 was partially funded by a scholarship from Royal Holloway University of London. R.J.Y.-M.
35 acknowledges general financial support from SMA UK (formerly The SMA Trust), through
36 the UK SMA Research Consortium, for SMA research in his laboratory.
37
38
39
40
41
42
43
44
45
46
47
48
49
50

51 **Conflicts of Interest Statement**

52 THG has served on advisory boards for SMA Europe, LifeArc, Roche and Novartis.
53
54
55
56
57

58 **References**

59
60

1. Lefebvre, S., Bürglen, L., Reboullet, S., Clermont, O., Burlet, P., Viollet, L., Benichou, B., Cruaud, C., Millasseau, P., Zeviani, M., *et al.* (1995) Identification and characterization of a Spinal Muscular Atrophy-determining gene. *Cell*, **80**, 155–165. DOI: [10.1016/0092-8674\(95\)90460-3](https://doi.org/10.1016/0092-8674(95)90460-3)
2. Rochette, C.F., Gilbert, N. and Simard, L.R. (2001) SMN gene duplication and the emergence of the SMN2 gene occurred in distinct hominids: SMN2 is unique to Homo sapiens. *Hum. Genet.*, **108**, 255–266. DOI: [10.1007/s004390100473](https://doi.org/10.1007/s004390100473)
3. Lorson, C.L. and Androphy, E.J. (2000) An exonic enhancer is required for inclusion of an essential exon in the SMA-determining gene SMN. *Hum. Mol. Genet.*, **9**, 259–265. DOI: [10.1093/hmg/9.2.259](https://doi.org/10.1093/hmg/9.2.259)
4. Feldkötter, M., Schwarzer, V., Wirth, R., Wienker, T.F. and Wirth, B. (2002) Quantitative analyses of SMN1 and SMN2 based on real-time lightcycler PCR: Fast and highly reliable carrier testing and prediction of severity of spinal muscular atrophy. *Am. J. Hum. Genet.*, **70**, 358–368. DOI: [10.1086/338627](https://doi.org/10.1086/338627)
5. Ramdas, S. and Servais, L. (2020) New treatments in spinal muscular atrophy: an overview of currently available data. *Expert Opin. Pharmacother.*, **21**, 307–315. DOI: [10.1080/14656566.2019.1704732](https://doi.org/10.1080/14656566.2019.1704732)
6. Simone, C., Ramirez, A., Bucchia, M., Rinchetti, P., Rideout, H., Papadimitriou, D., Re, D.B. and Corti, S. (2016) Is Spinal Muscular Atrophy a disease of the motor neurons only: pathogenesis and therapeutic implications? *Cell. Mol. Life Sci.*, **73**, 1003–1020. DOI: [10.1007/s00018-015-2106-9](https://doi.org/10.1007/s00018-015-2106-9).
7. Yeo, C.J.J. and Darras, B.T. (2020) Overturning the Paradigm of Spinal Muscular Atrophy as Just a Motor Neuron Disease. *Pediatr. Neurol.*, **109**, 12–19. DOI: [10.1016/j.pediatrneurol.2020.01.003](https://doi.org/10.1016/j.pediatrneurol.2020.01.003)

- 1
2
3 8. Huang, J.-J., Jong, Y.-J., Huang, M.-Y., Chiang, C.-H. and Huang, T.-Y. (1996)
4
5 Electrocardiographic Findings in Children with Spinal Muscular Atrophy. *Jpn. Heart J.*,
6
7 **37**, 239–242. DOI: 10.1536/ihj.37.239
8
9
- 10 9. Finsterer, J. and Stöllberger, C. (1999) Cardiac Involvement in Werdnig-Hoffmann's
11
12 Spinal Muscular Atrophy. *Cardiology*, **92**, 178–182. DOI: 10.1159/000006968
13
14
15
- 16 10. Bach, J.R. (2007) Medical considerations of long-term survival of Werdnig-Hoffmann
17
18 disease. *Am. J. Phys. Med. Rehabil.*, **86**, 349–355. DOI:
19
20 10.1097/PHM.0b013e31804b1d66
21
22
- 23 11. Rudnik-Schöneborn, S., Heller, R., Berg, C., Betzler, C., Grimm, T., Eggermann, T.,
24
25 Eggermann, K., Wirth, R., Wirth, B. and Zerres, K. (2008) Congenital heart disease is a
26
27 feature of severe infantile spinal muscular atrophy. *J. Med. Genet.*, **45**, 635–638. DOI:
28
29 10.1136/jmg.2008.057950
30
31
32
- 33 12. Bevan, A.K., Hutchinson, K.R., Foust, K.D., Braun, L., McGovern, V.L., Schmelzer,
34
35 L., Ward, J.G., Petruska, J.C., Lucchesi, P.A., Burghes, A.H.M., *et al.* (2010) Early heart
36
37 failure in the SMN Δ 7 model of spinal muscular atrophy and correction by postnatal
38
39 scAAV9-SMN delivery. *Hum. Mol. Genet.*, **19**, 3895–3905. DOI: 10.1093/hmg/ddq300
40
41
42
- 43 13. Shababi, M., Habibi, J., Ma, L., Glascock, J., Sowers, J.R. and Lorson, C.L. (2012)
44
45 Partial restoration of cardio-vascular defects in rescued severe model of Spinal Muscular
46
47 Atrophy. *J. Mol. Cell. Cardiol.*, **52**, 1074–1082. DOI: 10.1016/j.yjmcc.2012.01.005
48
49
50
- 51 14. Maxwell, G.K., Szunyogova, E., Shorrocks, H.K., Gillingwater, T.H. and Parson, S.H.
52
53 (2018) Developmental and degenerative cardiac defects in the Taiwanese mouse model
54
55 of severe spinal muscular atrophy. *J. Anat.*, **232**, 965–978. DOI: 10.1111/joa.12793
56
57
58
59
60

- 1
2
3 15. Šoltić, D., Shorrock, H.K., Allardyce, H., Wilson, E.L., Holt, I., Synowsky, S.A.,
4 Shirran, S.L., Parson, S.H., Gillingwater, T.H. and Fuller, H.R. (2019) Lamin A/C
5 dysregulation contributes to cardiac pathology in a mouse model of severe spinal
6 muscular atrophy. *Hum. Mol. Genet.*, **28**, 3515–3527. DOI: [10.1093/hmg/ddz195](https://doi.org/10.1093/hmg/ddz195)
7
8
9
- 10
11
12
13 16. Djordjevic, S.A., Milic-Rasic, V., Brankovic, V., Kosac, A., Vukomanovic, G.,
14 Topalovic, M., Marinkovic, D., Mladenovic, J., Pavlovic, A.S., Bijelic, M., *et al.* (2021)
15 Cardiac findings in pediatric patients with spinal muscular atrophy types 2 and 3. *Muscle*
16 *Nerve*, **63**, 75–83. DOI: [10.1002/mus.27088](https://doi.org/10.1002/mus.27088)
17
18
19
- 20
21
22
23 17. Lipnick, S.L., Agniel, D.M., Aggarwal, R., Makhortova, N.R., Finlayson, S.G., Brocato,
24 A., Palmer, N., Darras, B.T., Kohane, I. and Rubin, L.L. (2019) Systemic nature of
25 spinal muscular atrophy revealed by studying insurance claims. *PLoS One*, **14**,
26 e0213680. DOI: [10.1371/journal.pone.0213680](https://doi.org/10.1371/journal.pone.0213680)
27
28
29
- 30
31
32
33 18. Wijngaarde, C.A., Blank, A.C., Stam, M., Wadman, R.I., Van Den Berg, L.H. and Van
34 Der Pol, W.L. (2017) Cardiac pathology in spinal muscular atrophy: a systematic
35 review. *Orphanet J. Rare Dis.*, **12**, 67. DOI: [10.1186/s13023-017-0613-5](https://doi.org/10.1186/s13023-017-0613-5)
36
37
38
- 39
40
41
42 19. Rajendra, T.K., Gonsalvez, G.B., Walker, M.P., Shpargel, K.B., Salz, H.K. and Matera,
43 A.G. (2007) A *Drosophila melanogaster* model of spinal muscular atrophy reveals a
44 function for SMN in striated muscle. *J. Cell Biol.*, **176**, 831–841. DOI:
45 [10.1083/jcb.200610053](https://doi.org/10.1083/jcb.200610053)
46
47
48
- 49
50
51
52 20. Walker, M.P., Rajendra, T.K., Saieva, L., Fuentes, J.L., Pellizzoni, L. and Matera, A.G.
53 (2008) SMN complex localizes to the sarcomeric Z-disc and is a proteolytic target of
54 calpain. *Hum. Mol. Genet.*, **17**, 3399–3410. DOI: [10.1093/hmg/ddn234](https://doi.org/10.1093/hmg/ddn234)
55
56
57
58
59
60

- 1
2
3
4
5
6
7
8
9
10
11
12
13
14
15
16
17
18
19
20
21
22
23
24
25
26
27
28
29
30
31
32
33
34
35
36
37
38
39
40
41
42
43
44
45
46
47
48
49
50
51
52
53
54
55
56
57
58
59
60
21. Deguise, M.O., Boyer, J.G., McFall, E.R., Yazdani, A., De Repentigny, Y. and Kothary, R. (2016) Differential induction of muscle atrophy pathways in two mouse models of spinal muscular atrophy. *Sci. Rep.*, **6**, 28846. DOI: [10.1038/srep28846](https://doi.org/10.1038/srep28846)
 22. Khayrullina, G., Moritz, K.E., Schooley, J.F., Fatima, N., Viollet, C., McCormack, N.M., Smyth, J.T., Doughty, M.L., Dalgard, C.L., Flagg, T.P., *et al.* (2020) SMN-deficiency disrupts SERCA2 expression and intracellular Ca²⁺ signaling in cardiomyocytes from SMA mice and patient-derived iPSCs. *Skelet. Muscle*, **10**, 16. DOI: [10.1186/s13395-020-00232-7](https://doi.org/10.1186/s13395-020-00232-7)
 23. Mourelatos, Z., Dostie, J., Paushkin, S., Sharma, A., Charroux, B., Abel, L., Rappsilber, J., Mann, M. and Dreyfuss, G. (2002) miRNPs: A novel class of ribonucleoproteins containing numerous microRNAs. *Genes Dev.*, **16**, 720–728. DOI: [10.1101/gad.974702](https://doi.org/10.1101/gad.974702)
 24. Ripolone, M., Ronchi, D., Violano, R., Vallejo, D., Fagiolari, G., Barca, E., Lucchini, V., Colombo, I., Villa, L., Berardinelli, A., *et al.* (2015) Impaired Muscle Mitochondrial Biogenesis and Myogenesis in Spinal Muscular Atrophy. *JAMA Neurol.*, **72**, 666–675. DOI: [10.1001/jamaneurol.2015.0178](https://doi.org/10.1001/jamaneurol.2015.0178)
 25. Tsikitis, M., Galata, Z., Mavroidis, M., Psarras, S. and Capetanaki, Y. (2018) Intermediate filaments in cardiomyopathy. *Biophys. Rev.*, **10**, 1007–1031. DOI: [10.1007/s12551-018-0443-2](https://doi.org/10.1007/s12551-018-0443-2)
 26. Rudnik-Schöneborn, S., Botzenhart, E., Eggermann, T., Senderek, J., Schoser, B.G.H., Schröder, R., Wehnert, M., Wirth, B. and Zerres, K. (2007) Mutations of the LMNA gene can mimic autosomal dominant proximal spinal muscular atrophy. *Neurogenetics*, **8**, 137–142. DOI: [10.1007/s10048-006-0070-0](https://doi.org/10.1007/s10048-006-0070-0)
 27. Iwahara, N., Hisahara, S., Hayashi, T., Kawamata, J. and Shimohama, S. (2015) A novel *lamin A/C* gene mutation causing spinal muscular atrophy phenotype with cardiac

- 1
2
3 involvement: Report of one case. *BMC Neurol.*, **15**, 13. DOI: 10.1186/s12883-015-
4 0269-5
5
6
7
8
9 28. Nafchi, N.A.M., Chilcott, E.M., Brown, S., Fuller, H.R., Bowerman, M. and Yáñez-
10 Muñoz, R.J. (2023) Enhanced expression of the human *Survival motor neuron 1* gene
11 from a codon-optimised cDNA transgene *in vitro* and *in vivo*. *Gene Ther.*, Epub ahead
12 of print. PMID: 37322133. DOI: 10.1038/s41434-023-00406-0.
13
14
15
16
17
18 29. Deguise, M.-O., Beauvais, A., Schneider B.L. and Kothary, R. (2020) Blood flow to the
19 spleen is altered in a mouse model of Spinal Muscular Atrophy. *J. Neuromuscul. Dis.*,
20 **7**, 315-322. DOI: 10.3233/JND-200493
21
22
23
24
25
26 30. Harada, T., Swift, J., Irianto, J., Shin, J.-W., Spinler, K.R., Athirasala, A., Diegmiller,
27 R., Dingal, P.C.D.P., Ivanovska, I.L. and Discher, D.E. (2014) Nuclear lamin stiffness
28 is a barrier to 3D migration, but softness can limit survival. *J. Cell Biol.*, **204**, 669–682.
29 DOI: 10.1083/jcb.201308029
30
31
32
33
34
35
36 31. Swift, J., Ivanovska, I.L., Buxboim, A., Harada, T., Dingal, P.C.D.P., Pinter, J.,
37 Pajerowski, J.D., Spinler, K.R., Shin, J.-W., Tewari, M., *et al.* (2013) Nuclear Lamin-A
38 Scales with Tissue Stiffness and Enhances Matrix-Directed Differentiation. *Science*,
39 **341**, 1240104. DOI: 10.1126/science.1240104
40
41
42
43
44
45
46 32. Borbély, A., Van Der Velden, J., Papp, Z., Bronzwaer, J.G.F., Edes, I., Stienen, G.J.M.
47 and Paulus, W.J. (2005) Cardiomyocyte stiffness in diastolic heart failure. *Circulation*,
48 **111**, 774–781. DOI: 10.1161/01.CIR.0000155257.33485.6D
49
50
51
52
53
54 33. Røe, Å.T., Aronsen, J.M., Skårdal, K., Hamdani, N., Linke, W.A., Danielsen, H.E.,
55 Sejersted, O.M., Sjaastad, I. and Louch, W.E. (2017) Increased passive stiffness
56 promotes diastolic dysfunction despite improved Ca²⁺ handling during left ventricular
57 concentric hypertrophy. *Cardiovasc. Res.*, **113**, 1161–1172. DOI: 10.1093/cvr/cvx087
58
59
60

- 1
2
3
4
5
6
7
8
9
10
11
12
13
14
15
16
17
18
19
20
21
22
23
24
25
26
27
28
29
30
31
32
33
34
35
36
37
38
39
40
41
42
43
44
45
46
47
48
49
50
51
52
53
54
55
56
57
58
59
60
34. Chaytow, H., Huang, Y.-T., Gillingwater, T.H. and Faller, K.M.E. (2018) The role of survival motor neuron protein (SMN) in protein homeostasis. *Cell. Mol. Life Sci.*, **75**, 3877–3894. DOI: [10.1007/s00018-018-2849-1](https://doi.org/10.1007/s00018-018-2849-1)
35. Bernabò, P., Tebaldi, T., Groen, E.J.N., Lane, F.M., Perenthaler, E., Mattedi, F., Newbery, H.J., Zhou, H., Zuccotti, P., Potrich, V., *et al.* (2017) In Vivo Translatome Profiling in Spinal Muscular Atrophy Reveals a Role for SMN Protein in Ribosome Biology. *Cell Rep*, **21**, 953–965. DOI: [10.1016/j.celrep.2017.10.010](https://doi.org/10.1016/j.celrep.2017.10.010)
36. Fallini, C., Donlin-Asp, P.G., Rouanet, J.P., Bassell, G.J. and Rossoll, W. (2016) Deficiency of the survival of motor neuron protein impairs mRNA localization and local translation in the growth cone of motor neurons. *J. Neurosci.*, **36**, 3811–3820. DOI: [10.1523/JNEUROSCI.2396-15.2016](https://doi.org/10.1523/JNEUROSCI.2396-15.2016)
37. Kye, M.J., Niederst, E.D., Wertz, M.H., Gonçalves, I. do C.G., Akten, B., Dover, K.Z., Peters, M., Riessland, M., Neveu, P., Wirth, B., *et al.* (2014) SMN regulates axonal local translation via miR-183/mTOR pathway. *Hum. Mol. Genet.*, **23**, 6318–6331. DOI: [10.1093/hmg/ddu350](https://doi.org/10.1093/hmg/ddu350)
38. van Bergeijk, J., Rydel-Könecke, K., Grothe, C. and Claus, P. (2007) The spinal muscular atrophy gene product regulates neurite outgrowth: importance of the C terminus. *FASEB J.*, **21**, 1492–1502. DOI: [10.1096/fj.06-7136com](https://doi.org/10.1096/fj.06-7136com)
39. Acsadi, G., Lee, I., Li, X., Khaidakov, M., Pecinova, A., Parker, G.C. and Hüttemann, M. (2009) Mitochondrial dysfunction in a neural cell model of spinal muscular atrophy. *J. Neurosci. Res.*, **87**, 2748–2756. DOI: [10.1002/jnr.22106](https://doi.org/10.1002/jnr.22106)
40. Miller, N., Shi, H., Zelikovich, A.S. and Ma, Y.-C. (2016) Motor neuron mitochondrial dysfunction in spinal muscular atrophy. *Hum. Mol. Genet.*, **25**, 3395–3406. DOI: [10.1093/hmg/ddw262](https://doi.org/10.1093/hmg/ddw262)

- 1
2
3 41. Thelen, M.P., Wirth, B. and Kye, M.J. (2020) Mitochondrial defects in the respiratory
4 complex I contribute to impaired translational initiation via ROS and energy
5 homeostasis in SMA motor neurons. *Acta Neuropathol. Commun.*, **8**, 223. DOI:
6 [10.1186/s40478-020-01101-6](https://doi.org/10.1186/s40478-020-01101-6)
7
8
9
10
11
12
13 42. Towbin, J.A. and Bowles, N.E. (2006) Dilated cardiomyopathy: A tale of cytoskeletal
14 proteins and beyond. *J. Cardiovasc. Electrophysiol.*, **17**, 919–926. DOI: [10.1111/j.1540-](https://doi.org/10.1111/j.1540-8167.2006.00530.x)
15 [8167.2006.00530.x](https://doi.org/10.1111/j.1540-8167.2006.00530.x)
16
17
18
19
20
21 43. Davies, B.S.J., Fong, L.G., Yang, S.H., Coffinier, C. and Young, S.G. (2009) The
22 posttranslational processing of prelamin A and disease. *Annu. Rev. Genomics Hum.*
23 *Genet.*, **10**, 153–174. DOI: [10.1146/annurev-genom-082908-150150](https://doi.org/10.1146/annurev-genom-082908-150150)
24
25
26
27
28 44. Carmosino, M., Torretta, S., Procino, G., Gerbino, A., Forleo, C., Favale, S. and Svelto,
29 M. (2014) Role of nuclear Lamin A/C in cardiomyocyte functions. *Biol. Cell*, **106**, 346–
30 358. DOI: [10.1111/boc.201400033](https://doi.org/10.1111/boc.201400033)
31
32
33
34
35
36 45. Gruenbaum, Y. and Foisner, R. (2015) Lamins: Nuclear intermediate filament proteins
37 with fundamental functions in nuclear mechanics and genome regulation. *Annu. Rev.*
38 *Biochem.*, **84**, 131–164. DOI: [10.1146/annurev-biochem-060614-034115](https://doi.org/10.1146/annurev-biochem-060614-034115)
39
40
41
42
43 46. Šoltić, D. and Fuller, H.R. (2020) Molecular Crosstalk Between Non-SMN-Related and
44 SMN-Related Spinal Muscular Atrophy. *Neurosci. Insights*, **15**, 2633105520914301.
45 DOI: [10.1177/2633105520914301](https://doi.org/10.1177/2633105520914301)
46
47
48
49
50
51 47. Mutsaers, C.A., Lamont, D.J., Hunter, G., Wishart, T.M. and Gillingwater, T.H. (2013)
52 Label-free proteomics identifies Calreticulin and GRP75/Mortalin as peripherally
53 accessible protein biomarkers for spinal muscular atrophy. *Genome Med.*, **5**, 95. DOI:
54 [10.1186/gm498](https://doi.org/10.1186/gm498)
55
56
57
58
59
60

- 1
2
3
4
5
6
7
8
9
10
11
12
13
14
15
16
17
18
19
20
21
22
23
24
25
26
27
28
29
30
31
32
33
34
35
36
37
38
39
40
41
42
43
44
45
46
47
48
49
50
51
52
53
54
55
56
57
58
59
60
48. Aghamaleky Sarvestany, A., Hunter, G., Tavendale, A., Lamont, D.J., Llaverro Hurtado, M., Graham, L.C., Wishart, T.M. and Gillingwater, T.H. (2014) Label-free quantitative proteomic profiling identifies disruption of ubiquitin homeostasis as a key driver of Schwann cell defects in spinal muscular atrophy. *J. Proteome Res.*, **13**, 4546–4557. DOI: [10.1021/pr500492j](https://doi.org/10.1021/pr500492j)
49. Fuller, H.R., Gillingwater, T.H. and Wishart, T.M. (2016) Commonality amid diversity: Multi-study proteomic identification of conserved disease mechanisms in spinal muscular atrophy. *Neuromuscul. Disord.*, **26**, 560–569. DOI: [10.1016/j.nmd.2016.06.004](https://doi.org/10.1016/j.nmd.2016.06.004)
50. Captur, G., Arbustini, E., Bonne, G., Syrris, P., Mills, K., Wahbi, K., Mohiddin, S.A., McKenna, W.J., Pettit, S., Ho, C.Y., *et al.* (2018) Lamin and the heart. *Heart*, **104**, 468–479. DOI: [10.1136/heartjnl-2017-312338](https://doi.org/10.1136/heartjnl-2017-312338)
51. Fatkin, D., MacRae, C., Sasaki, T., Wolff, M.R., Porcu, M., Frenneaux, M., Atherton, J., Vidaillet, H.J., Spudich, S., de Girolami, U., *et al.* (1999) Missense Mutations in the Rod Domain of the Lamin A/C Gene As Causes of Dilated Cardiomyopathy and Conduction-System Disease. *N. Engl. J. Med.*, **341**, 1715–1724. DOI: [10.1056/NEJM199912023412302](https://doi.org/10.1056/NEJM199912023412302)
52. Van Berlo, J.H., De Voogt, W.G., Van Der Kooi, A.J., Van Tintelen, J.P., Bonne, G., Yaou, R.B., Duboc, D., Rossenbacker, T., Heidbüchel, H., De Visser, M., *et al.* (2005) Meta-analysis of clinical characteristics of 299 carriers of LMNA gene mutations: Do lamin A/C mutations portend a high risk of sudden death? *J. Mol. Med.*, **83**, 79–83. DOI: [10.1007/s00109-004-0589-1](https://doi.org/10.1007/s00109-004-0589-1)
53. van Rijsingen, I.A.W., Nannenberg, E.A., Arbustini, E., Elliott, P.M., Mogensen, J., Hermans-van Ast, J.F., van der Kooi, A.J., van Tintelen, J.P., van den Berg, M.P.,

- 1
2
3 Grasso, M., *et al.* (2013) Gender-specific differences in major cardiac events and
4 mortality in lamin A/C mutation carriers. *Eur. J. Heart Fail.*, **15**, 376–384. DOI:
5
6 [10.1093/eurjhf/hfs191](https://doi.org/10.1093/eurjhf/hfs191)
7
8
9
10
11 54. Cattin, M.E., Muchir, A. and Bonne, G. (2013) ‘State-of-the-heart’ of cardiac
12 laminopathies. *Curr. Opin. Cardiol.*, **28**, 297–304. DOI:
13
14 [10.1097/HCO.0b013e32835f0c79](https://doi.org/10.1097/HCO.0b013e32835f0c79)
15
16
17
18 55. Brayson, D. and Shanahan, C.M. (2017) Current insights into LMNA cardiomyopathies:
19 Existing models and missing LINC. *Nucleus*, **8**, 17–33. DOI:
20
21 [10.1080/19491034.2016.1260798](https://doi.org/10.1080/19491034.2016.1260798)
22
23
24
25
26 56. Storey, E.C. and Fuller, H.R. (2022) Genotype-Phenotype Correlations in Human
27 Diseases Caused by Mutations of LINC Complex-Associated Genes: A Systematic
28 Review and Meta-Summary. *Cells*, **11**.4065. DOI: [10.3390/cells11244065](https://doi.org/10.3390/cells11244065)
29
30
31
32
33 57. Battey, E., Stroud, M.J. and Ochala, J. (2020) Using nuclear envelope mutations to
34 explore age-related skeletal muscle weakness. *Clin. Sci.*, **134**, 2177–2187. DOI:
35
36 [10.1042/CS20190066](https://doi.org/10.1042/CS20190066)
37
38
39
40
41 58. Cho, S., Vashisth, M., Abbas, A., Majkut, S., Vogel, K., Xia, Y., Ivanovska, I.L., Irianto,
42 J., Tewari, M., Zhu, K., *et al.* (2019) Mechanosensing by the lamina protects against
43 nuclear rupture, DNA damage, and cell cycle arrest. *Dev. Cell*, **49**, 920–935. DOI:
44
45 [10.1016/j.devcel.2019.04.020](https://doi.org/10.1016/j.devcel.2019.04.020)
46
47
48
49
50
51 59. Buxboim, A., Swift, J., Irianto, J., Spinler, K.R., Dingal, P.C.D.P., Athirasala, A., Kao,
52 Y.-R.C., Cho, S., Harada, T., Shin, J.-W., *et al.* (2014) Matrix elasticity regulates lamin-
53 A,C phosphorylation and turnover with feedback to actomyosin. *Curr. Biol.*, **24**, 1909–
54
55 1917. DOI: [10.1016/j.cub.2014.07.001](https://doi.org/10.1016/j.cub.2014.07.001)
56
57
58
59
60

- 1
2
3
4
5
6
7
8
9
10
11
12
13
14
15
16
17
18
19
20
21
22
23
24
25
26
27
28
29
30
31
32
33
34
35
36
37
38
39
40
41
42
43
44
45
46
47
48
49
50
51
52
53
54
55
56
57
58
59
60
60. Uzer, G., Rubin, C.T. and Rubin, J. (2016) Cell mechanosensitivity is enabled by the LINC nuclear complex. *Curr. Mol. Biol. Rep.*, **2**, 36–47. DOI: 10.1007/s40610-016-0032-8
61. Pradhan, R., Ranade, D. and Sengupta, K. (2018) Emerin modulates spatial organization of chromosome territories in cells on softer matrices. *Nucleic Acids Res.*, **46**, 5561–5586. DOI: 10.1093/nar/gky288
62. Lammerding, J., Schulze, P.C., Takahashi, T., Kozlov, S., Sullivan, T., Kamm, R.D., Stewart, C.L. and Lee, R.T. (2004) Lamin A/C deficiency causes defective nuclear mechanics and mechanotransduction. *J. Clin. Invest.*, **113**, 370–378. DOI: 10.1172/JCI200419670
63. Lanzicher, T., Martinelli, V., Puzzi, L., Del Favero, G., Codan, B., Long, C.S., Mestroni, L., Taylor, M.R.G. and Sbaizero, O. (2015) The cardiomyopathy lamin A/C D192G mutation disrupts whole-cell biomechanics in cardiomyocytes as measured by atomic force microscopy loading-unloading curve analysis. *Sci. Rep.*, **5**, 13388. DOI: 10.1038/srep13388
64. Nikolova, V., Leimena, C., McMahon, A.C., Tan, J.C., Chandar, S., Jogia, D., Kesteven, S.H., Michalicek, J., Otway, R., Verheyen, F., *et al.* (2004) Defects in nuclear structure and function promote dilated cardiomyopathy in lamin A/C-deficient mice. *J. Clin. Invest.*, **113**, 357–369. DOI: 10.1172/JCI200419448
65. Ramos, F.J., Chen, S.C., Garelick, M.G., Dai, D.-F., Liao, C.-Y., Schreiber, K.H., MacKay, V.L., An, E.H., Strong, R., Ladiges, W.C., *et al.* (2012) Rapamycin reverses elevated mTORC1 signaling in lamin A/C-deficient mice, rescues cardiac and skeletal muscle function, and extends survival. *Sci. Transl. Med.*, **4**, 144ra103. DOI: 10.1126/scitranslmed.3003802

- 1
2
3 66. Cahill, T.J., Ashrafian, H. and Watkins, H. (2013) Genetic cardiomyopathies causing
4 heart failure. *Circ. Res.*, **113**, 660–675. DOI: 10.1161/CIRCRESAHA.113.300282
5
6
7
8
9 67. Soussi-Yanicostas, N., Ben Hamida, C., Bejaoui, K., Hentati, F., Ben Hamida, M. and
10 Butler-Browne, G.S. (1992) Evolution of muscle specific proteins in Werdnig-
11 Hoffman's disease. *J. Neurol. Sci.*, **109**, 111–120. DOI: 10.1016/0022-510x(92)90103-
12
13
14
15
16
17
18 68. Capetanaki, Y., Bloch, R.J., Kouloumenta, A., Mavroidis, M. and Psarras, S. (2007)
19 Muscle intermediate filaments and their links to membranes and membranous
20 organelles. *Exp. Cell Res.*, **313**, 2063–2076. DOI: 10.1016/j.yexcr.2007.03.033
21
22
23
24
25
26 69. Heffler, J., Shah, P.P., Robison, P., Phyto, S., Veliz, K., Uchida, K., Bogush, A.,
27 Rhoades, J., Jain, R. and Prosser, B.L. (2020) A Balance Between Intermediate
28 Filaments and Microtubules Maintains Nuclear Architecture in the Cardiomyocyte.
29
30
31
32
33
34
35
36 70. Granger, B.L. and Lazarides, E. (1978) The existence of an insoluble Z disc scaffold in
37 chicken skeletal muscle. *Cell*, **15**, 1253–1268. DOI: 10.1016/0092-8674(78)90051-x
38
39
40
41 71. Hijikata, T., Murakami, T., Imamura, M., Fujimaki, N. and Ishikawa, H. (1999) Plectin
42 is a linker of intermediate filaments to Z-discs in skeletal muscle fibers. *J. Cell Sci.*, **112**,
43
44
45
46
47
48
49 72. Maggi, L., Mavroidis, M., Psarras, S., Capetanaki, Y. and Lattanzi, G. (2021) Skeletal
50 and cardiac muscle disorders caused by mutations in genes encoding intermediate
51 filament proteins. *Int. J. Mol. Sci.*, **22**, 4256. DOI: 10.3390/ijms22084256
52
53
54
55
56
57
58
59
60

- 1
2
3 73. Jaka, O., Casas-Fraile, L., López De Munain, A. and Sáenz, A. (2015) Costamere
4 proteins and their involvement in myopathic processes. *Expert Rev. Mol. Med.*, **17**, e12.
5
6 *DOI: 10.1017/erm.2015.9*
7
8
9
10 74. Bär, H., Strelkov, S. V., Sjöberg, G., Aebi, U. and Herrmann, H. (2004) The biology of
11 desmin filaments: How do mutations affect their structure, assembly, and organisation?
12
13 *J. Struct. Biol.*, **148**, 137–152. *DOI: 10.1016/j.jsb.2004.04.003*
14
15
16
17 75. Milner, D.J., Weitzer, G., Tran, D., Bradley, A. and Capetanaki, Y. (1996) Disruption
18 of muscle architecture and myocardial degeneration in mice lacking desmin. *J. Cell*
19 *Biol.*, **134**, 1255–1270. *DOI: 10.1083/jcb.134.5.1255*
20
21
22
23 76. Li, Z., Mericskay, M., Agbulut, O., Butler-Browne, G., Carlsson, L., Thornell, L.-E.,
24 Babinet, C. and Paulin, D. (1997) Desmin is essential for the tensile strength and
25 integrity of myofibrils but not for myogenic commitment, differentiation, and fusion of
26 skeletal muscle. *J. Cell Biol.*, **139**, 129–144. *DOI: 10.1083/jcb.139.1.129*
27
28
29
30 77. Lovering, R.M., O'Neill, A., Muriel, J.M., Prosser, B.L., Strong, J. and Bloch, R.J.
31 (2011) Physiology, structure, and susceptibility to injury of skeletal muscle in mice
32 lacking keratin 19-based and desmin-based intermediate filaments. *Am. J. Physiol. Cell*
33 *Physiol.*, **300**, C803–C813. *DOI: 10.1152/ajpcell.00394.2010*
34
35
36 78. Meyer, G.A. and Lieber, R.L. (2012) Skeletal muscle fibrosis develops in response to
37 desmin deletion. *Am. J. Physiol. Cell Physiol.*, **302**, C1609–C1620. *DOI:*
38 *10.1152/ajpcell.00441.2011*
39
40
41
42 79. Carlsson, L. and Thornell, L.-E. (2001) Desmin-related myopathies in mice and man.
43 *Acta Physiol. Scand.*, **171**, 341–348. *DOI: 10.1046/j.1365-201X.2001.00837.x*
44
45
46
47
48
49
50
51
52
53
54
55
56
57
58
59
60

- 1
2
3 80. Anderson, J., Li, Z. and Goubel, F. (2001) Passive stiffness is increased in soleus muscle
4 of desmin knockout mouse. *Muscle Nerve*, **24**, 1090–1092. DOI: 10.1002/mus.1115
5
6
7
8
9 81. Münch, J. and Abdelilah-Seyfried, S. (2021) Sensing and Responding of
10 Cardiomyocytes to Changes of Tissue Stiffness in the Diseased Heart. *Front. Cell Dev.*
11 *Biol.*, **9**, 642840. DOI: 10.3389/fcell.2021.642840
12
13
14
15
16 82. Parker, K.K. and Ingber, D.E. (2007) Extracellular matrix, mechanotransduction and
17 structural hierarchies in heart tissue engineering. *Phil. Trans. R. Soc. B*, **362**, 1267–1279.
18 DOI: 10.1098/rstb.2007.2114
19
20
21
22
23 83. Farquharson, C. and Robins, S.P. (1989) The distribution of elastin in developing and
24 adult rat organs using immunocytochemical techniques. *J. Anat.*, **165**, 225–36.
25
26
27
28
29 84. Montero, P., Flandes-Iparraguirre, M., Musquiz, S., Pérez Araluce, M., Plano, D.,
30 Sanmartín, C., Orive, G., Gavira, J.J., Prosper, F. and Mazo, M.M. (2020) Cells,
31 Materials, and Fabrication Processes for Cardiac Tissue Engineering. *Front. Bioeng.*
32 *Biotechnol.*, **8**, 955. DOI: 10.3389/fbioe.2020.00955
33
34
35
36
37
38
39 85. Li, S.-H., Sun, Z., Guo, L., Han, M., Wood, M.F.G., Ghosh, N., Vitkin, I.A., Weisel,
40 R.D. and Li, R.-K. (2012) Elastin overexpression by cell-based gene therapy preserves
41 matrix and prevents cardiac dilation. *J. Cell Mol. Med.*, **16**, 2429–2439. DOI:
42 10.1111/j.1582-4934.2012.01560.x
43
44
45
46
47
48
49 86. Cociolone, A.J., Hawes, J.Z., Staiculescu, M.C., Johnson, E.O., Murshed, M. and
50 Wagenseil, J.E. (2018) Elastin, arterial mechanics, and cardiovascular disease. *Am. J.*
51 *Physiol. Heart Circ. Physiol.*, **315**, H189–H205. DOI: 10.1152/ajpheart.00087.2018
52
53
54
55
56 87. Engler, A.J., Carag-Krieger, C., Johnson, C.P., Raab, M., Tang, H.-Y., Speicher, D.W.,
57 Sanger, J.W., Sanger, J.M. and Discher, D.E. (2008) Embryonic cardiomyocytes beat
58
59
60

- best on a matrix with heart-like elasticity: scar-like rigidity inhibits beating. *J. Cell Sci.*, **121**, 3794–3802. DOI: 10.1242/jcs.029678
88. Sato, S., Ashraf, M., Millard, R.W., Fujiwara, H. and Schwartz, A. (1983) Connective tissue changes in early ischemia of porcine myocardium: An ultrastructural study. *J. Mol. Cell Cardiol.*, **15**, 261–275. DOI: 10.1016/0022-2828(83)90281-x
89. Sugayama, S.M.M., Moisés, R.L., Wagênfur, J., Ikari, N.M., Abe, K.T., Leone, C., Da Silva, C.A.A., Ferrari Chauffaille, M.de L.L. and Kim, C.A. (2003) Williams-Beuren syndrome. Cardiovascular abnormalities in 20 patients diagnosed with fluorescence in situ hybridization. *Arq. Bras. Cardiol.*, **81**, 468–473. DOI: 10.1590/S0066-782X2003001300003
90. Hou, C., Zheng, J., Liu, W., Xie, L., Sun, X., Zhang, Y., Xu, M., Li, Y. and Xiao, T. (2021) Identification and characterization of a novel ELN mutation in congenital heart disease with pulmonary artery stenosis. *Sci. Rep.*, **11**, 14154. DOI: 10.1038/s41598-021-93736-1
91. Shi, X., Zhang, S., Liu, Y., Brazile, B., Cooley, J., Butler, J.R., McMahan, S.R., Perez, K.L., Xu, J., Eastep, T., *et al.* (2023) Spatial distribution and network morphology of epicardial, endocardial, interstitial, and Purkinje cell-associated elastin fibers in porcine left ventricle. *Bioact. Mater.*, **19**, 348–359. DOI: 10.1016/j.bioactmat.2022.04.019
92. Fomovsky, G.M., Thomopoulos, S. and Holmes, J.W. (2010) Contribution of extracellular matrix to the mechanical properties of the heart. *J. Mol. Cell Cardiol.*, **48**, 490–496. DOI: 10.1016/j.yjmcc.2009.08.003
93. Boyden, P.A., Dun, W. and Robinson, R.B. (2016) Cardiac Purkinje fibers and Arrhythmias; The GK Moe Award Lecture 2015. *Heart Rhythm*, **13**, 1172–1181. DOI: 10.1016/j.hrthm.2016.01.011

- 1
2
3 94. Tanaka, H., Nishi, S., Nuruki, K. and Tanaka, N. (1977) Myocardial ultrastructural
4 changes in Kugelberg-Welander syndrome. *Br. Heart J.*, **39**, 1390–1393. DOI:
5
6 [10.1136/hrt.39.12.1390](https://doi.org/10.1136/hrt.39.12.1390)
7
8
9
10
11 95. Dawood, A.F., Alzamil, N.M., Hewett, P.W., Momenah, M.A., Dallak, M., Kamar, S.S.,
12 Abdel Kader, D.H., Yassin, H., Haidara, M.A., Maarouf, A., *et al.* (2022) Metformin
13 Protects against Diabetic Cardiomyopathy: An Association between Desmin–Sarcomere
14 Injury and the iNOS/mTOR/TIMP-1 Fibrosis Axis. *Biomedicines*, **10**, 984. DOI:
15
16 [10.3390/biomedicines10050984](https://doi.org/10.3390/biomedicines10050984)
17
18
19
20
21
22
23 96. Palmisano, M.G., Bremner, S.N., Hornberger, T.A., Meyer, G.A., Domenighetti, A.A.,
24 Shah, S.B., Kiss, B., Kellermayer, M., Ryan, A.F. and Lieber, R.L. (2015) Skeletal
25 muscle intermediate filaments form a stress-transmitting and stress-signaling network.
26
27 *J. Cell Sci.*, **128**, 219–224. DOI: [10.1242/jcs.142463](https://doi.org/10.1242/jcs.142463)
28
29
30
31
32
33 97. Berciano, M.T., Castillo-Iglesias, M.S., Val-Bernal, J.F., Lafarga, V., Rodriguez-Rey,
34 J.C., Lafarga, M. and Tapia, O. (2020) Mislocalization of SMN from the I-band and M-
35 band in human skeletal myofibers in spinal muscular atrophy associates with primary
36 structural alterations of the sarcomere. *Cell Tissue Res.*, **381**, 461–478. DOI:
37
38 [10.1007/s00441-020-03236-3](https://doi.org/10.1007/s00441-020-03236-3)
39
40
41
42
43
44
45 98. Liu, H.-X., Jing, Y.-X., Wang, J.-J., Yang, Y.-P., Wang, Y.-X., Li, H.-R., Song, L., Li,
46 A.-H., Cui, H.-L. and Jing, Y. (2020) Expression patterns of intermediate filament
47 proteins desmin and lamin A in the developing conduction system of early human
48 embryonic hearts. *J. Anat.*, **236**, 540–548. DOI: [10.1111/joa.13108](https://doi.org/10.1111/joa.13108)
49
50
51
52
53
54
55 99. Brodsky, G.L., Muntoni, F., Miodic, S., Sinagra, G., Sewry, C.A. and Mestroni, L.
56 (2000) Lamin A/C gene mutation associated with dilated cardiomyopathy with variable
57
58
59
60

- 1
2
3 skeletal muscle involvement. *Circulation*, **101**, 473–476. DOI:
4
5 [10.1161/01.cir.101.5.473](https://doi.org/10.1161/01.cir.101.5.473)
6
7
8
9 100. Lindgren, M., Robertson, J., Adiels, M., Schaufelberger, M., Åberg, M., Torén, K.,
10
11 Waern, M., Åberg, N.D. and Rosengren, A. (2020) Elevated resting heart rate in
12
13 adolescent men and risk of heart failure and cardiomyopathy. *ESC Heart Fail.*, **7**, 1178–
14
15 1185. DOI: [10.1002/ehf2.12726](https://doi.org/10.1002/ehf2.12726)
16
17
18 101. Heier, C.R., Satta, R., Lutz, C. and Didonato, C.J. (2010) Arrhythmia and cardiac defects
19
20 are a feature of spinal muscular atrophy model mice. *Hum. Mol. Genet.*, **19**, 3906–3918.
21
22 DOI: [10.1093/hmg/ddq330](https://doi.org/10.1093/hmg/ddq330)
23
24
25 102. Afilalo, J., Sebag, I.A. Chalifour, L.E., Rivas, D., Akter, R., Sharma, K. and Duque, G.
26
27 (2007) Age-related changes in lamin A/C expression in cardiomyocytes. *Am. J. Physiol.*
28
29 *Heart Circ. Physiol.*, **293**, H1451-H1456. DOI: [10.1152/ajpheart.01194.2006](https://doi.org/10.1152/ajpheart.01194.2006)
30
31
32
33 103. Lieber, S.C., Qiu, H., Chen, L., Shen, Y.-T., Hong, C., Hunter, W.C., Aubry, N., Vatner,
34
35 S.F. and Vatner, D.E. (2008) Cardiac dysfunction in aging conscious rats: altered cardiac
36
37 cytoskeletal proteins as a potential mechanism. *Am. J. Physiol. Heart Circ. Physiol.*,
38
39 **295**, H860-H866. DOI: [10.1152/ajpheart.00146.2008](https://doi.org/10.1152/ajpheart.00146.2008)
40
41
42
43 104. Sarbacher, C.A. and Halper, J.T. (2019) Connective tissue and age-related diseases.
44
45 *Subcell. Biochem.*, **91**, 281-310. DOI: [10.1007/978-981-13-3681-2_11](https://doi.org/10.1007/978-981-13-3681-2_11)
46
47
48 105. Russ, D.W. and Grandy, J.S. (2011) Increased desmin expression in hindlimb muscles
49
50 of aging rats. *J. Cachexia Sarcopenia Muscle*, **2**, 175-180. DOI: [10.1007/s13539-011-](https://doi.org/10.1007/s13539-011-0033-7)
51
52 [0033-7](https://doi.org/10.1007/s13539-011-0033-7)
53
54
55 106. Bowerman, M., Murray, L.M., Beauvais, A., Pinheiro, B. and Kothary, R. (2012) A
56
57 critical smn threshold in mice dictates onset of an intermediate spinal muscular atrophy
58
59
60

- 1
2
3 phenotype associated with a distinct neuromuscular junction pathology. *Neuromuscul.*
4
5 *Disord.*, **22**, 263–276. DOI: 10.1016/j.nmd.2011.09.007
6
7
8
9 107. DiDonato, C.J., Lorson, C.L., De Repentigny, Y., Simard, L., Chartrand, C., Androphy,
10 E.J. and Kothary, R. (2001) Regulation of murine survival motor neuron (Smn) protein
11 levels by modifying Smn exon 7 splicing. *Hum. Mol. Genet.*, **10**, 2727–2736. DOI:
12 10.1093/hmg/10.23.2727
13
14
15
16
17
18 108. Hammond, S.M., Gogliotti, R.G., Rao, V., Beauvais, A., Kothary, R. and DiDonato, C.J.
19 (2010) Mouse survival motor neuron alleles that mimic SMN2 splicing and are inducible
20 rescue embryonic lethality early in development but not late. *PLoS One*, **5**, e15887. DOI:
21 10.1371/journal.pone.0015887
22
23
24
25
26
27
28 109. Hsieh-Li, H.M., Chang, J.-G., Jong, Y.-J., Wu, M.-H., Wang, N.M., Tsai, C.H. and Li,
29 H. (2000) A mouse model for spinal muscular atrophy. *Nat. Genet.*, **24**, 66–70. DOI:
30 10.1038/71709
31
32
33
34
35
36 110. Fuller, H.R., Hurtado, M.L., Wishart, T.M. and Gates, M.A. (2014) The rat striatum
37 responds to nigro-striatal degeneration via the increased expression of proteins
38 associated with growth and regeneration of neuronal circuitry. *Proteome Sci.*, **12**, 20.
39 DOI: 10.1186/1477-5956-12-20
40
41
42
43
44
45 111. Huang, D.W., Sherman, B.T. and Lempicki, R.A. (2009) Systematic and integrative
46 analysis of large gene lists using DAVID bioinformatics resources. *Nat. Protoc.*, **4**, 44–
47 57. DOI: 10.1038/nprot.2008.211
48
49
50
51
52
53 112. Huang, D.W., Sherman, B.T. and Lempicki, R.A. (2009) Bioinformatics enrichment
54 tools: Paths toward the comprehensive functional analysis of large gene lists. *Nucleic*
55 *Acids Res.*, **37**, 1–13. DOI: 10.1093/nar/gkn923
56
57
58
59
60

- 1
2
3
4
5
6
7
8
9
10
11
12
13
14
15
16
17
18
19
20
21
22
23
24
25
26
27
28
29
30
31
32
33
34
35
36
37
38
39
40
41
42
43
44
45
46
47
48
49
50
51
52
53
54
55
56
57
58
59
60
113. Krämer, A., Green, J., Pollard, J. and Tugendreich, S. (2014) Causal analysis approaches in Ingenuity Pathway Analysis. *Bioinformatics*, **30**, 523–530. DOI: [10.1093/bioinformatics/btt703](https://doi.org/10.1093/bioinformatics/btt703)
114. Blessing, D., Vachey, G., Pythoud, C., Rey, M., Padrun, V., Wurm, F.M., Schneider, B.L. and Déglon, N. (2018) Scalable Production of AAV9 Vectors in Orbitally Shaken HEK293 Cells. *Mol. Ther. Methods Clin. Dev.*, **13**, 14–26. DOI: [10.1016/j.omtm.2018.11.004](https://doi.org/10.1016/j.omtm.2018.11.004)
115. Šoltić, D., Bowerman, M., Stock, J., Shorrock, H.K., Gillingwater, T.H. and Fuller, H.R. (2018) Multi-Study Proteomic and Bioinformatic Identification of Molecular Overlap between Amyotrophic Lateral Sclerosis (ALS) and Spinal Muscular Atrophy (SMA). *Brain Sci.*, **8**, 212. DOI: [10.3390/brainsci8120212](https://doi.org/10.3390/brainsci8120212)
116. Young, P.J., Le, T.T., Thi Man, N., Burghes, A.H.M. and Morris, G.E. (2000) The relationship between SMN, the spinal muscular atrophy protein, and nuclear coiled bodies in differentiated tissues and cultured cells. *Exp. Cell Res.*, **256**, 365–374. DOI: [10.1006/excr.2000.4858](https://doi.org/10.1006/excr.2000.4858)
117. Abramoff, M.D., Magalhães, P.J. and Ram, S.J. (2004) Image processing with imageJ. *Biophotonics Intern.*, **11**, 36–41. DOI: [10.1201/9781420005615.ax4](https://doi.org/10.1201/9781420005615.ax4)
118. Jensen, E.C. (2013) Quantitative Analysis of Histological Staining and Fluorescence Using ImageJ. *Anat. Rec.*, **296**, 378–381. DOI: [10.1002/ar.22641](https://doi.org/10.1002/ar.22641)
119. Heberle, H., Meirelles, G.V., da Silva, F.R., Telles, G.P. and Minghim, R. (2015) InteractiVenn: A web-based tool for the analysis of sets through Venn diagrams. *BMC Bioinformatics*, **16**, 169. DOI: [10.1186/s12859-015-0611-3](https://doi.org/10.1186/s12859-015-0611-3)

Legends to Figures

Figure 1. Summary and bioinformatics analysis of the proteomic profiles of heart tissues differentially abundant in the *Smn*^{2B/-} and Taiwanese mice models of SMA compared to age-matched WT mice. (A) Venn diagram showing an overlap of 50 proteins identified as significantly up- or down-regulated in both *Smn*^{2B/-} and Taiwanese mouse models of SMA (an unused ProtScore (conf) > 0.05, detected by ≥2 unique peptides, and a statistically significant (p≤0.05) fold change of ≥1.25 or ≤0.8). **(B)** Heat map illustrating the size of fold-change in proteins found to be dysregulated in both mice models of SMA. Two-way comparisons generated in IPA® in which the following were ranked by -log(p-value) for each SMA mouse model: **(C)** Disease & disorders, physiological system development & function; **(D)** Molecular & cellular functions and **(E)** Canonical pathways. **(F)** Schematic illustrating the cellular components impacted by the significantly dysregulated proteins of the *Smn*^{2B/-} mouse model of SMA as determined following DAVID analysis. Image created with BioRender.com.

Figure 2. Levels and distribution of SMN in heart tissues from *Smn*^{2B/-} mice following AAV9-mediated *SMN1* delivery at P0. (A) Representative western blots of SMN levels in heart tissues from untreated *Smn*^{2B/-} mice, *Smn*^{2B/-} mice following AAV9-mediated treatment with and without *SMN1* from two sources plus a corresponding age-matched WT mouse (P18). The bar graph represents average SMN levels expressed relative to the corresponding WT mouse. **(B)** Representative immunofluorescent images (IMFs) for SMN staining within heart tissues from untreated *Smn*^{2B/-} mice and *Smn*^{2B/-} mice following treatment with AAV9-mediated *SMN1* from two sources. ***p<0.001. Scale bars represent 75 μm.

Figure 3. Levels and distribution of lamin A/C in heart tissues from *Smn*^{2B/-} mice following AAV9-mediated *SMN1* delivery at P0. (A) Representative western blots of lamin

1
2
3 A/C levels in heart tissues from WT mice (P18), untreated *Smn*^{2B/-} mice and *Smn*^{2B/-} mice
4 following AAV9-mediated treatment with *SMNI* from two sources. The bar graph represents
5 average lamin A/C levels expressed relative to WT mice. **(B)** Representative western blots of
6 lamin A/C levels in heart tissues from untreated *Smn*^{2B/-} mice and *Smn*^{2B/-} mice following
7 AAV9-mediated treatment without *SMNI* (vehicle control) from two different vector sources.
8 The bar graph represents average lamin A/C levels expressed relative to untreated *Smn*^{2B/-} mice.
9
10 **(C)** Representative IMFs for lamin A/C staining within heart tissues from WT mice (P18),
11 untreated *Smn*^{2B/-} mice and *Smn*^{2B/-} mice following AAV9-mediated treatment with *SMNI* from
12 two vector sources. Corresponding bar graph reflects the area of cells stained for lamin A/C
13 corrected for number of cells present (DAPI stain) as determined by ImageJ analysis and
14 expressed relative to corresponding WT mice. Dashed line represents the average lamin A/C
15 levels in WT mice and error bars represent the standard deviation from the mean. **(D)** Images
16 demonstrating dual staining of sarcomeres with alpha-actinin 2 (red) and lamin A/C (green) in
17 WT mice. * $p < 0.05$; ** $p < 0.01$. Scale bars represent 25 μm except the lower panel of **(D)** where
18 they represent 5 μm . Δ represents a combined sample not included in the analysis.

19
20
21
22
23
24
25
26
27
28
29
30
31
32
33
34
35
36
37
38
39
40 **Figure 4. Levels and distribution of desmin in heart tissues from *Smn*^{2B/-} mice following**
41 **AAV9-mediated *SMNI* delivery at P0. (A)** Representative western blots of desmin levels in
42 heart tissues from WT mice (P18), untreated *Smn*^{2B/-} mice and *Smn*^{2B/-} mice following AAV9-
43 mediated treatment with *SMNI* from two sources. The bar graph represents average desmin
44 levels expressed relative to WT mice. **(B)** Representative western blots of desmin levels in
45 heart tissues from untreated *Smn*^{2B/-} mice and *Smn*^{2B/-} mice following AAV9-mediated
46 treatment without *SMNI* (vehicle control) from two different vector sources. The bar graph
47 represents average desmin levels expressed relative to untreated *Smn*^{2B/-} mice. **(C)**
48 Representative IMFs for desmin staining within heart tissues from WT mice (P18), untreated
49
50
51
52
53
54
55
56
57
58
59
60

1
2
3 *Smn*^{2B/-} mice and *Smn*^{2B/-} mice following AAV9-mediated treatment with *SMNI* from two
4 vector sources. Zoomed images to highlight the reduction in desmin positive striations in
5 untreated *Smn*^{2B/-} mice in comparison to WT mice and AAV9-mediated *SMNI* treated *Smn*^{2B/-}
6 mice. Corresponding bar graph reflects the area of cells stained for desmin corrected for
7 number of cells present (DAPI stain) as determined by ImageJ analysis and expressed relative
8 to corresponding WT mice. Dashed line represents the average desmin levels in WT mice and
9 error bars represent the standard deviation from the mean. * $p < 0.05$; ** $p < 0.01$; *** $p < 0.001$.
10 Scale bars represent 75 μm (panels a-d), 25 μm (panels e-g) and 10 μm (panel h).
11
12
13
14
15
16
17
18
19
20
21
22
23

24 **Figure 5. Levels and distribution of elastin in heart tissues from *Smn*^{2B/-} mice following**
25 **AAV9-mediated *SMNI* delivery at P0. (Panels a-d)** Representative heart sections stained
26 with Miller's Elastin van Gieson from WT mice (P18), untreated *Smn*^{2B/-} mice and *Smn*^{2B/-} mice
27 following AAV9-mediated treatment with *SMNI* from two different vector sources. Elastic
28 fibres (blue/black); mature collagen (red); other tissues such as muscle and red blood cells
29 (yellow). **(Panels e-l)** Representative IMFs for elastin staining within heart tissues from WT
30 mice (P18), untreated *Smn*^{2B/-} mice and *Smn*^{2B/-} mice following AAV9-mediated treatment with
31 *SMNI* from two vector sources. Corresponding bar graph reflects the area of cells stained for
32 elastin corrected for number of cells present (DAPI stain) as determined by ImageJ analysis
33 and expressed relative to corresponding WT mice. Dashed line represents the average elastin
34 levels in WT mice and error bars represent the standard deviation from the mean. *** $p < 0.001$.
35 Black scale bars represent 10 μm (panels a-d). White scale bars represent 75 μm (panels e-h)
36 and 10 μm (panels i-l).
37
38
39
40
41
42
43
44
45
46
47
48
49
50
51
52
53

54 **Abbreviations**

55
56
57
58 AWERB Animal Welfare Ethical Review Body
59
60

1		
2		
3	DAVID	Database for Annotation, Visualization and Integrated Discovery
4		
5	ECM	Extracellular matrix
6		
7	Gems	Gemini of the coiled bodies
8		
9		
10	IMF	Immunofluorescent image
11		
12	IPA	Ingenuity Pathway Analysis
13		
14	iPSCs	Induced pluripotent stem cells
15		
16		
17	iTRAQ	Isobaric tags for relative and absolute quantitation
18		
19	P	Post-natal day
20		
21	SMA	Spinal muscular atrophy
22		
23		
24	SMN	Survival motor neuron
25		
26	WT	Wild type
27		
28		
29		
30		
31		
32		
33		
34		
35		
36		
37		
38		
39		
40		
41		
42		
43		
44		
45		
46		
47		
48		
49		
50		
51		
52		
53		
54		
55		
56		
57		
58		
59		
60		

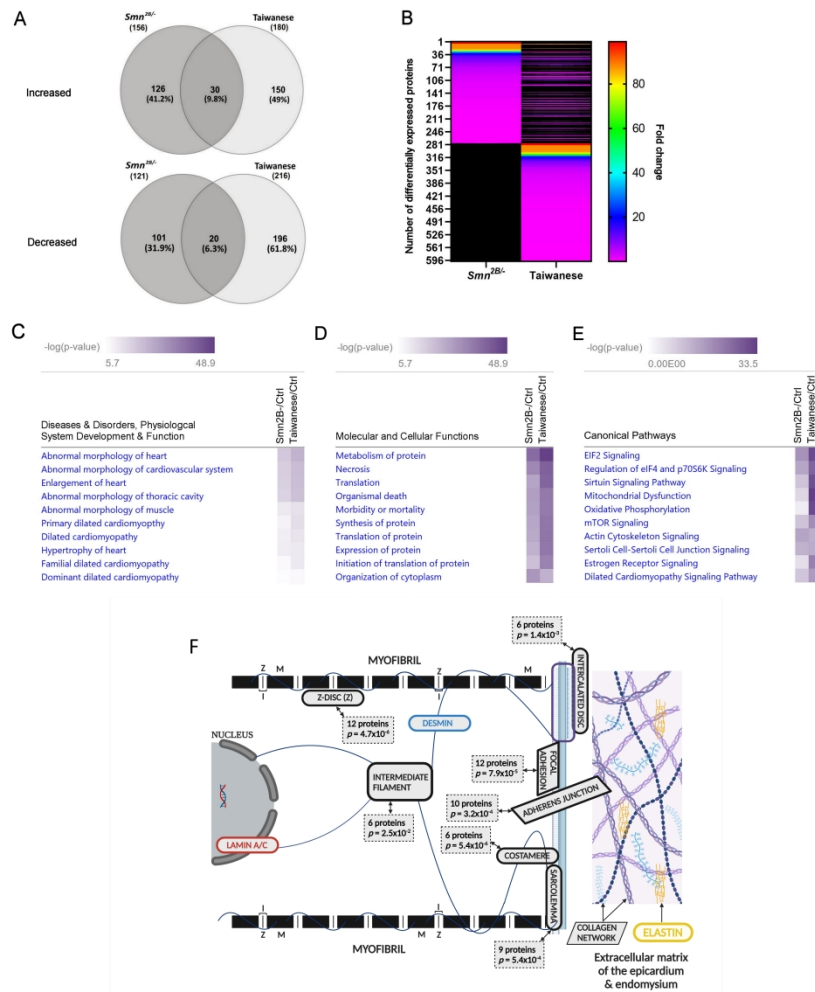


Figure 1. Summary and bioinformatics analysis of the proteomic profiles of heart tissues differentially abundant in the *Smn2B^{-/-}* and Taiwanese mice models of SMA compared to age-matched WT mice. (A) Venn diagram showing an overlap of 50 proteins identified as significantly up- or down-regulated in both *Smn2B^{-/-}* and Taiwanese mouse models of SMA (an unused ProtScore (conf) > 0.05, detected by ≥ 2 unique peptides, and a statistically significant ($p < 0.05$) fold change of >1.25 or <0.8). (B) Heat map illustrating the size of fold-change in proteins found to be dysregulated in both mice models of SMA. Two-way comparisons generated in IPA® in which the following were ranked by $-\log(p\text{-value})$ for each SMA mouse model: (C) Disease & disorders, physiological system development & function; (D) Molecular & cellular functions and (E) Canonical pathways. (F) Schematic illustrating the cellular components impacted by the significantly dysregulated proteins of the *Smn2B^{-/-}* mouse model of SMA as determined following DAVID analysis. Image created with BioRender.com.

1518x1643mm (96 x 96 DPI)

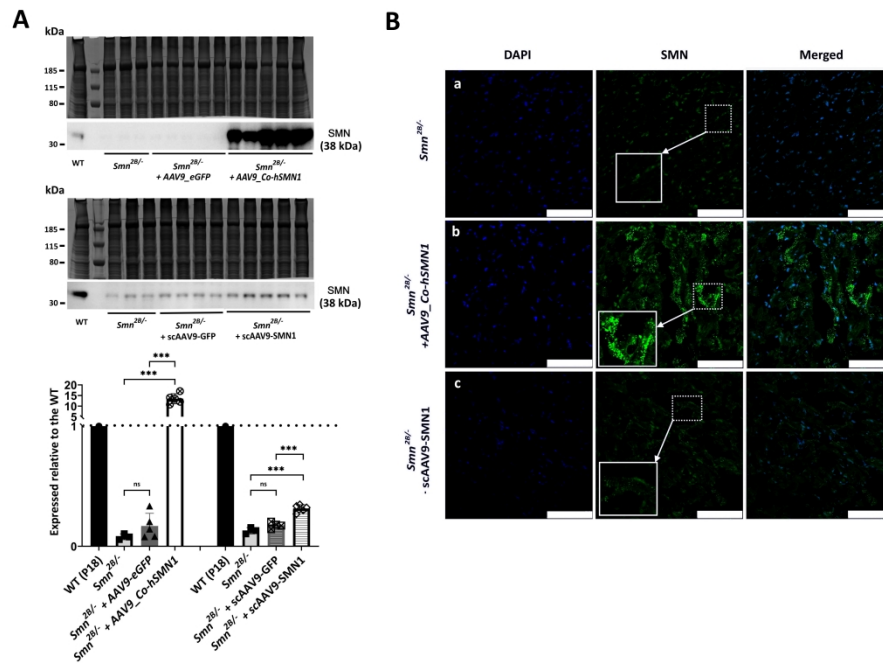


Figure 2. Levels and distribution of SMN in heart tissues from *Smn*2B^{-/-} mice following AAV9-mediated SMN1 delivery at P0. (A) Representative western blots of SMN levels in heart tissues from untreated *Smn*2B^{-/-} mice, *Smn*2B^{-/-} mice following AAV9-mediated treatment with and without SMN1 from two sources plus a corresponding age-matched WT mouse (P18). The bar graph represents average SMN levels expressed relative to the corresponding WT mouse. (B) Representative immunofluorescent images (IMFs) for SMN staining within heart tissues from untreated *Smn*2B^{-/-} mice and *Smn*2B^{-/-} mice following treatment with AAV9-mediated SMN1 from two sources. ***p < 0.001. Scale bars represent 75 μm.

1865x1337mm (96 x 96 DPI)

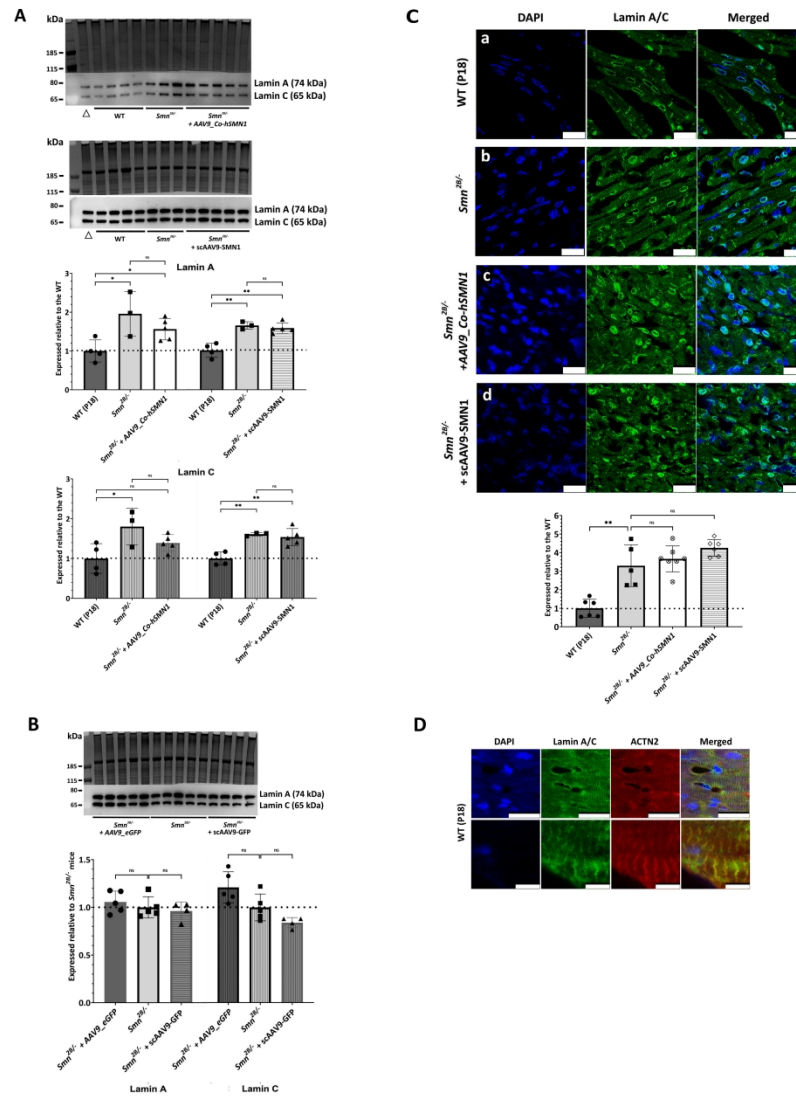


Figure 3. Levels and distribution of lamin A/C in heart tissues from *Smn*^{2B/-} mice following AAV9-mediated SMN1 delivery at P0. (A) Representative western blots of lamin A/C levels in heart tissues from WT mice (P18), untreated *Smn*^{2B/-} mice and *Smn*^{2B/-} mice following AAV9-mediated treatment with SMN1 from two sources. The bar graph represents average lamin A/C levels expressed relative to WT mice. (B) Representative western blots of lamin A/C levels in heart tissues from untreated *Smn*^{2B/-} mice and *Smn*^{2B/-} mice following AAV9-mediated treatment without SMN1 (vehicle control) from two different vector sources. The bar graph represents average lamin A/C levels expressed relative to untreated *Smn*^{2B/-} mice. (C) Representative IMFs for lamin A/C staining within heart tissues from WT mice (P18), untreated *Smn*^{2B/-} mice and *Smn*^{2B/-} mice following AAV9-mediated treatment with SMN1 from two vector sources. Corresponding bar graph reflects the area of cells stained for lamin A/C corrected for number of cells present (DAPI stain) as determined by ImageJ analysis and expressed relative to corresponding WT mice. Dashed line represents the average lamin A/C levels in WT mice and error bars represent the standard deviation from the mean. (D) Images demonstrating dual staining of sarcomeres with alpha-actinin 2 (red) and lamin A/C (green) in WT mice. * $p < 0.05$; ** $p < 0.01$. Scale bars represent 25 μm except the lower panel of (D)

1
2
3 where they represent 5 μm . Δ represents a combined sample not included in the analysis.
4

5 1400x1782mm (96 x 96 DPI)
6
7
8
9
10
11
12
13
14
15
16
17
18
19
20
21
22
23
24
25
26
27
28
29
30
31
32
33
34
35
36
37
38
39
40
41
42
43
44
45
46
47
48
49
50
51
52
53
54
55
56
57
58
59
60

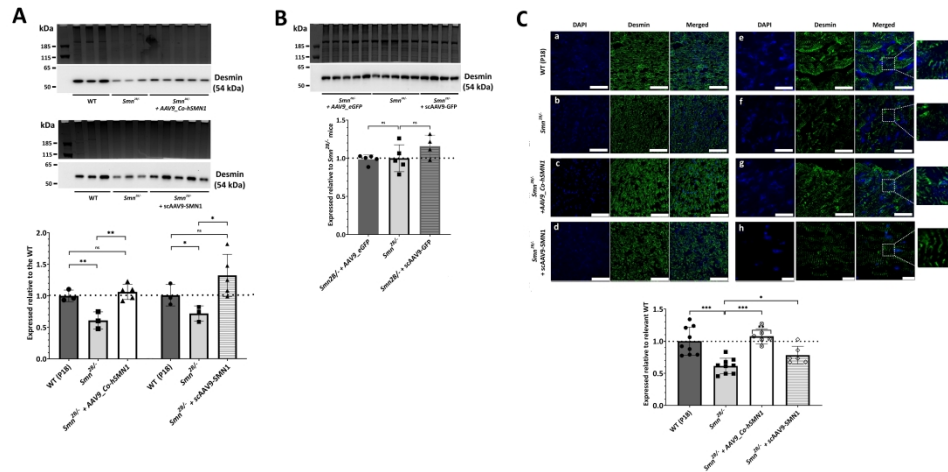


Figure 4. Levels and distribution of desmin in heart tissues from *Smn2B*^{-/-} mice following AAV9-mediated SMN1 delivery at P0. (A) Representative western blots of desmin levels in heart tissues from WT mice (P18), untreated *Smn2B*^{-/-} mice and *Smn2B*^{-/-} mice following AAV9-mediated treatment with SMN1 from two sources. The bar graph represents average desmin levels expressed relative to WT mice. (B) Representative western blots of desmin levels in heart tissues from untreated *Smn2B*^{-/-} mice and *Smn2B*^{-/-} mice following AAV9-mediated treatment without SMN1 (vehicle control) from two different vector sources. The bar graph represents average desmin levels expressed relative to untreated *Smn2B*^{-/-} mice. (C) Representative IMFs for desmin staining within heart tissues from WT mice (P18), untreated *Smn2B*^{-/-} mice and *Smn2B*^{-/-} mice following AAV9-mediated treatment with SMN1 from two vector sources. Zoomed images to highlight the reduction in desmin positive striations in untreated *Smn2B*^{-/-} mice in comparison to WT mice and AAV9-mediated SMN1 treated *Smn2B*^{-/-} mice. Corresponding bar graph reflects the area of cells stained for desmin corrected for number of cells present (DAPI stain) as determined by ImageJ analysis and expressed relative to corresponding WT mice. Dashed line represents the average desmin levels in WT mice and error bars represent the standard deviation from the mean. * $p < 0.05$; ** $p < 0.01$; *** $p < 0.001$. Scale bars represent 75 μm (panels a-d), 25 μm (panels e-g) and 10 μm (panel h).

660x330mm (300 x 300 DPI)

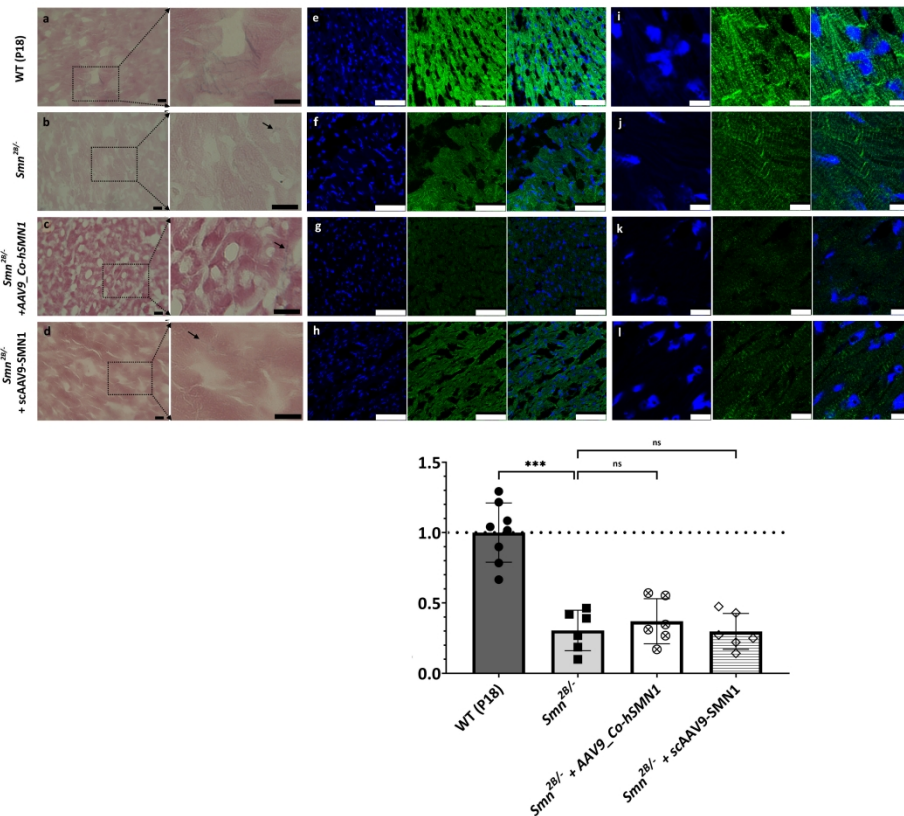


Figure 5. Levels and distribution of elastin in heart tissues from *Smn*^{2B/-} mice following AAV9-mediated SMN1 delivery at P0. (Panels a-d) Representative heart sections stained with Miller's Elastin van Gieson from WT mice (P18), untreated *Smn*^{2B/-} mice and *Smn*^{2B/-} mice following AAV9-mediated treatment with SMN1 from two different vector sources. Elastic fibres (blue/black); mature collagen (red); other tissues such as muscle and red blood cells (yellow). (Panels e-l) Representative IMFs for elastin staining within heart tissues from WT mice (P18), untreated *Smn*^{2B/-} mice and *Smn*^{2B/-} mice following AAV9-mediated treatment with SMN1 from two vector sources. Corresponding bar graph reflects the area of cells stained for elastin corrected for number of cells present (DAPI stain) as determined by ImageJ analysis and expressed relative to corresponding WT mice. Dashed line represents the average elastin levels in WT mice and error bars represent the standard deviation from the mean. ****p*<0.001. Black scale bars represent 10 μ m (panels a-d). White scale bars represent 75 μ m (panels e-h) and 10 μ m (panels i-l).

1645x1516mm (96 x 96 DPI)